

<sub>1</sub> White Paper on the Electron-Ion Collider in Preparation for  
<sub>2</sub> the NSAC Long Range Plan

<sub>3</sub> (DRAFT)

<sub>4</sub> EIC User Group

<sub>5</sub> November 14, 2022

# Contents

1	<b>1 Executive Summary</b>	<b>2</b>
2	1.1 The EIC Science Case . . . . .	2
3	1.2 The Electron-Ion Collider and EPIC Detector . . . . .	4
4	1.3 The Case for Two Detectors . . . . .	6
5	1.4 Recommendations and Initiatives . . . . .	6
6		
7	<b>2 The Science Case</b>	<b>8</b>
8	2.1 Origin of Nucleon Spin . . . . .	8
9	2.2 Origin of Nucleon Mass . . . . .	10
10	2.3 Imaging the 3D Parton Structure of Nucleons and Nuclei . . . . .	12
11	2.3.1 Imaging the Transverse Spatial Distributions of Quarks and Gluons	14
12	2.3.2 Multi-Dimensional Imaging of the Nucleon in Momentum Space . .	15
13	2.4 The Nucleus: A Laboratory for QCD . . . . .	16
14	2.4.1 Physics of High Gluon Densities in Nuclei . . . . .	17
15	2.4.2 Quarks and Gluons in the Nucleus . . . . .	19
16	2.5 Opportunities for Electro-Weak and Beyond the Standard Model Physics .	25
17		
18	<b>3 Synergy and Uniqueness of EIC</b>	<b>29</b>
19	3.1 Synergy with low energy nuclear physics and nuclear structure . . . . .	29
20	3.2 Synergy of eA, pA and AA . . . . .	31
21	3.3 Synergy with High-Energy LHC Program and Other Science Programs Worldwide . . . . .	32
22	3.4 Synergy with Lattice QCD and QCD Phenomenology . . . . .	36
23		
24	<b>4 Detectors</b>	<b>39</b>
25	4.1 Introduction - Detector Requirements . . . . .	39
26	4.2 The EPIC Detector . . . . .	41
27	4.2.1 Vertex and Tracking Detector . . . . .	41
28	4.2.2 Particle Identification Detector Systems . . . . .	43
29	4.2.3 Calorimeter Detector Systems . . . . .	48
30	4.2.4 Far-Forward Detector Systems . . . . .	51
31	4.2.5 Far-Backward Detector Systems . . . . .	53
32	4.3 Electron Polarimetry . . . . .	54
33	4.4 Hadron Polarimetry . . . . .	56
33	4.5 The Need for Two Detectors . . . . .	57

<b>1</b>	<b>5 Wider Impact</b>	<b>63</b>
2	5.1 Accelerator Science and Technology . . . . .	63
3	5.2 Detector Technology . . . . .	65
4	5.3 Advanced Computing . . . . .	67
5	5.4 International and Domestic Interest . . . . .	69
<b>6</b>	<b>References</b>	<b>71</b>

# <sup>1</sup> Chapter 1

## <sup>2</sup> Executive Summary

<sup>3</sup> The scientific foundation for the Electron Ion Collider (EIC) has been built for over two  
<sup>4</sup> decades. Throughout, the EIC initiative was driven by maintaining U.S. leadership in both  
<sup>5</sup> nuclear science and accelerator physics. These dual goals were clear from the outset, starting  
<sup>6</sup> with the 2002 NSAC Long Range Plan [1] where “*R&D over the next three years to address*  
<sup>7</sup> *EIC design issues*” was placed at high priority. Support from the community continued  
<sup>8</sup> with the 2007 Long Range Plan [2] which recommended “*the allocation of resources to*  
<sup>9</sup> *develop accelerator and detector technology necessary to lay the foundation for a polarized*  
<sup>10</sup> *Electron-Ion Collider*” and culminated in the 2015 plan, where the EIC was identified as  
<sup>11</sup> the “*highest priority for new facility construction following the completion of FRIB*” [3].

<sup>12</sup> During this period the science case underpinning these recommendations was continually  
<sup>13</sup> developed and documented by the growing EIC community, as illustrated in Fig. 1.1. A  
<sup>14</sup> series of workshops hosted by the Institute of Nuclear Theory laid the foundation for a  
<sup>15</sup> White Paper titled ”Understanding the glue that binds us all” [6]. The studies developed  
<sup>16</sup> for this White Paper, combined with continued progress in accelerator *R&D*, served as  
<sup>17</sup> input to a critical review in 2018 by the National Academy of Sciences (NAS). Their final  
<sup>18</sup> report, An Assessment of the U.S. Based Electron-Ion Collider Science, concluded that “*the*  
<sup>19</sup> *EIC science is compelling, fundamental, and timely.*” [7].

<sup>20</sup> The present White Paper serves as a compendium for these two decades of work. It  
<sup>21</sup> will briefly summarize the flagship components of the EIC science case and discuss the  
<sup>22</sup> current design of the collider and interaction regions. An update on the status of the  
<sup>23</sup> project will be presented, including the ongoing design of the EPIC detector that will be  
<sup>24</sup> built at the 6 o’clock interaction region and plans for a second, complementary detector  
<sup>25</sup> to be constructed at the 8 o’clock region. Synergies with ongoing and future nuclear and  
<sup>26</sup> particle physics programs will be discussed.

### <sup>27</sup> 1.1 The EIC Science Case

<sup>28</sup> Decades of scattering experiments and their theoretical interpretation have produced an  
<sup>29</sup> intriguing picture of the proton and neutron. These particles are held inside the atomic  
<sup>30</sup> nucleus by the strong force, the same force that generates the dynamic landscape of quarks  
<sup>31</sup> and gluons that form the substructure of the nucleon. Some quantum numbers of the

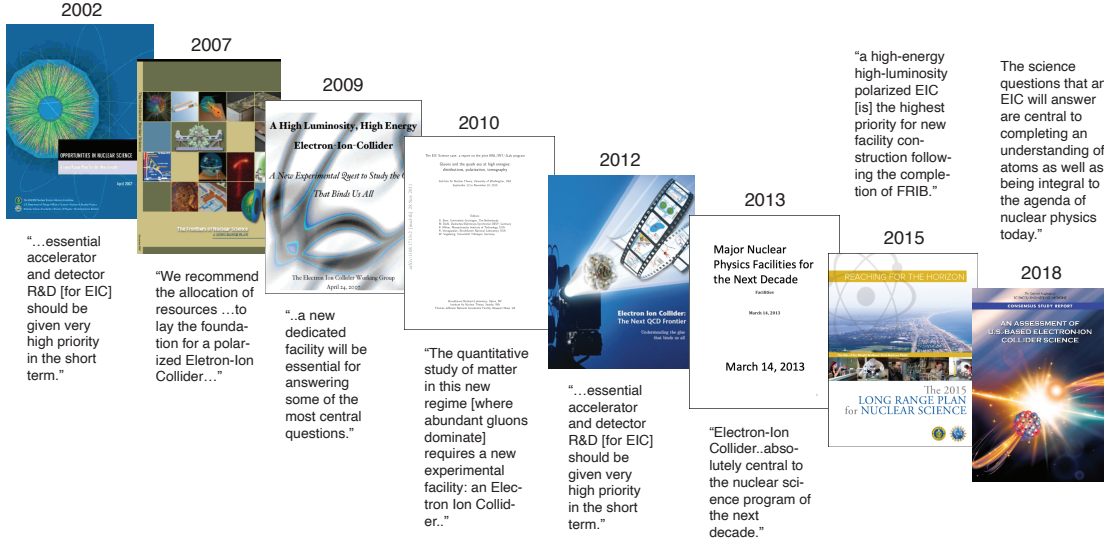


Figure 1.1: A chronological display of the publications that document the development of the EIC science case. From left to right: The 2002 [1] and 2007 [2] Long Range Plans, a 2009 report of the EIC Working Group [4], a report on the joint 2010 BNL/INT/JLab program on EIC [5], the 2012 EIC White Paper [6], the 2013 NSAC Subcommittie Report on Scientific Facilities, the 2015 Long Range Plan [3], and the NAS report [7].

1 nucleon, like its electric charge, are easily reproduced by simply summing the properties of  
 2 the three valence quarks. Yet, the quarks contribute only a third of the total nucleon spin  
 3 and an even smaller fraction of the total mass. Clearly, many of the fundamental properties  
 4 of the nucleon must emerge from the gluons, the carriers of the strong force that confine the  
 5 quarks inside of the nucleon, and from the copious  $q\bar{q}$  pairs that form the quark sea. Our  
 6 interest goes beyond reconstructing the fundamental properties of the parent nucleon: our  
 7 ultimate goal is understanding the dynamics of the dense partonic environment found in  
 8 nucleons and nuclei. The EIC is an amazingly versatile machine that will allow experiments  
 9 to map out the spatial and momentum distributions for quarks and gluons, study how the  
 10 gluon density evolves with the resolution of the electron probe and with the momentum  
 11 fraction  $x$  carried by the interacting gluon, and observe how transitions from partonic to  
 12 hadronic degrees of freedom are modified in increasingly dense nuclear matter. These key  
 13 science questions (and more!) can be summarized by the following four lines of inquiry:

- 14     • How do the nucleonic properties such as mass and spin emerge from partons and their  
 15       underlying interactions?
- 16     • How are partons inside the nucleon distributed in both momentum and position space?
- 17     • Where does the saturation of gluon densities in the nucleus set in? What happens to  
 18       the gluon density in nucleons and nuclei at small  $x$ ? Does it saturate at high energy,  
 19       giving rise to gluonic matter with universal properties in all nuclei (and perhaps even  
 20       in nucleons)?

- How do color-charged quarks and gluons, and jets, interact with a nuclear medium?
- How do the confined hadronic states emerge from these quarks and gluons? How do the quark-gluon interactions create nuclear binding?
- Do signals from beyond-the-standard-model physics manifest in electron-proton/ion collisions? If so, what can we learn about the nature of these new particles and forces?

## 1.2 The Electron-Ion Collider and EPIC Detector

The EIC will be a new, innovative, large-scale particle accelerator facility capable of colliding high energy beams of polarized electrons with heavy ions and polarized protons and light ions. It is a joint endeavor between Brookhaven National Laboratory (BNL) and the Thomas Jefferson National Accelerator Facility (JLAB) that will be built on the current site of the Relativistic Heavy Ion Collider (RHIC). In December 2019, the EIC was launched as an official project of the US government when it was granted Critical Decision Zero (CD0). Soon after, in June of 2021, the project was awarded CD1 status and it is on track to achieving CD2/3A by early 2024. Construction is expected to start in 2025, with beam operations (CD4) to commence in the early 2030s.

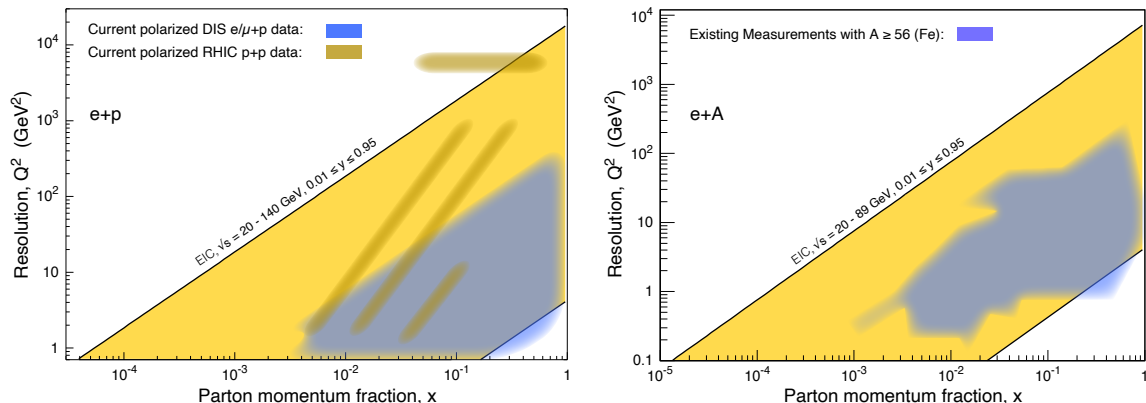


Figure 1.2: Left: The  $x-Q^2$  range covered by the EIC (yellow) in comparison with past and existing polarized  $e/\mu+p$  experiments at CERN, DESY, JLab and SLAC, and  $p+p$  experiments at RHIC. Right: The  $x-Q^2$  range for  $e+A$  collisions for ions heavier than iron (yellow) compared to existing world data. [Update with RHIC forward coverage](#)

The EIC is being designed to cover a center-of-mass energy range for  $e+p$  collisions of  $28 \text{ GeV} \leq \sqrt{s} \leq 140 \text{ GeV}$ , which in turn allows for a broad kinematic reach in  $x$  and  $Q^2$  as shown in Figure 1.2. The quantity  $x$  is a measure of the momentum fraction of the struck parton inside the parent-proton, while  $Q^2$  refers to the square of the four-momentum transfer between the electron and proton and is inversely proportional to the square of the spatial resolution. The diagonal lines in each plot represent lines of constant inelasticity  $y$ , which is the ratio of the virtual photon's energy to the electron's energy in the target rest frame.

- 1 The quantities  $x$ ,  $y$ , and  $Q^2$  are obtained from measurements of energies and angles of final  
 2 state objects, i.e., the scattered electron, the hadronic final-state or a combination of both.  
 3 The left panel in Fig. 1.2 shows the kinematic coverage for  $e+p$  collisions, and the right  
 4 panel shows the coverage for  $e+A$  collisions. The EIC will open the door to entirely new  
 5 regions in both  $x$  and  $Q^2$  while providing critical overlap with present and past experiments.  
 6 Access to the low- $x$  region is particularly important as this is the gluon-dominated regime  
 7 where saturation effects are expected to emerge.

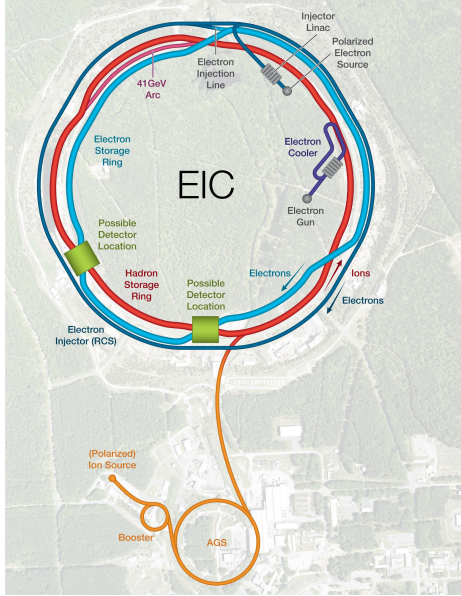


Figure 1.3: Planned EIC accelerator.

In order to address the crucial scientific questions discussed in the previous sections, the EIC must provide:

- Highly polarized electron ( $\sim 70\%$ ) and proton ( $\sim 70\%$ ) beams;
- Ion beams from deuterons to heavy nuclei such as gold, lead, or uranium;
- Variable  $e+p$  center-of-mass energies from 28–100 GeV, upgradable to 140 GeV;
- High collision electron-nucleon luminosity  $10^{33}–10^{34} \text{ cm}^{-2} \text{ s}^{-1}$ ;
- The possibility to have more than one interaction region.

- 8 Shown schematically in Fig. 1.3, the EIC will collide bright, intense counter-circulating  
 9 beams of electrons and ions at two possible interactions regions, IP6 and IP8. The De-  
 10 partment of Energy (DOE) has committed to building a general-purpose, large acceptance  
 11 detector that is capable of addressing the science case outlined in the NAS report. In 2020  
 12 the EIC Users Group launched a year-long effort to explore possible detector technologies  
 13 and codify the detector requirements needed to address the NAS science case. The results  
 14 of this study have been collected and published as the EIC Yellow Report [8]. With the de-  
 15 tector requirements defined, BNL and JLAB extended a call to the community in March of  
 16 2021 for Collaboration Proposals for the reference detector. A Detector Proposal Advisory  
 17 Panel (DPAP), an international committee of detector experts and theorists, was assembled  
 18 to review the submitted proposals. The outcome of that competitive review process is the  
 19 EPIC collaboration, which is in the process of finalizing the technology choices and detector  
 20 designs for the detector at IP6.

### **1 1.3 The Case for Two Detectors**

**2** A key deliverable of the EIC Project is a design that accommodates a second interaction  
**3** region and detector. Due to constrained resources, the EIC Project is committed to sup-  
**4** porting only one interaction region and detector, but it is recognized by all stakeholders  
**5** that a second detector is essential to fully exploit the science potential of the EIC. His-  
**6** torically, projects of similar scientific impact and scope were designed to include two or  
**7** more complementary detectors and the importance of this model has been demonstrated  
**8** time and again. Multiple detectors will expand scientific opportunities, draw a more vivid  
**9** and complete picture of the science, provide independent confirmation for discovery mea-  
**10** surements and mitigate potential risks when entering uncharted territories. Two detectors  
**11** will expand the opportunities for a new generation of scientists and encourage technological  
**12** development and innovation by fostering a natural and healthy competition between the  
**13** two collaborations.

**14** The timeline for a second experiment is crucial, the two experiments should be separated  
**15** by no more than a few years for scientific validation to be productive. In turn, this delayed  
**16** time frame can be used to explore new and complementary detector technologies that may  
**17** not have been utilized in the reference detector, EPIC. The EIC community has emphasized  
**18** the need for at least two detectors for many years and the DPAP echoed this support stating  
**19** in their report that "*There is significant support in the community and from the panel for a*  
**20** *second general-purpose detector system to be installed in IR8 when resources are available.*"  
**21** The EIC Users Group is in the process of refining the science case for a second detector and  
**22** is actively working to engage additional national and international resources for this effort.

### **23 1.4 Recommendations and Initiatives**

**24** The EIC Users Group (EICUG) currently consists of 1363 members from 267 institutions  
**25** located in 36 countries around the world. The EICUG community proposes the following  
**26** recommendation and initiative. These proposals were presented, discussed and received  
**27** overwhelming support at the QCD Town Hall Meeting in September of 2022.

**28**  
**29** **Recommendation:** We recommend the expeditious completion of the EIC as  
**30** the highest priority for facility construction.

**31**  
**32** *The Electron-Ion Collider (EIC) is a powerful and versatile new accelerator facility, capable*  
**33** *of colliding high-energy beams ranging from heavy ions to polarized light ions and protons*  
**34** *with high-energy polarized electron beams. In the 2015 Long Range Plan the EIC was put*  
**35** *forward as the highest priority for new facility construction and the expeditious completion*  
**36** *remains a top priority for the nuclear physics community. The EIC, accompanied by the*  
**37** *general-purpose large-acceptance detector, EPIC, will be a discovery machine that addresses*  
**38** *fundamental questions such as the origin of mass and spin of the proton as well as probing*  
**39** *dense gluon systems in nuclei. It will allow for the exploration of new landscapes in QCD,*  
**40** *permitting the “tomography”, or high-resolution multidimensional mapping of the quark and*  
**41** *gluon components inside of nucleons and nuclei. Realizing the EIC will keep the U.S. on*  
**42** *the frontiers of nuclear physics and accelerator science technology.*

- 1     ● *Building on the recent EIC project CD-1 approval, the community-led Yellow-Report,*  
2     *and detector proposals, the QCD research community is committed to continue the*  
3     *development and timely realization of the EIC and its first detector, EPIC. We rec-*  
4     *ommend supporting the growth of a diverse and active research workforce for the EPIC*  
5     *collaboration, in support of the expeditious realization of the first EIC detector.*
- 6     ● *We recommend new investments to establish a national EIC theory alliance to enhance*  
7     *and broaden the theory community needed for advancing EIC science and the experi-*  
8     *mental program. This theory alliance will contribute to a diverse workforce through*  
9     *a competitive national EIC theory fellow program and tenure-track bridge positions,*  
10     *including appointments at minority serving institutions.*

11 **Initiative: We recommend targeted efforts to enable the timely realization of a**  
12 **second, complementary detector at the Electron-Ion Collider.**

13  
14     *The EIC is a transformative accelerator that will enable studies of nuclear matter with un-*  
15     *precedented precision. The EIC encapsulates a broad physics program with experimental*  
16     *signatures ranging from exclusive production of single particles in ep scattering to very high*  
17     *multiplicity final states in eA collisions. Two detectors will expand the scientific opportu-*  
18     *nities, draw a more complete picture of the science, and mitigate the inherent risks that*  
19     *come with exploring uncharted territory by providing independent confirmation of discovery*  
20     *measurements. High statistical precision matched with a similar or better level of systematic*  
21     *precision is vital for the EIC and this can only be achieved with carefully optimized instru-*  
22     *mentation. A natural and efficient way to reduce systematic errors is to equip the EIC*  
23     *with two complementary detectors using different technologies. The second detector effort*  
24     *will rely heavily on the use of generic detector R&D funds and accelerator design effort to*  
25     *integrate the detector into the interaction region. The design and construction of such a*  
26     *complementary detector and interaction region are interwoven and must be synchronized*  
27     *with the current EIC project and developed in the context of a broad and engaged interna-*  
28     *tional EIC community.*

29

# <sup>1</sup> Chapter 2

## <sup>2</sup> The Science Case

### <sup>3</sup> 2.1 Origin of Nucleon Spin

The decomposition of the nucleon spin in terms of quark and gluon helicities and orbital angular momenta (OAM) has been an essential goal for nuclear scientists for several decades. The problem, known as the proton spin puzzle, is central to our understanding of the proton's or neutron's internal structure. The nucleon spin of  $1/2$  (in units of  $\hbar$ ) can be divided among its components according to [9] (see also [10]) as

$$\frac{1}{2} = \frac{1}{2} \Delta\Sigma(\mu^2) + \Delta G(\mu^2) + L_Q(\mu^2) + L_G(\mu^2), \quad (2.1)$$

where  $\Delta\Sigma$ ,  $\Delta G$ ,  $L_Q$ , and  $L_G$  are the contributions from the quark plus antiquark helicity, the gluon helicity, and the quark and gluon OAM, respectively. All terms in the spin decomposition depend on the resolution (renormalization) scale  $\mu$ . The quark and gluon spin contributions follow from the respective helicity distribution functions  $\Delta\Sigma(x, \mu^2)$  and  $\Delta g(x, \mu^2)$  upon integration of the latter over the whole  $x$ -range from 0 to 1:

$$\Delta\Sigma(\mu^2) = \int_0^1 dx \Delta\Sigma(x, \mu^2), \quad \Delta G(\mu^2) = \int_0^1 dx \Delta g(x, \mu^2). \quad (2.2)$$

<sup>4</sup> Here  $x$  is the fraction of the proton momentum carried by the measured quark or gluon while  $\Delta\Sigma = \Delta u + \Delta \bar{u} + \Delta d + \Delta \bar{d} + \dots$ . The discovery by the EMC experiment at CERN in the 1980s that the  $\Delta\Sigma$  term can only explain a small fraction of the nucleon spin signaled a breakdown of the constituent-quark model of the proton. The question of where the missing proton spin resides became known as the proton spin crisis, with the ‘proton spin puzzle’ being a term used more recently. Numerous fixed-target polarized electron/muon DIS experiments and polarized  $p + p$  experiments at RHIC covering the range  $0.005 \lesssim x \lesssim 0.6$ , not only confirmed the general finding of the EMC experiment with the present value of the quark helicity contribution  $\Delta\Sigma(\mu^2 = 10 \text{ GeV}^2) \approx 0.35$ , but also suggested that  $\Delta G(\mu^2 = 10 \text{ GeV}^2) \approx 0.2$  with large error bars [11–14].

<sup>14</sup> The non-zero gluon helicity integral  $\Delta G$ , while significant, is not large enough to make up the missing contribution to the nucleon spin. The missing spin, therefore, either comes

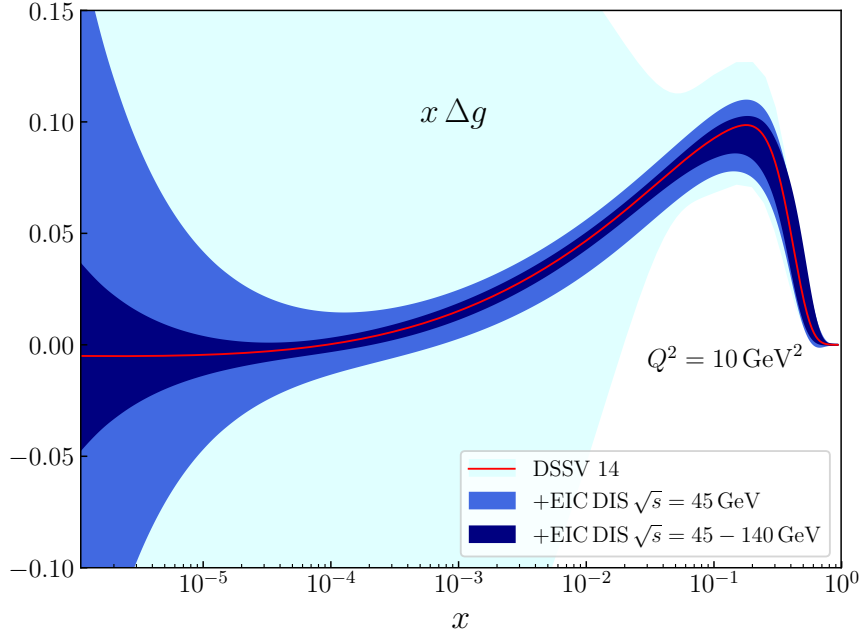


Figure 2.1: Impact of the projected EIC  $A_{LL}$  pseudodata on the gluon helicity distribution as a function of  $x$  for  $Q^2 = 10 \text{ GeV}^2$  [15]. In addition to the DSSV14 collaboration estimate (light-blue), the uncertainty bands resulting from the fit including the  $\sqrt{s} = 45 \text{ GeV}$  DIS pseudodata (blue) and, subsequently, the reweighting with  $\sqrt{s} = 140 \text{ GeV}$  pseudodata (dark blue), are also shown.

1 from the OAM contributions  $L_Q$  and  $L_G$  or is carried by the small- $x$  quarks and gluons,  
2 not yet probed in experiments.

3 Indeed, the numerical values for  $\Delta\Sigma$  and  $\Delta G$  quoted above have large uncertainties  
4 because, thus far, we have no information at all about the parton helicity distributions  
5  $\Delta\Sigma(x, \mu^2)$  and  $\Delta g(x, \mu^2)$  for  $x \lesssim 0.005$ . These uncertainties are illustrated in Fig. 2.1,  
6 which depicts the DSSV14 extraction of the gluon helicity distribution (light blue) and the  
7 impact the EIC data will make on it (blue and dark blue). One can see from Fig. 2.1 that the  
8 uncertainties will be drastically reduced when the existing measurements are combined with  
9 precision measurements over the full kinematic range accessible to EIC. Therefore, the EIC  
10 will put the nucleon spin decomposition phenomenology on a much firmer ground s [6,16,17]  
11 and will, additionally, allow us to test the theoretical predictions for helicity distributions at  
12 small  $x$  [18–22]. The latter predictions are important, because they are based on the novel  
13 evolution equations in  $x$  [19, 22], very different from the  $Q^2$ -evolution-based approaches  
14 used in the standard PDF fits. If these predictions are confirmed, the formalism behind  
15 them [19, 22] would allow us to extrapolate helicity distributions to the values of  $x$  even  
16 lower than those to be probed at the EIC, thus evaluating the remaining quark and gluon  
17 helicity contributions to the proton spin. An example of such extrapolation employing EIC  
18 pseudodata is shown in Fig. 2.2. There is also ongoing work [23] on the extraction of OAM  
19 contributions from the EIC data.

20 Lattice QCD has made enormous progress in recent years capitalizing on the novel

methods of calculating parton distribution functions proposed in [24, 25]. Lattice predictions for helicity distributions [26, 27] along with the calculations of  $x$ -integrated contributions to the proton spin [28], when combined with the EIC data and the small- $x$  extrapolations mentioned above, would help better constrain the proton spin decomposition (see, e.g., [29]) and, hopefully, resolve the proton spin puzzle.

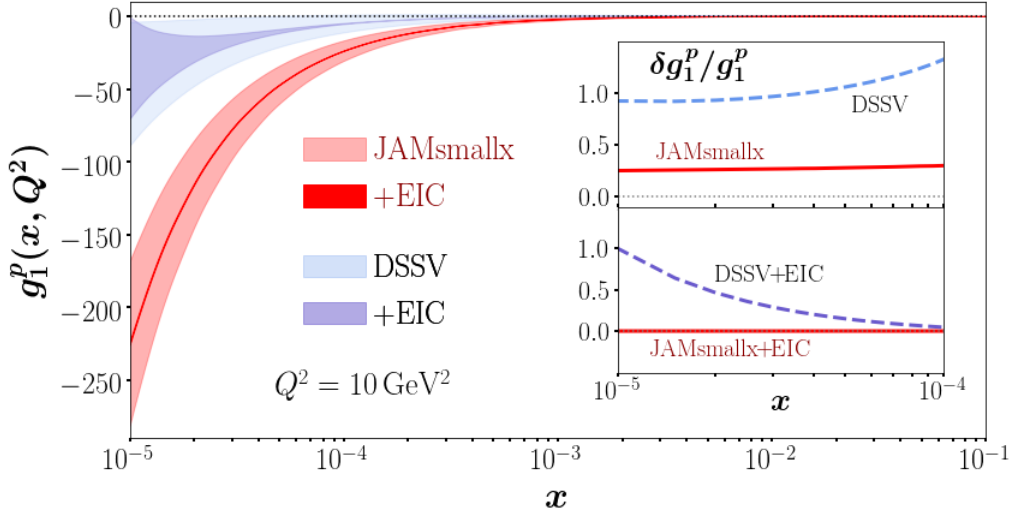


Figure 2.2: JAMsmallx collaboration [30] result for the  $g_1^p$  structure function obtained from existing polarized DIS data (light red band) as well as with EIC pseudodata (dark red band). For comparison, we include  $g_1^p$  from the DSSV fit to existing data [11, 12] (light blue band) and with EIC pseudodata at  $\sqrt{S} = 45$  and 141 GeV [31] (light purple band). The inset gives the relative uncertainty  $\delta g_1^p/g_1^p$  for each fit at small  $x$ . The difference between the red and blue bands at the  $x$  values below those to be probed at the EIC,  $x < 10^{-4}$ , is due in part to different theoretical approaches: the former is due to evolution in  $x$ , while the latter is due to evolution in  $Q^2$ , which cannot fully predict the  $x$  dependence.

## 2.2 Origin of Nucleon Mass

More than 99% of the mass of the visible universe resides in atomic nuclei, whose mass, in turn, is primarily determined by the masses of the proton and neutron. Therefore, it is of utmost importance to understand the origin of the proton (and neutron) mass, particularly how it emerges from the strong interaction dynamics. This goes well beyond simply adding the constituent masses that originate from the Higgs mechanism. Indeed, the large bulk of the nucleon mass can be attributed to contributions from quark and gluon (kinetic and potential) energies as highlighted in the NAS report [7]. Modern Lattice QCD calculations closely reproduce the hadron spectrum and support that QCD dynamics leads to mass.

One way to address the hadron mass question is to determine how current quarks and gluons contribute. There exist essentially two types of mass decomposition: one consists in a decomposition of the trace of the energy-momentum tensor (EMT), and the other

1 corresponds to an energy decomposition in the rest frame of the system. These two types of  
 2 mass decomposition can help gaining further intuition about the QCD dynamics responsible  
 3 for the emergence of mass (and also structure). It should be noted that mass is a number, one  
 4 decomposes into various operators of quark and gluon fields – and these are not observable.  
 5 The interpretation of each term would have an impact, *i.e.*, a physical meaning, if one can  
 6 connect each term to a physical observable within a controlled approximation. Therefore,  
 7 the various mass decompositions add significant physical interest if each component can  
 8 be extracted from experimental observables. The EIC with its versatile CM energy range,  
 9  $\sim 20\text{-}140 \text{ GeV}$  will have a unique role in this providing unique data on the QCD transition  
 10 region at the Fermi scale.

11 An essential role for an understanding of the proton mass is played by the trace anomaly  
 12 of the QCD energy-momentum tensor [32–35], that can give insight into the mass contribu-  
 13 tion from the vacuum. This contribution can be experimentally studied through heavy-  
 14 quark production near threshold ( $J/\Psi$ ,  $\Upsilon$ ). In such measurements one always introduces  
 15 quarks in the vacuum, so the issue is how to cleanly link the data to the trace anomaly.  
 16 This requires sophisticated QCD analysis methods, and sufficient data to constrain them.  
 17 In the Yellow Report [8], the impact of  $J/\Psi$  production on the mass of the proton and on  
 18 our understanding of the reaction mechanism (2-gluon mechanism) is shown. The 2-gluon  
 19 mechanism is most closely connected to the operator related to the trace anomaly.

20 The  $Q^2$  dependence of threshold  $J/\Psi$  production gives empirical information about the  
 21 2-gluon mechanism. Currently, experiments are ongoing at JLab, and the first results for  
 22 near-threshold  $J/\Psi$  exclusive photoproduction have been reported recently. However, these  
 23 measurements cannot provide information either on the  $Q^2$  dependence for  $J/\Psi$  produc-  
 24 tion or the complementary heavier-mass  $\Upsilon$  production, and so EIC can provide a unique  
 25 opportunity.

26 Beyond protons and neutrons, pions and kaons are the necessary main building blocks  
 27 of nuclear matter. If we really want to claim we understand QCD dynamics we have  
 28 to understand at least the structure of the pion, kaon, proton, neutron, and likely also  
 29 the lambda at the same level. Paradoxically, the chiral-symmetry features that manifest  
 30 themselves in the lightest pseudoscalar mesons appear to be key to the further understanding  
 31 of the emergent mass and structure mechanisms. In this picture, the properties of the  
 32 nearly massless pion are the cleanest expressions of the mechanism that is responsible for  
 33 the emergence of the mass and have measurable implications for the pion form factor and  
 34 meson structure functions [36].

35 Measurements of the pion structure can be done at EIC through the Sullivan process  
 36 with high, near-100% tagging detection fraction, in sharp contrast with earlier HERA mea-  
 37 surements, and with decades better statistics. The pion structure can give us key insights  
 38 in the emergent-mass contributions. Any mass decomposition must fulfill the cancellations  
 39 that lead to the small pion mass where various terms are expected to remain non-zero  
 40 (trace anomaly, quark/gluon momentum fractions). Pion structure function measurements  
 41 inform about the quark/gluon momentum fractions, and, separate pion form factor mea-  
 42 surements at the EIC, up to  $Q^2$  momentum transfer scales of  $\sim 30 \text{ (GeV}/c)^2$ , informing us  
 43 how emergent mass manifests itself in the wave function.

44 At variance with the pion, the effects of the Higgs mechanism, which gives a non-  
 45 vanishing mass to the quarks, play a more substantial role for the kaon mass due to its

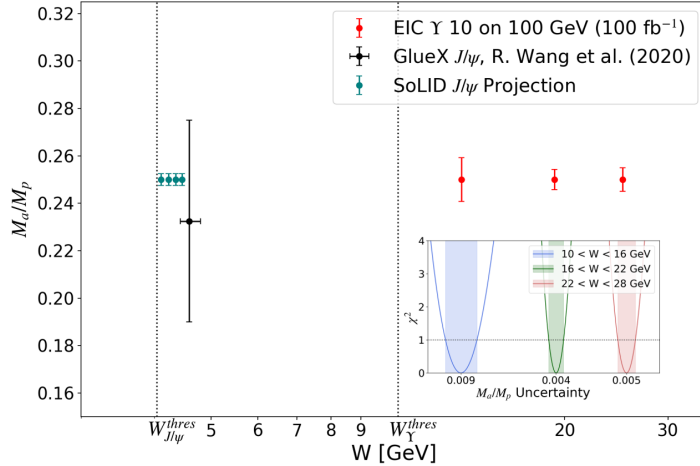


Figure 2.3: Projection of experimental uncertainty on the trace anomaly contribution to the proton mass ( $M_a/M_p$ ) extracted from  $\Upsilon$  photoproduction on the proton at the EIC in  $10 \times 100$  GeV electron/proton beam-energy configuration. The insert panel illustrates the minimization used to determine the uncertainty for each data point. The black circles are the results from the analysis of the GlueX  $J/\Psi$  data [191], while the dark green circles correspond the JLab SoLID  $J/\Psi$  projections. The  $\Upsilon$  projections were generated following the approach from Ref. [192] with the lAger Monte Carlo generator [193].

1 strange quark content. Therefore, a comparison of the charged pion and charged kaon form  
 2 factors over a wide range in  $Q^2$  would provide unique information relevant to understanding  
 3 the generation of hadronic mass. The EIC can also, similar as for pions, open a vast land-  
 4 scape of structure function measurements constraining quark and gluon energy distributions  
 5 in kaons.

6 Lastly, gluon tomography measurements discussed separately (see Section 2.3) can in-  
 7 form how gluons spread out in radial space as compared to quarks, and how confinement  
 8 and the emergent-mass mechanism manifest themselves in the gluon radius. Information on  
 9 such gluonic radii in hadrons is an essential component of understanding the QCD dynamics  
 10 and modeling.

## 11 2.3 Imaging the 3D Parton Structure of Nucleons and Nuclei

12 The EIC will significantly extend our knowledge of the distribution of quarks and gluons  
 13 in nucleons and nuclei. Most of our knowledge to date has been gathered from inclu-  
 14 sive electron-proton scattering, augmented with hard scattering reactions in hadron-hadron  
 15 collisions, that provides a 1-dimensional picture of the nucleon as it describes the  $x$ - or mo-  
 16 mentum fraction distribution of (longitudinal) quark and gluon momenta in the direction of  
 17 the nucleon momentum. Examples of processes that can provide information beyond this  
 18 1-dimensional picture are illustrated in Fig. 2.5.

19 Additional data gained by detecting the full final state of the proton beam provides

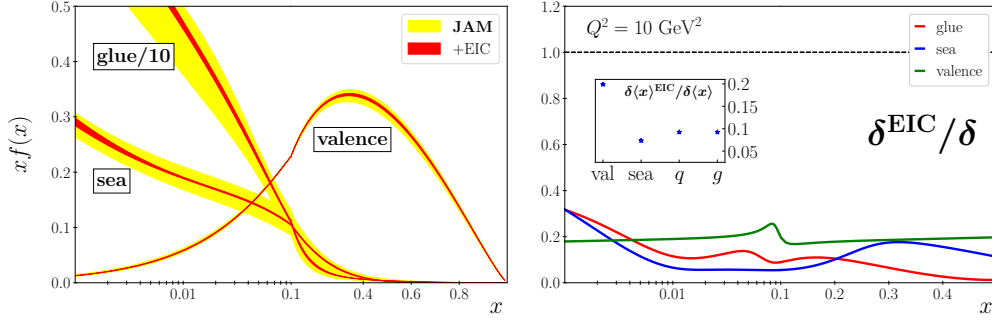


Figure 2.4: Comparison of uncertainties on the pion valence, sea quark and gluon PDFs before (yellow bands) and after (red bands) inclusion of EIC data. Right: Ratio of uncertainties of the PDFs with EIC data to PDFs without EIC data,  $\delta^{EIC}/\delta$ , for the valence (green line), sea quark (blue) and gluon (red) PDFs, assuming 1.2% systematic uncertainty, and (inset) the corresponding ratios of the momentum fraction uncertainties,  $\delta \langle x \rangle^{EIC}/\delta \langle x \rangle$ , for valence, sea, total quark and gluon PDFs [149], at the scale  $Q^2 = 10 \text{ GeV}^2$ . Fits were obtained using a Monte Carlo procedure, using DGLAP at NLL with VFNS, NLL as and both Drell-Yan and  $F_2$  for leading neutrons at NLO.

1 information about the impact parameter, related to the transverse position of the partons –  
 2 quarks and gluons – that reside inside nucleons and nuclei. These measurements will enable  
 3 parton tomography, a series of two-dimensional (2D) images of the nucleon, stacked along  
 4 the Bjorken  $x$  direction. Starting at large  $x$ , in the domain of valence quarks, and proceeding  
 5 toward lower  $x$ , the regime of sea quarks and gluons, these images will reveal where quarks  
 6 and gluons are located in the transverse plane. If the target beam is unpolarized, or if  
 7 the target spin is aligned with the direction of motion, then the distribution is rotationally  
 8 symmetric in the transverse plane. In this case, parton tomography provides a series of  
 9 radial distributions.

10 Using a related class of observables gathered from data where the scattered electron is  
 11 measured in tandem with an electro-produced hadron, or a jet, or a pair of hadrons, an  
 12 EIC will also measure the transverse motion of partons. The uncertainty principle relates  
 13 the typical transverse momentum of a parton to the spatial extent of the quark or gluon  
 14 field that produced it. Because the quark or gluon transverse momentum is not a Fourier  
 15 conjugate of its impact parameter, the transverse position and momentum distributions are  
 16 not Fourier conjugates of each other. These transverse momentum-dependent measurements  
 17 then provide additional clues that will help to identify the nature of fluctuations of the  
 18 color field in the nucleon [37–39]. This enhances sensitivity to features following from the  
 19 essence of quantum theory, resulting in observables, notably spin asymmetries, that become  
 20 sensitive to quantum phases generated by the color force (analogous to the Berry phase)  
 21 when transverse motion is studied. The full richness of transverse momentum information is  
 22 explored when transverse polarization (with the spin direction orthogonal to the direction  
 23 of motion) is added. In this case, orbital motion leads to correlations between spin and  
 24 transverse momentum, and parton tomography provides a series of images of transverse  
 25 momentum distributions that are fully 2+1 dimensional.

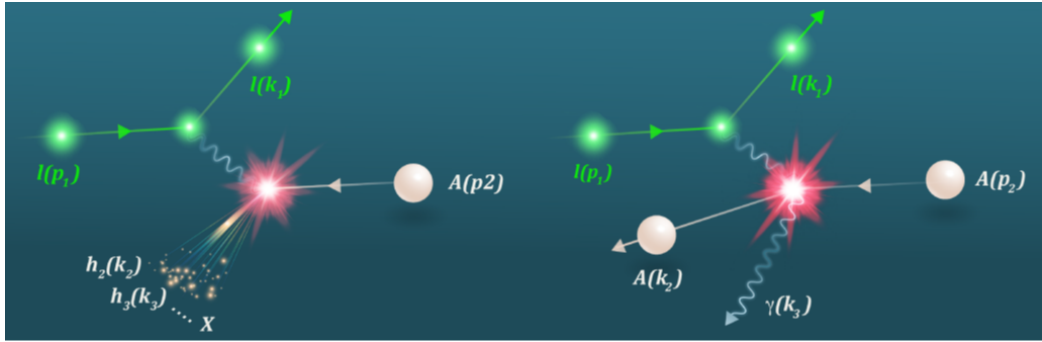


Figure 2.5: Illustration of the two types of processes that occur in lepton-nucleus collisions. The left-panel shows a semi-inclusive process where a hadron, hadron pair, jet or dijet is measured and the remnant nucleus is destroyed. The right panel shows an exclusive process were the nucleus remains intact.

1 The science potential of the processes sensitive to the multi-dimensional structure of  
 2 nucleons and nuclei is illustrated in Fig. 2.6. Further information on the challenge to image  
 3 quarks and gluons at the subatomic scale can be found in [40].

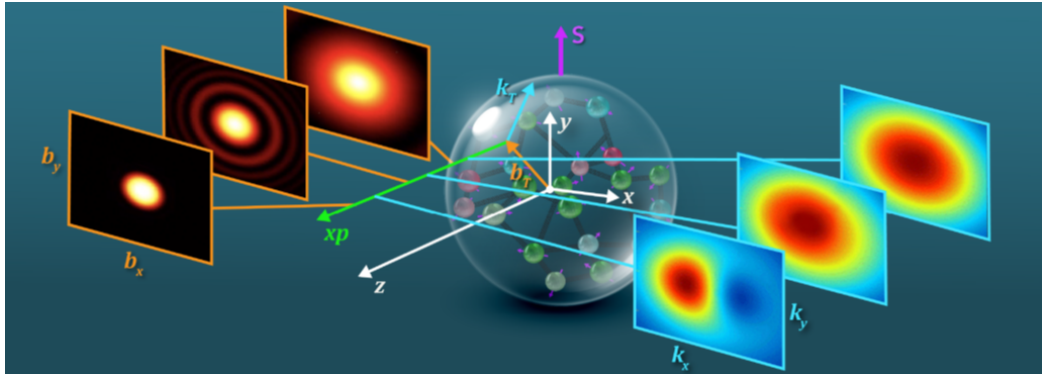


Figure 2.6: Tomographic images in slices of  $x$  for the quarks and gluons in a nucleus. The images on the left give a (transverse) spatial tomography in  $b_T$ -space provided by exclusive processes. The images on the right give a (transverse) momentum tomography in  $k_T$ -space provided by semi-inclusive processes.

#### 4 2.3.1 Imaging the Transverse Spatial Distributions of Quarks and Gluons

5 We live macroscopically in a 3D world. Yet we know very little about the transverse  
 6 spatial distributions of quarks and gluons in the microscopic sub-atomic world, with our  
 7 main knowledge constrained by information on the 1-dimensional parton distributions as  
 8 function of the longitudinal momentum fraction  $x$ .

9 From elastic form factor measurements we have learned that the (integrated over  $x$ )  
 10 charge and magnetization distributions of nucleons and nuclei differ, but so far our level  
 11 of knowledge of the spatial distributions for valence quarks, sea quarks, and gluons is still

<sup>1</sup> relatively low.

<sup>2</sup> It is possible to determine the transverse spatial distributions of quarks and gluons  
<sup>3</sup> experimentally, where their study requires a particular category of measurements, that of  
<sup>4</sup> exclusive reactions. Examples are deeply virtual Compton scattering (DVCS) and deeply  
<sup>5</sup> virtual meson production (DVMP). For those reactions, the proton remains intact, and  
<sup>6</sup> a photon or a meson is produced. Exclusivity demands that all final-state products are  
<sup>7</sup> detected, i.e., the scattered electron, the produced photon or meson, and the scattered  
<sup>8</sup> proton. The spatial distributions of quarks and gluons in these measurements are extracted  
<sup>9</sup> from the Fourier transform of the differential cross-section with respect to the momentum  
<sup>10</sup> transfer  $t$  between the incoming and the scattered proton. The non-perturbative quantities  
<sup>11</sup> that encode the spatial distributions are called generalized parton distributions (GPDs)  
<sup>12</sup> [41–43]. In addition to the fundamental role of GPDs concerning the spatial distribution  
<sup>13</sup> of partons inside hadrons [44], the second moment of particular sets of GPDs will provide  
<sup>14</sup> in-depth insight into the total angular momentum of quarks and gluons in the proton [10].  
<sup>15</sup> GPDs offer a unique opportunity to probe the energy-momentum tensor through their form  
<sup>16</sup> factors. GPDs contain information about the spin, the pressure and shear forces inside  
<sup>17</sup> hadrons [45], and open a further door to deepen our understanding of the nucleon mass.

<sup>18</sup> Our knowledge of GPDs is currently limited and mainly based on DVCS data based on  
<sup>19</sup> fixed-target experiments at intermediate to high- $x$  or on the HERA collider measurements  
<sup>20</sup> at low- $x$ . The polarized beams and higher luminosity at EIC, along with forthcoming data  
<sup>21</sup> from JLab at 12 GeV, will make a very significant impact on those measurements. It is  
<sup>22</sup> anticipated that measurements made for protons in the range  $0.04 \lesssim t < 1.5 \text{ GeV}^2$  will  
<sup>23</sup> enable maps of parton distributions all the way down to  $0.1 \text{ fm}$  [17, 46]. The range of ion  
<sup>24</sup> beams at EIC will allow such exclusive measurements to be performed on nuclei, and will  
<sup>25</sup> enable us to understand the transverse quark and gluon distributions within.

### <sup>26</sup> 2.3.2 Multi-Dimensional Imaging of the Nucleon in Momentum Space

<sup>27</sup> As in the case of the transverse spatial distribution of partons inside a hadron, we know  
<sup>28</sup> very little about their distribution in the transverse momentum space. Due to the confined  
<sup>29</sup> QCD bound state, to gluon emission and to multiple rescattering, the partons must have  
<sup>30</sup> nonzero momenta in the (transverse) plane perpendicular to the nucleon momentum.

<sup>31</sup> The 3D parton structure of hadrons in momentum space is encoded in transverse mo-  
<sup>32</sup> mentum dependent parton distributions (TMDs). Quarks and gluons inside a spin- $\frac{1}{2}$  hadron  
<sup>33</sup> are described by 8 TMDs each [39]. These functions quantify different correlations between  
<sup>34</sup> longitudinal and transverse spin of the proton with the quark and gluons polarizations and  
<sup>35</sup> transverse momenta, revealing deep insights into the internal structure of the proton (or  
<sup>36</sup> neutron). Some of the better known TMDs are the Sivers [37, 38] and Boer-Mulders [39]  
<sup>37</sup> functions, along with the unpolarized and helicity-dependent TMDs.

<sup>38</sup> The Boer-Mulders functions quantifies the correlation that can exist between the quark  
<sup>39</sup> transverse polarization and transverse momentum even in an unpolarized nucleon. The  
<sup>40</sup> Sivers function measures the correlation between the quark or gluon transverse momentum  
<sup>41</sup> and the transverse polarization of the nucleon (proton): it has been suggested that this  
<sup>42</sup> correlation is related to the spin-orbit coupling inside the nucleon. For such spin-orbit  
<sup>43</sup> correlations to manifest themselves as spin asymmetries, a second ingredient is required:

that the struck parton acquires a quantum-mechanical phase from traveling through the color field of the nucleon. As a consequence, spin asymmetries probe the dynamics of QCD in novel ways, providing substantial different information on the nucleon structure dynamics from that provided by a series of radial (or transverse spatial) distributions.

An essential aspect of TMDs concerns their  $Q^2$  scale-dependence (evolution) as predicted in QCD [47–51], which is very different from the evolution of the collinear 1D parton distribution functions. There is, therefore, a substantial interest in a quantitative understanding of the TMD evolution. The EIC will be ideal for such studies, complementing the high precision data becoming available from JLab at larger values of  $x$ . It would allow to explore TMDs over an extensive range in  $Q^2$  while covering transverse momenta of the final-state hadrons over a wide range from low (non-perturbative) to high (perturbative) values. The EIC data will also be complementary to the data reported by RHIC and LHC, which probes similar values of  $Q^2$  but in different processes, therefore testing factorization and universality of TMDs. Theoretically anticipated violations of TMD universality, such as the well-known sign reversal of the Sivers function between the semi-inclusive DIS (SIDIS) and Drell-Yan (DY) processes [52, 53], can also be tested at the EIC.

TMDs can be measured at EIC via the SIDIS process, where one detects an identified hadron or jet, or identified di-hadrons or dijets, in addition to the scattered lepton. The data sets used to constrain TMDs are currently even more limited in  $x$  and  $Q^2$  than those shown in the left panel of Fig. 1.2 used to constrain helicity-dependent parton distribution functions. With its polarized beams, high luminosity and broad energy range, the EIC will dramatically advance our knowledge of TMDs. Unpolarized beams at the EIC are just as relevant to map in detail, e.g., the Boer-Mulders TMD as already mentioned earlier. With its range of ion beams, from deuterons to heavy nuclei, the EIC will allow studies of TMDs in nucleons and nuclei alike, which will be discussed more in Section 2.4 below. The nuclear medium modification of TMDs is essentially unknown; for example a modification of the orbital motion of quarks in the medium is expected. The 3D momentum structure of the nucleon for the different quark flavors and the gluons will be mapped out over a wide range in  $x$  and  $Q^2$  [6, 54]. The EIC is therefore expected to have a transformative impact on the field of the nucleon’s 3D structure in momentum space.

## 2.4 The Nucleus: A Laboratory for QCD

In this Section we outline the physics potential of  $e+A$  collisions at the EIC building on the strong physics case detailed in the EIC White Paper [6] and the report of the National Academy of Science [7].

With its wide range in energy and nuclear beams, high luminosity and clean collider environment, the EIC offers an unprecedented opportunity for precision studies and discovery. As we detail below, this is also true in  $e+A$  collisions, where the EIC would be able to discover gluon saturation, map the momentum and spatial distribution of gluons and sea quarks in nuclei, measure the response of the cold nuclear medium to the propagation of high-momentum (hard) probes, and study hadronization of quarks and gluons inside the nucleus. Compared to the proton, the nucleus has an additional parameter, the atomic number  $A$ , which the EIC would be able to vary by colliding different nuclei with the electrons. Below we will explain that due to this  $A$  parameter, the nucleus serves as an

1 efficient amplifier of the physics of gluon saturation and high gluon densities. It also serves  
 2 as a powerful analyzer of physics across the full range of  $x$ ,  $Q^2$  and  $A$ .

3 The  $e+A$  measurements at the EIC will also deepen and corroborate our understanding  
 4 of the formation and properties of the strongly interacting Quark Gluon Plasma (QGP) in  
 5 high energy heavy ion collisions at RHIC and the LHC, of the dynamics of proton–nucleus  
 6 collisions, of the hadronization process of high energy cosmic ray showers, and of many  
 7 other neighboring fields.

#### 8 2.4.1 Physics of High Gluon Densities in Nuclei

9 It is well-established that gluon and sea quark PDFs in the proton grow rather rapidly  
 10 with decreasing Bjorken  $x$  at small values of  $x$  (see Fig. 2.7). The dynamical mechanism  
 11 responsible for the growth is driven by the splitting of gluons into pairs of gluons (and  
 12 splitting of quarks into quarks and gluons) [55–59]. The large number of gluons and sea  
 13 quarks at low  $x$ , all of them confined within the few fm<sup>2</sup> transverse area of the proton is  
 14 bound to generate high density of partons (gluons and quarks). But will this high density  
 15 keep increasing as we probe lower and lower values of  $x$ ? Would the physics change in  
 16 the high density regime? As was originally conjectured in [60], the growth of the gluon  
 17 density should saturate at some small value of  $x$ , leading to the novel regime of gluon  
 18 saturation (see [61–67] for reviews). The new dynamics in the saturation regime is due to  
 19 gluon mergers: the mergers compensate for the splittings, leading to saturation of the gluon  
 20 density. The transition from the splittings-dominated regime to the saturation regime is  
 21 described by the nonlinear small- $x$  evolution equations, [68–77], which are a manifestation  
 22 of the nonlinear nature of QCD.

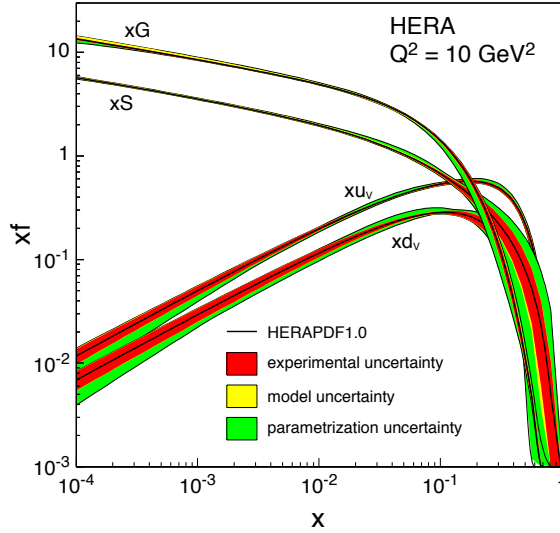


Figure 2.7: HERAPDF extraction of parton distribution functions. The plot depicts  $x$  times the PDF versus  $x$  for  $Q^2 = 10 \text{ GeV}^2$ . The PDFs plotted are for the valence up and down quarks ( $u_v$  and  $d_v$ ), along with the gluon ( $G$ ) and “sea” quarks ( $S$ ) PDFs. Please note the logarithmic scale of the vertical axis.

1     A key feature of gluon saturation is the emergence of a momentum scale  $Q_s$ , known as  
 2     the saturation scale. The scale is predicted by the nonlinear evolution equations [68–77] and  
 3     designates a transition from the low-density regime ( $Q > Q_s$ ) to the high-density saturated  
 4     regime ( $Q < Q_s$ ) as indicated in Fig. 2.8. The saturation scale grows with decreasing  $x$ ,  
 5      $Q_s^2 \sim 1/x^{0.3}$ . When this scale significantly exceeds the QCD confinement scale  $\Lambda_{QCD}$ , the  
 6     dynamics of strongly correlated gluons can be described by weak coupling QCD methods.  
 7     The framework that enables such computations is an effective field theory called the Color  
 8     Glass Condensate (CGC) [61–67]. It is expected that the saturation phenomenon should  
 9     exist in nuclei as well, with the saturation scale growing with the nuclear atomic number  
 10      $A$ ,  $Q_s^2 \propto A^{1/3}$  [78–81]; thus, the novel domain of saturated gluon fields can be accessed  
 11     especially well in large nuclei. This saturation regime of QCD is predicted to exist in all  
 12     hadrons and nuclei when boosted to high energies where one can probe the low- $x$  region in  
 13     full detail. While some tantalizing evidence in favor of saturation physics has been collected  
 14     by the accelerators around the world, a definitive discovery is yet to come. Unambiguously  
 15     establishing this novel domain of QCD and its detailed study is one of the most critical EIC  
 16     goals.

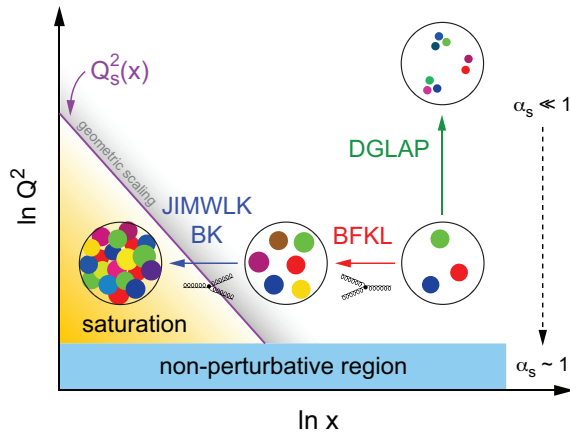


Figure 2.8: Schematic illustration of the probe resolution,  $Q^2$ , versus  $x$ , indicating regions of non-perturbative (band at the bottom) and perturbative QCD (everything above the non-perturbative region), including in the latter, low to high saturated parton density, and the transition region between them. The perturbative (low-parton density) region is described by the standard DGLAP evolution [55–57] and the linear small- $x$  BFKL evolution [58, 59], denoted by the vertical and horizontal arrows correspondingly. The BFKL equation evolves the gluon distribution towards small  $x$ , where the parton density becomes large and parton saturation sets in. The transition to saturation is described by the non-linear BK [68–71] and JIMWLK [72–77] evolution equations. The saturation region is shown in yellow.

17     Multiple experimental signatures of saturation have been discussed in the literature [6].  
 18     The EIC program follows a multi-pronged approach taking advantage of the versatility of the  
 19     EIC facility. Day-one measurements include the proton and nuclear structure functions  $F_2$   
 20     and  $F_L$ , which are sensitive to saturation physics. One of the other key signatures concerns  
 21     the suppression of di-hadron angular correlations in the process  $e + A \rightarrow e' + h_1 + h_2 + X$ .  
 22     The angle between the two hadrons  $h_1$  and  $h_2$  in the azimuthal plane,  $\Delta\phi$ , is sensitive to the

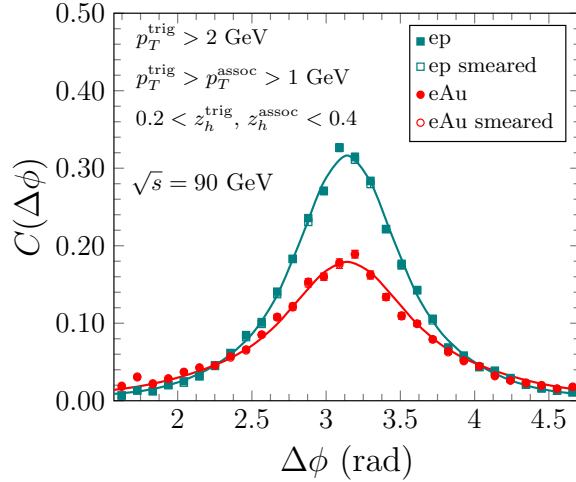


Figure 2.9: A saturation model prediction of the hadron-hadron correlation function  $C(\Delta\phi)$  to be measured in  $e+p$  and  $e+A$  collisions at EIC plotted versus the azimuthal angle  $\Delta\phi$ : the away side peak at  $\Delta\phi = \pi$  decreases as one goes from  $e+p$  to  $e+A$  due to the increase in the saturation scale with  $A$ . The ranges of transverse momenta ( $p_T$ ) and longitudinal momentum fractions ( $z_h$ ) of the trigger and associate hadrons are specified in the plot.

1 transverse momentum of gluons to and their self-interaction — the mechanism that leads  
 2 to saturation. The experimental signature of saturation is a progressive suppression of the  
 3 away-side ( $\Delta\phi = \pi$ ) correlations of hadrons with increasing atomic number  $A$  at a fixed  
 4 value of  $x$ , as demonstrated in Fig. 2.9. Diffraction and diffractive particle production in  
 5  $e+A$  scattering is another promising avenue to establish the existence of saturation and to  
 6 study the underlying dynamics. Diffraction entails the exchange of a color-neutral object  
 7 between the virtual photon and the proton remnant. As a consequence, there is a rapidity  
 8 gap between the scattered target and the diffractively produced system. At HERA, these  
 9 types of diffractive events made up a large fraction of the total  $e+p$  cross-section (10–  
 10 15%). Saturation models predict that at the EIC, more than 20% of the cross-section  
 11 will be diffractive. In simplified terms, since diffractive cross-sections are proportional to  
 12 the square of the nuclear gluon distribution,  $\sigma \propto g(x, Q^2)^2$ , they are very sensitive to the  
 13 onset of non-linear dynamics in QCD. An early measurement of coherent diffraction in  $e+A$   
 14 collisions at the EIC would provide the first unambiguous evidence for gluon saturation.

### 15 2.4.2 Quarks and Gluons in the Nucleus

#### 16 Propagation of a Fast Moving Color Charge in QCD Matter

17

18 The EIC will address not only many outstanding questions about hadron *structure*, in-  
 19 cluding the qualitatively new constraints on parton dynamics in saturation, as described  
 20 earlier, but also will make substantial progress in our understanding of hadron *formation*,  
 21 including parton propagation through nuclear matter. In the standard regime of pertur-  
 22 bative QCD at high  $Q^2$  and moderate to high  $x$ , in  $e+A$  scattering events, the virtual

1 photon transmits a large fraction of the electron's energy. It interacts with a quark from a  
 2 nucleon in the nucleus. The struck quark will subsequently traverse the nucleus, interacting  
 3 with the color charges within, and continually lose energy. At some point, this quark will  
 4 hadronize, forming a color-neutral hadron. Whether the hadronization process happens  
 5 inside or outside the nucleus depends on the interplay between the quark's energy and the  
 6 atomic number of the nucleus. If the virtual photon energy (in the nuclear rest frame)  
 7 is high, the quark kicked out of the nucleon will have considerable energy and produce a  
 8 jet. Measuring the jets experimentally provides several advantages over studies of leading  
 9 hadrons. Reconstructed from multiple (ideally all) final state particles produced by  
 10 hadronization of the scattered parton, jets are much closer proxies for the parton kinemat-  
 11 ics than any single-particle observable. Using jets, in many cases, removes (or minimizes)  
 12 hadronization uncertainties. On the other hand, jets are composite objects with rich inter-  
 13 internal substructure encoding shower evolution and hadronization details, which the EIC will  
 14 be uniquely positioned to study.

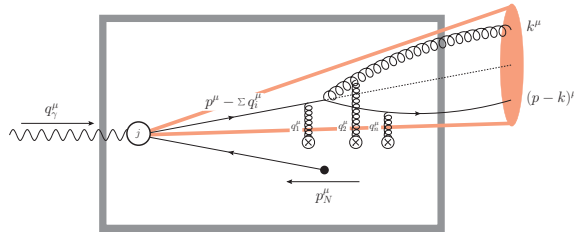


Figure 2.10: Illustration of the indicated jet kinematics for semi-inclusive Deep-Inelastic Scattering (SIDIS) in the Breit frame. The dark box represents the medium (nucleus), and the red cone represents the jet.

15 At the EIC, the jets will be used as multipurpose tools to study, for example, the gluon  
 16 helicity in polarized protons in  $e+p$  collisions [17]. A comparison of the cross-section in  
 17  $e+p$  and  $e+A$  collisions is expected to be sensitive to in-medium shower broadening effects.  
 18 Key measurements relying on jets were identified for their sensitivity to parton energy loss  
 19 in the nucleus [82]. Similarly, new measurements of several variables assessed via lepton-jet  
 20 correlations can constrain the parton transport coefficient in nuclei [83]. The energy loss  
 21 of fast color-charged partons in the cold nuclear matter exhibited in  $e+A$  collisions spans  
 22 different regimes or scales. Specifically, a partially coherent Landau-Pomeranchuk-Migdal  
 23 (LPM) regime, with the gluon formation times of the order of the medium length, and a  
 24 fully coherent (factorization) regime, dominating for significantly longer time frames. The  
 25 latter part could be evaluated in hadronic collisions elsewhere, while the EIC will provide  
 26 the most direct access to the energy loss in nuclei in the LPM regime via identified hadron  
 27 in semi-inclusive deep inelastic scattering events.

28 Energy loss is expected to occur in both hot and cold QCD matter through the gluon  
 29 radiation and/or collisional losses. The quantitative assessments of the related processes  
 30 in both media types are central to relativistic heavy ion collisions, as a critical reference  
 31 for complete modeling of the QGP, and the field of nuclear physics in general for under-  
 32 standing the transport properties of nuclear matter. Detailed mapping of color-charge and  
 33 flavor effects in cold-QCD reactions with nuclei of different sizes will provide additional

1 experimental handles for understanding the transport properties of nuclear matter. These  
 2 assessments will provide new quantitative constraints on strong interactions in the nuclear  
 3 medium. These advances will be a significant part of synergistic activities with the ongoing  
 4 hot QCD program studies of the quark-gluon plasma (QGP).

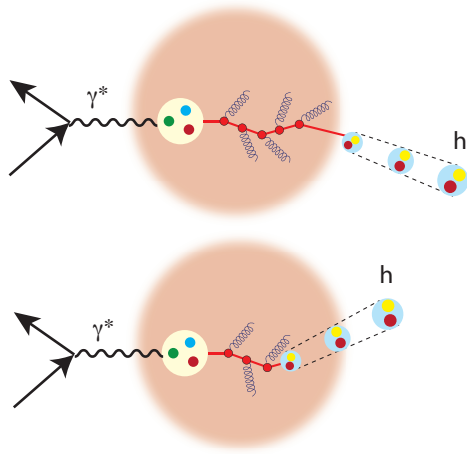


Figure 2.11: Illustration of a parton moving through cold nuclear matter when the produced hadron is formed outside (upper) and inside (lower) the nucleus, demonstrating how nuclei can be used as an analyzer of the hadronization process.

## 5 Understanding Hadronization

6  
 7 The nucleus is also a laboratory for understanding the dynamics of confinement, the pro-  
 8 cess by which a high-energy parton created by the interaction of a virtual photon with the  
 9 nucleus is color neutralized and evolves into a hadron. The processes involved in *hadroniza-*  
 10 *tion*, the transition of colored partons to colorless hadrons, still lack detailed understanding  
 11 from the first principles in QCD. A high-energy parton is known to radiate soft gluons and  
 12 quark-antiquark pairs; all involved partons will eventually form a stream of hadrons, collec-  
 13 tively termed "jet." Hadronization has been studied through jets, correlations, and identified  
 14 particle distributions at many collider facilities, including the only electron-proton collider  
 15 to date, HERA, and electron-positron, as well as proton-proton and heavy ion colliders.  
 16 The best experimental tool available to disentangle the various mechanisms and time scales  
 17 involved in the hadron formation is DIS with nuclei.

18 In studying the propagation of energetic quarks, the nucleus becomes a QCD laboratory,  
 19 providing femtometer-scale detectors and a medium with known properties, such as size  
 20 and density. Hadronization in the cold nuclear matter is only qualitatively understood to  
 21 date. Questions remaining about its space-time dynamics include its dependence on the  
 22 quark mass and flavor and the mechanisms by which quarks and gluons lose their energy  
 23 and become hadrons. Such questions are not surprising as one cannot fully understand  
 24 hadronization without understanding confinement. Electron-nucleus collisions in which a  
 25 meson is detected are an excellent tool for furthering our understanding of hadronization.

With electrons as the probe, one can select the energy of the virtual photon, thus controlling the momentum transfer to the quark, and obtain clean measurements of medium-induced energy loss by choosing high-photon energies, which lead to hadronization outside of the nucleus (see figure 2.11, left). Similar techniques can delineate the interplay between quark propagation and hadron formation mechanisms (see figure 2.11, right).

Studying hadronization for light and heavy quarks in the cold nuclear matter can unravel some of the mysteries surrounding energy loss in a quark-gluon plasma. For example, experiments at RHIC and the LHC showed that light and heavy quarks lose energy at a similar rate, even though if the QCD interactions were weak, heavy quarks would be less likely to lose energy via medium-induced radiation of gluons. At the EIC, the large  $Q^2$  range will permit measurements in the perturbative regime with enough leverage to determine nuclear modifications of the fragmentation functions – that describe the probabilities for a parton (or jet) to convert into a specific hadron. The high luminosity will permit the multidimensional binning necessary for separating the many competing mechanisms. The large  $\nu \approx 10 - 1000$  GeV range will allow one to isolate in-medium parton propagation effects (large  $\nu$ ), and to cleanly extract color neutralization and hadron formation times (small  $\nu$ ). Required are studies of particle production for identified hadron species (see figure 2.12). The existing phenomenological description of in-medium fragmentation describes the observed attenuation of light hadron production through modification of splitting functions in the presence of nuclear matter. Jet substructure studies at the EIC will provide direct experimental input for constraining the evolution of splitting functions in nuclear matter.

It is argued that mechanisms other than parton fragmentation should also be considered for understanding particle production in lepton-hadron collisions: threshold production, string-breaking, and coalescence or recombination. The latter arguably plays a critical role in particle production in higher-density environments of larger nuclei. Baryon over meson enhancement of hot QCD matter was first discovered in ultra-relativistic A+A collisions and successfully described by coalescence models of QGP was since observed in much smaller  $p+p$  systems. The baryon production enhancements of  $p+p$  collisions with respect to what is measured in  $e^+e^-$  events were found to be multiplicity dependent and persistent across all flavor sectors. The excellent hadron identification capabilities play an essential role in exploring and differentiating these phenomena, positioning the EIC detectors to make groundbreaking progress in our understanding of hadronization mechanisms. Systematic studies of baryon-to-meson ratios with different ion species may offer sensitivity to density dependence of coalescence/recombination contributions. In parallel, semi-inclusive measurements of identified hadrons with or in jets will provide differentiating capabilities on light, strange and heavy quarks.

At the EIC, one will also be able to study the hadronization of light mesons versus open charm and open bottom mesons and the in-medium propagation of heavy mesons. The second aspect of hadronization studies at an EIC is the possibility of using colored probes to study the gluon distribution in nuclei. In addition, for the first time, one will be able to measure jets and their substructure in  $e+A$  collisions. Lastly, the production of quarkonia in  $e+p$  and  $e+A$  collisions will also provide unique insight into the hadronization processes in more unknown regimes, such as those for exclusive backward u-channel production and the remnants of the ion beam (target region fragmentation).

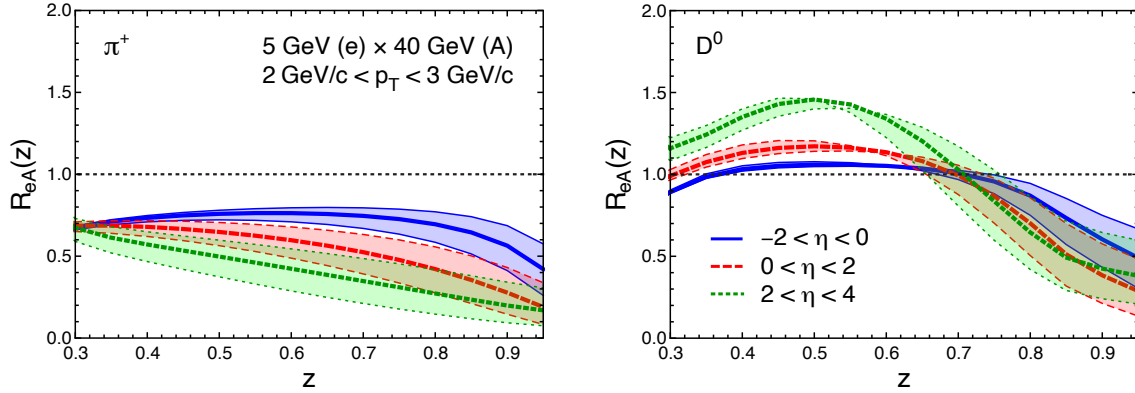


Figure 2.12: Ratio of relative particle production ( $N_h/N_{\text{incl}}$ ) in  $e+A$  over that in  $e+p$  as a function of  $z$ , the momentum fraction of the parton carried by the respective hadron. Light pions (left) show the largest nuclear suppression at the EIC. However, heavy flavor meson ratios (right) have to be measured to differentiate models of hadronization since they show a substantially different modification in  $e+A$ . From [84].

## 1 Nuclear Modifications of Parton Distributions

2 As described above, the EIC will enable dramatic improvements in description of parton  
 3 distribution functions of the proton and its complete three-dimensional imaging. In contrast  
 4 to proton PDFs, our understanding of the nuclear PDFs (nPDFs) is significantly more  
 5 limited, as most of the existing constraints come from fixed-target experiments in a region  
 6 of intermediate to high- $x$  values. The hadronic and nuclear collisions data from the LHC  
 7 have had so far little impact on extracting nuclear PDFs [85].

8 High energy electron-nucleus collisions at the EIC will enable measurements of nuclear  
 9 PDFs over a broad and continuous range in  $Q^2$ , all the way from  $Q^2 \sim 2 \text{ GeV}^2$  to the highest  
 10  $Q^2$  reachable ( $\sim 500 \text{ GeV}^2$ ). This will lead to the study of the nPDFs with unprecedented  
 11 precision and to the understanding of the collective phenomena that result in the PDF  
 12 differences between the bound and unbound nucleons. These differences are often quantified  
 13 via ratio to the proton PDF, with modifications ranging from suppression (below unity)  
 14 in the so-called "shadowing" domain of small- $x$ , different level of enhancements in the  
 15 "anti-shadowing" and "EMC" regimes, that for the large part are only phenomenologically  
 16 modeled.

17 Nuclear PDFs are determined through global fits driven by the reduced cross-section,  
 18  $\sigma_r$ , from existing inclusive DIS data off nuclei. Measurements of nuclear structure functions  
 19 elucidate to what extent a nucleus could be described by a collection of independent nucleons  
 20 - a fundamental question about nuclei properties in QCD.

21 An additional constraint on the gluon distribution at moderate to high- $x$  comes from  
 22 charm production via photon-gluon fusion. The fraction of charm production grows with the  
 23 energy, reaching about  $\sim 15\%$  of the total cross-section at the highest  $\sqrt{s}$ , thus permitting  
 24 one to set a robust and independent constraint on the gluon distribution in nuclei at high-  
 25  $x$  [6, 17]. This is illustrated in figure 2.13.

26 High-energy lepton scattering off light (polarized) nuclei ( $d$ ,  ${}^3\text{He}$ ,  ${}^4\text{He}$ ) at EIC will be

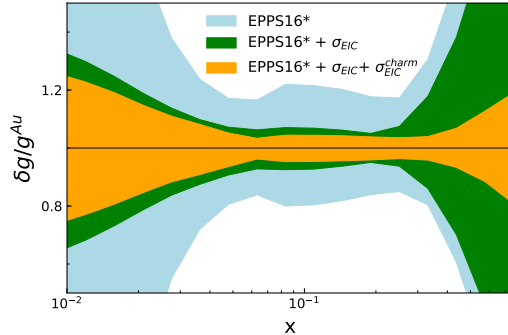


Figure 2.13: Relative uncertainty bands of the gluon for  $Au$  at  $Q^2 = 1.69 \text{ GeV}^2$ . The blue band is the original EPPS16\* fit, the green band incorporates inclusive  $\sigma$  cross section pseudodata and the orange one adds also the charm cross section  $\sigma_{EIC}^{charm}$ .

1 used not only for neutron studies, but also for detailed probing of nPDF-related effects,  
2 investigation of the EMC effect in position space, exploring the pressure distributions in  
3 light nuclei, and exploiting the very unique opportunities which the spin-1 deuteron target  
4 offers through its possible tensor polarization. The EIC will also provide novel insight  
5 into the physics of short range correlations (SRC) in nuclei and how they relate to the  
6 mechanism by which QCD generates the nuclear force, as well as possible connections to  
7 the nPDF EMC effect and the SRC of nucleon pairs with high internal nucleon momentum.  
8 Regardless of the EMC connection, the EIC will investigate the underlying physics of SRC in  
9 kinematic regions that so far could not be reached. Finally, the relation between diffraction  
10 and nuclear shadowing could be tested at the EIC. The relation is a rigorous theoretical  
11 result for the deuteron case, while its extension to larger nuclei is model dependent.

12 The nucleus is a QCD molecule, with a complex structure corresponding to bound states  
13 of nucleons. Understanding the formation of nuclei in terms of QCD degrees-of-freedom is  
14 an ultimate long-term goal of nuclear physics. In addition to the one-dimensional nPDFs  
15 studies, the EIC operations with different ion species will allow complete three-dimensional  
16 imaging of parton densities in the nuclei. With its broad kinematic reach, as shown in  
17 Fig. 1.2, the capability to probe a variety of nuclei in both inclusive and semi-inclusive  
18 DIS measurements, the EIC will be the first experimental facility capable of exploring the  
19 internal 3-dimensional sea quark and gluon structure of a nucleus at low  $x$ . As has been  
20 discussed earlier, it will allow precision measurement of differential parton distributions for  
21 protons as well as nuclei, providing insights about the longitudinal and transverse motion of  
22 partons in fast-moving nucleons. The EIC data are expected to make a profound impact on  
23 the nuclear TMDs and GPDs, with the 3D imaging for nuclei in the transverse momentum  
24 and impact parameter space, respectively.

25 The EIC is a unique facility for nuclear TMD studies, as it will deliver polarization of  
26 both the electron and (light) nuclei beams. It will bring new advances in understanding of  
27 the motion and contribution of gluons and sea quarks, that are not accessible elsewhere.  
28 In particular, the gluon TMDs in general and the gluon Sivers function, in particular,  
29 are largely unexplored by the existing facilities, but at the EIC multiple processes with

sensitivity to the transverse momentum dependent gluon distributions will be pursued. A traditional way of accessing TMDs is, of course, semi-inclusive DIS where at least one hadron is detected, in addition to the scattered lepton. However, The TMDs on nucleons and nuclei alike, can also be studied via different final states with di-hadrons or jets, or the Drell-Yan process. Another example is an electroproduction of open-charm meson pairs. Additionally, jet production measurements are expected to become a useful tool for studies of nuclear structure [86] and gluon helicity in polarized protons [17] and nuclei; jet measurements constrain polarized and unpolarized parton distribution functions providing additional handle for probing gluon TMDs.

Having the  $e+A$  and  $e+p$  data simultaneously at the same facility will allow to minimize the systematic uncertainties by constraining the medium modifications of spin dependent and independent azimuthal asymmetries in SIDIS, which provide access to medium modified parton distributions, and to relative magnitude of the transverse momentum width of the nucleon TMDs. The orbital motion of quarks is known to be modified in the medium [YR642], i.e. the ratio of the TMDs for bound and unbound nucleons is not equal to 1 and is not constant with  $x$  and  $Q^2$ . That makes a variety of physics observables sensitive to orbital motion, in particular various spin and azimuthal asymmetries, good candidates to provide important information on partonic distributions in bound nucleons. One of the main theoretical tools to study hadronic matter are factorization theorems that introduce universal distributions of partons such as the TMDs discussed above.

Another prominent example are Generalized parton distributions (GPDs) that can be probed in hard exclusive processes. Complimentary to proton GPDs discussed earlier, nuclear GPDs (nGPDs) involve proton and neutron GPDs. In fact DVCS on light nuclei is the only way to measure neutron GPDs, a measurement that the EIC can perform with ease. As is the case with nPDFs, nGPD will be modified by nuclear effects which will prove wide valuable information on our 3D image of partons in the nucleus. Studies of nGPDs might even access novel nuclear effects not present in DIS on nuclear targets (effects associated with the real part of the DVCS amplitude) and will put stringent constraints on theoretical models of the nuclear structure. DVCS is more sensitive to details of small- $x$  physics (shadowing, anti-shadowing, black disk limit) than inclusive DIS on nuclear targets.

## 2.5 Opportunities for Electro-Weak and Beyond the Standard Model Physics

The EIC is designed for precision measurements in the QCD sector, but the high luminosity, polarized lepton and hadron beams and wide kinematic coverage provided by the EPIC detector afford unique opportunities for a variety of sub-fields in nuclear and particle physics. The most extensive point of contact is with electroweak (EW) and beyond-the-standard model (BSM) physics. This section will briefly discuss five focus areas where an EIC could make significant contributions. A more comprehensive review of possible EW and BSM studies at the EIC may be found in the EIC Yellow Report [8] and the Snowmass White Paper: Electron Ion Collider for High Energy Physics [87].

Precision measurements of parity violating electron asymmetries over a wide range of  $Q^2$  will constrain the quark and electron neutral current couplings, which in turn depend on the

1 Weinberg's weak mixing angle ( $\theta_W$ ). Deviations between precision theory calculations and  
2 measurements of the  $Q^2$  dependence of  $\sin^2 \theta_W$  would point to new physics. For example,  
3 the dark-Z ( $Z_d$ ), a light dark boson originating from a spontaneously broken U(1) gauge  
4 symmetry in the dark sector, gives rise to an additional source of parity violation through  
5 its coupling to the weak neutral current by mixing with the Z-boson. In parity-violating  
6 DIS, its effects can be absorbed into a shift in the measured weak mixing angle,

$$\Delta \sin^2 \theta_W(Q^2) \simeq -0.42 \varepsilon \delta \frac{M_Z}{m_{Z_d}} \frac{m_{Z_d}^2}{Q^2 + m_{Z_d}^2}. \quad (2.3)$$

7 For  $m_{Z_d} \ll M_Z$ , this shift is negligible near the Z-pole  $Q^2 \sim M_Z^2$ . However, at low  $Q^2$ ,  
8 below the Z-pole, the shift can be significant. In the region explored by the EIC,  $10 \text{ GeV} < Q < 70 \text{ GeV}$ ,  
9 the mass range  $m_{Z_d} \sim 10 - 30 \text{ GeV}$  could result in deviations in the running  
10 of the weak mixing angle, large enough to be within reach of the projected EIC sensitivities.

11 The lepton flavor violation observed in neutrino oscillations implies a similar violation  
12 in the charged lepton flavor (CLF) sector. While CLF violations due to standard model  
13 processes are too suppressed to be observed by current or planned experiments, many BSM  
14 scenarios predict much higher rates, those that could be detected by a future EIC. The  
15 electron-to-tau conversion ( $e + p \rightarrow \tau + X$ ), mediated by leptoquarks, is one of the most  
16 promising CLFV channels at an EIC. The limits placed by an EIC on searches for massive  
17 leptoquarks will surpass the HERA collider and the kinematic reach of the EIC will be  
18 sensitive to the differences between scalar and vector leptoquarks. Another opportunity in  
19 the  $e - \tau$  channel is the measurement of CLFV mediated by Axion-Like Particles (ALPs),  
20 for example via  $e + A \rightarrow \tau + A + a$  where  $A$  is a high Z ion and  $a$  is an ALP. Electron  
21 scattering from high Z beams, such as heavy ions, could lead to enhanced production of  
22 GeV scale ALPs. Furthermore, the polarized beams provide a unique sensitivity to parity  
23 violating ALPs.

24 The dark photon ( $A'$ ) is a hidden sector boson that has been proposed as a force mediator  
25 that interacts directly with dark matter but also couples weakly with the standard model  
26 (SM) photon. In principle this coupling allows dark photons to be produced in any final  
27 state where a SM photon is produced, for example radiative production in diffractive events  
28 where the dark photon decays to a lepton pair ( $ep \rightarrow epA' \rightarrow epl^+l^-$ ). In these types of  
29 searches, the invariant mass of the dilepton pairs would show a narrow reconstructed  $A'$   
30 peak sitting on top of a smooth background of SM processes. Current limits for  $M_{A'} < 1$   
31 GeV are set primarily by BaBar, LHCb, and CMS [88, 89]. The center-of-mass energy of  
32 the EIC reaches above the  $Z^0$  threshold, competitive with the CMS dimuon result [90], the  
33 highest mass range currently probed by a collider experiment. In particular, the presence  
34 of an initial-state lepton with large center-of-mass energy may also make it possible to  
35 substantially expand probing of the parameter space in models with new force mediators  
36 with leptonic couplings.

37 Lorentz and CPT symmetry are among the best established symmetries in physics.  
38 However, many BSM theories admit regimes where one or both of these symmetries can be  
39 spontaneously broken. Low-energy tests of Lorentz and CPT symmetry can be performed  
40 using the effective field theory known as the Standard-Model Extension (SME) [91–93].  
41 To date, SME operators describing Lorentz- and CPT-violating effects on QCD degrees  
42 of freedom are largely unconstrained. Recent studies suggest that differential cross section

1 measurements at the EIC will allow for precision tests of Lorentz and CPT symmetry in the  
2 quark sector [94–96]. Data for unpolarized inclusive DIS at  $100 \text{ fb}^{-1}$  integrated luminosity  
3 can increase bounds on quark-sector coefficients by two orders of magnitude compared to  
4 HERA data. Symmetry violations would be visible as variations of the cross section as a  
5 function of sidereal time. Additional processes that can be measured at the EIC, including  
6 those with polarization effects, charged-current exchange, and QCD corrections, can place  
7 first constraints on a number of completely unexplored effects stemming from Lorentz and  
8 CPT violation.

9 Finally, there will be significant synergy between the EIC and HL-LHC programs of new-  
10 physics searches, especially if periods of operation of the two colliders overlap. The EIC has  
11 the potential to significantly constrain the PDFs and their flavor composition in the region  
12 of large partonic momentum fractions,  $x > 0.01$ , where the main constraints on the nucleon  
13 structure are currently provided by the fixed-target experiments. The measurements of the  
14 PDFs at the EIC will not be affected by possible new physics contributions that may be  
15 present in the relevant kinematic region at the LHC.



<sup>1</sup> **Chapter 3**

<sup>2</sup> **Synergy and Uniqueness of EIC**

<sup>3</sup> **3.1 Synergy with low energy nuclear physics and nuclear  
4 structure**

<sup>5</sup> Even though the EIC is a high-energy collider with typical energy scales in the tens-to-  
<sup>6</sup> hundreds of GeV range, there are key measurements that are of relevance to nuclear physics  
<sup>7</sup> at much lower energies. Conversely, guidance from low-energy nuclear structure physics is  
<sup>8</sup> important for realizing key aspects of the broad EIC science program.

<sup>9</sup> **Hadron elastic form factors:** Even though the EIC is a high-energy collider, it can  
<sup>10</sup> provide elastic form factor data at small  $1/Q^2$  resolution scales that constrain the charge and  
<sup>11</sup> magnetism distributions. An EIC would provide valuable data on the proton and neutron  
<sup>12</sup> form factors as well as the light mesons, pions and kaons, that are responsible for the long-  
<sup>13</sup> range part of the nuclear force. This includes through the GPD formalism of exclusive  
<sup>14</sup> reactions the possibility to determine gravitational form factors of the energy-momentum  
<sup>15</sup> tensor.

<sup>16</sup> **Input from nuclear structure data** Accurate nuclear structure input is needed both  
<sup>17</sup> in coherent exclusive reactions with light ions — enabling the study of nuclear tomography  
<sup>18</sup> in partonic degrees of freedom — and in light-ion reactions with spectator tagging. The  
<sup>19</sup> goal of the tagging is to provide additional control over the initial nuclear configuration. A  
<sup>20</sup> further challenge is to identify and isolate final-state interactions in such reactions (FSIs).  
<sup>21</sup> The dominant FSI will be between the slow-moving (relative to the nucleus center-of-mass)  
<sup>22</sup> breakup products. Re-interactions of slow hadrons with other spectator fragments also  
<sup>23</sup> contribute in the target fragmentation region of nuclear Deep-Inelastic Scattering with  
<sup>24</sup> tagging. All these FSIs have in common their low relative momenta, and as such the  
<sup>25</sup> dynamics are similar to those in low- and medium-energy nuclear breakup reactions.

<sup>26</sup> Neutron structure information can be determined by tagging a spectator proton from  
<sup>27</sup> electron-deuteron collisions. In inclusive Deep-Inelastic Scattering, the dominant neutron  
<sup>28</sup> structure uncertainty in the high- $x$  region arises from nuclear structure corrections. How-  
<sup>29</sup> ever, in the weakly-bound deuteron these effects are small, and the deuteron is thus the  
<sup>30</sup> obvious candidate to extract neutron information. Making use of baseline nuclear struc-  
<sup>31</sup> ture calculations can further pin down the link between medium modifications and nuclear  
<sup>32</sup> interactions or inferring the size of non-nucleonic components in nuclei (like  $\Delta$  isobars).

1   **Using light nuclei to study exotic effects** Light nuclei play an important role in  
2 general; their conventional structure is well known so that exotic effects can be exposed.  
3 This allows the use of light nuclei to probe the interplay between high-energy QCD dynamics  
4 and low-energy nuclear interactions. As one example, a novel way to explore gluon degrees of  
5 freedom in the nucleon-nucleon potential is to look at exclusive heavy quarkonium (“onium”)  
6 production in coincidence with knock-out reactions of protons and neutrons. The simplest  
7 example to consider is exclusive scattering off the deuteron with diffractive breakup. There  
8 can either be a color-singlet two-gluon exchange between the onium and a “leading” proton  
9 (or neutron) with the other neutron (or proton) a spectator counterpart. In this case, at  
10 large relative momentum transfer between the two final-state nucleons, the scattering is  
11 sensitive to color-singlet short-range correlations in the deuteron wave function. Or the  
12 color-singlet exchange between the onium and the deuteron occurs by one gluon exchanged  
13 to the proton and the other to the neutron. The interaction is then necessarily sensitive to  
14 color-octet, or gluon-dominated, short-range correlations in the deuteron wave function to  
15 preserve color. Polarized deuteron beams are envisioned as an upgrade to the EIC, allowing  
16 access to observables such as the deuteron tensor  $b_1$  structure function. The deuteron  $b_1$   
17 encodes the difference between the unpolarized quark distributions between a deuteron in  
18 the polarization state  $M = \pm 1$  (“dumbbell”) and  $M = 0$  (“donut”) and are thus inherently  
19 sensitive to nuclear interactions. Can the quarks “see” the deuteron long-range structure,  
20 or that of other light ions?

21   **Diffractive and exclusive processes on heavy nuclei:** The collider environment  
22 enables the potential for measurements of nuclear fragments following  $eA$  scattering with  
23 its far-forward detectors, and the high luminosity, which can provide novel insights into  
24 low-energy nuclear reactions and correlations. At the EIC, where the relativistic  $\gamma$  is 100,  
25 energies of nuclear fragments, of nuclear de-excitation products such as low-energy photons  
26 and neutrons, and nuclear lifetimes get boosted with this factor.

27   The most relevant measurements are diffractive observables corresponding to a low-  
28 momentum transfer color-singlet exchange (of momenta larger than the nuclear Fermi mo-  
29 mentum) and a large rapidity gap separating nuclear fragments from the current fragments  
30 for a wide range of invariant masses  $M_X$ . At high energies, there is a very clean separation  
31 of time scales between the hard QCD physics of the current fragmentation region and the  
32 soft physics of nuclear fragments. Nuclear structure can play a decisive role in the separa-  
33 tion of the coherent and incoherent parts of the cross section for diffractive and exclusive  
34 processes on heavy nuclei. This is critical for studies of gluonic fluctuations and the effects  
35 of heavy, dense nuclei, and studies of nuclear femtography for light ions. This could provide  
36 a detailed map of the gluonic radius of a variety of nuclei, at par with for example the  
37 charge radius or neutron skin measurements. Similar, correlations among nucleons in the  
38 target fragmentation region have the potential to provide novel insight into the underlying  
39 quark-gluon correlations that generate short-range nuclear forces.

40   Studies of diffractive scattering and nuclear femtography further benefit from an excel-  
41 lent forward acceptance for isotopes that undergo small changes in rigidity compared with  
42 the ion beam (which is equivalent to small changes in  $p_T$  for light ions). This is at the  
43 root of the concept to introduce a secondary focus of the proton/heavy ion beam optics  
44 far downstream. Experimentally, identification of produced ions would use the far-forward  
45 detectors located 30-50 meters downstream of the collision point. This enables fully exclu-

sive measurement of nuclear fragments from heavy nuclei up to  $A = 90$ , and measurements to the heaviest  $A \sim 250$  nuclei, including a possible access to exotic nuclei at the EIC. The former allows more detailed maps at the quark-gluon sublevel of light ions. The latter benefits from the large relativistic  $\gamma$ -factor at the EIC, boosting nuclear lifetimes to allow study of even short-lived isotopes far from stability. EIC production rates seem sufficiently high to provide opportunities for complementary measurements to those at FRIB.

### 3.2 Synergy of eA, pA and AA

Deeply inelastic scattering and photo-nuclear processes have natural ties with the physics of hadronic collisions. These relate to the issue of small- $x$  gluons and factorization in  $e+p$  and  $e+A$  versus  $p+p$  and  $p+A$ , and to the implications of the determination of parton distributions for  $p+A$  collision for an improved understanding of the initial conditions in heavy-ion collisions. In return, ultra-peripheral nucleus-nucleus and proton-nucleus collisions at RHIC and LHC allow one to study high-energy photoproduction processes at high center-of-mass energies using the heavy nucleus as a source of Weizäcker-Williams photons. The physics explored in these electromagnetic processes has many connections with the scientific program of a future Electron-Ion Collider on topics such as nuclear shadowing, gluon saturation and non-linear QCD, as well as nuclear imaging.

**Implications of PDF determinations for proton-nucleus collisions:** Many studies have shown [8, 97, 98] that measurements at EIC are bound to significantly improve our knowledge of the nuclear PDFs. In particular, it should be possible to tightly constrain the gluon distribution at  $x \gtrsim 10^{-2}$  at scales comparable to the charm-quark mass,  $Q \sim m_{\text{charm}}$ . Due to DGLAP dynamics, this translates to well-constrained gluons even at  $x \ll 10^{-2}$  at higher  $Q^2$ . Such an improved description will lead to more precise predictions for  $p+A$  collisions at the LHC and thereby allow for stringent tests of factorization. Since the EIC will constrain nuclear PDFs at much lower  $x$  than the existing DIS data, the improved PDFs will increase the chances for discovering the onset of non-linear evolution at the LHC using, for example, low- $x$  forward  $D$ -meson measurements by the LHCb collaboration [99]. Similar conclusions hold in the case of other observables such as the direct photon production in the forward direction to be, possibly, measured by the ALICE collaboration [100]. Therefore, extraction of nuclear PDFs in a clean DIS environment at the EIC will allow for precision searches of new phenomena in a broad range of observables in  $p+A$  collisions at LHC.

**Initial conditions for hydrodynamics in A+A collisions:** Heavy ion collision experiments at RHIC and LHC study a deconfined state of quark and gluons, the Quark-Gluon Plasma (QGP). The evolution of two colliding cold nuclei into a QGP is complex and consists of several stages. The initial particle production is followed by a phase of thermalization and equilibration leading to the creation of the plasma which then expands and cools. The plasma phase is usually modeled by relativistic hydrodynamics, before undergoing a phase transition to ordinary hadronic matter which then decouples into the hadronic final states that are observed by the detectors. This model of heavy-ion collisions is able to predict observations starting from a given initial condition at the time of equilibration, and from a given set of transport coefficients describing the evolving matter. Inverting this process to infer both the matter properties and the initial conditions is a daunting task.

This is where the physics program of the EIC is relevant in several ways. Firstly, exclusive and diffractive measurements of protons and nuclei at the EIC, will provide accurate information on the spatial distributions of quarks and gluons in protons and nuclei and their fluctuations [101]. This spatial structure is one of the most important inputs into hydrodynamical calculations of the QGP, because collective interactions in the QGP can transform initial spatial structures into momentum space correlations among the produced particles.

Multi-particle correlations that are present in the wave functions of the colliding systems [102–105] can have effects that are very similar to ones resulting from hydrodynamical flow [106, 107]. This is especially true in what are referred to in the heavy ion context as “small systems”, i.e., proton-proton and proton-nucleus collisions, where it can be difficult to disentangle the effects of hydrodynamical correlations (e.g. “flow”) from such multigluon “initial state” correlations. The “initial state” correlations can be studied very precisely at the EIC, and analyzed in terms of concepts like color dipoles and quadrupoles, improving our knowledge of the linear gluon polarization at small  $x$  [108, 109] and of the quark and gluon Wigner functions. A precise understanding of the CGC wave function from the EIC, which is related to the above-mentioned objects, will also help constrain our understanding of the pre-equilibrium thermalization stage of the heavy ion collision.

**Parton interactions in matter:** The importance of understanding parton and particle propagation and parton energy loss in DIS was discussed earlier in Sec. 2.4.2. Advances in this direction will facilitate the interpretation of the data from  $p+A$  and  $A+A$  reactions. In  $p+A$  collisions, final-state effects associated with the QGP are expected to be absent/suppressed. However, experimental results on the impact parameter dependence of high energy jet cross sections in  $p+Pb$  collisions at LHC and in  $d+Au$  collisions at RHIC show highly nontrivial and large nuclear effects from different centrality selections. These are observed at all transverse momenta  $p_T$  at forward rapidities (in the direction of the proton beam) and for large  $p_T$  at mid-rapidity: they manifest themselves as suppression of the jet yield in central events and enhancement in peripheral collisions [110]. Theoretical work on hadron, jet, Drell-Yan, and  $J/\psi$  production in  $p+A$  reactions has emphasized the importance of measuring and understanding energy loss in cold nuclear matter [111–114]. Calculations that incorporate this physics are qualitatively consistent with the central to peripheral cross section ratio,  $R_{CP}$  [115]. Away from kinematic bounds, cold nuclear matter energy-loss effects are small but can still contribute to the observed quenching in AA [116]. The impact on cross sections and particle correlation is amplified at smaller center-of-mass energies [117, 118]. Theoretical predictions for the energy loss in cold nuclear matter describing the data in  $p+A$  and  $A+A$  collisions will be experimentally tested and further constrained at the EIC.

### 3.3 Synergy with High-Energy LHC Program and Other Science Programs Worldwide

A new generation of high-energy physics experiments will deepen our knowledge of the subatomic matter and evolution of the Universe. Particle interactions through the fundamental strong force are of crucial importance in their own right and play the key role across many

1 studies, from electroweak precision tests and Beyond-Standard-Model (BSM) searches at  
 2 the Large Hadron Collider (LHC) to high-intensity experiments and neutrino and cosmic  
 3 ray physics. There is significant potential for cross-fertilization between studies of hadronic  
 4 matter in particle and nuclear physics experiments. Just as the EIC will provide essential  
 5 new inputs about the structure of nucleons and nuclei for particle physics experiments,  
 6 decades of experience in QCD studies at high energy colliders will benefit various aspects  
 7 of the EIC program.

8 **Hadron tomography:** The EIC is expected to have a significant impact on the reach  
 9 in precision of hadron scattering experiments at future hadron colliders. The program of  
 10 the High-Luminosity LHC (HL-LHC) is premised on achieving the next-generation sensitiv-  
 11 ity to a wide variety of SM and BSM processes. The success of this program in testing  
 12 the SM and performing impact measurements at the TeV scale is critically dependent upon  
 13 advancements in knowledge of the internal structure of hadrons within QCD. The EIC will  
 14 undertake a dedicated tomography program to measure the 2+1-dimensional (dependent on  
 15 two transverse and one longitudinal direction) structure of the nucleons and a broad range of  
 16 nuclei [119]. This program envisions measurement of observables sensitive to various parton  
 17 distributions in the proton and other QCD bound states, including TMDs and GPDs, in ad-  
 18 dition to (un)polarized collinear (longitudinal) PDFs. By facilitating controlled extractions  
 19 of these various parton distributions and testing relations among them predicted by QCD,  
 20 the EIC will provide unique data that will clarify detailed mechanisms of formation of QCD  
 21 bound states. The EIC measurements will be confronted with advanced predictions from  
 22 multi-loop QCD and lattice QCD. While currently fixed-target DIS experiments provide  
 23 leading constraints on the spin-independent nucleon PDFs at large  $x$  [120, 121] relevant for  
 24 new-physics searches at the HL-LHC, the EIC will significantly advance in constraining  
 25 these PDFs and separating parton flavors in the same kinematic region.

26 Precise determinations of PDFs and TMDs at the EIC will elevate accuracy of the  
 27 HL-LHC measurements of electroweak parameters: weak mixing angle and weak boson  
 28 mass. For example, precision measurements of the weak boson mass at the LHC rely  
 29 on the theoretical formalism of TMD factorization to model the transverse recoil of weak  
 30 bosons against QCD radiation. The EIC will constrain TMD PDFs associated with the  
 31 nonperturbative radiation from up- and down-type quarks. The knowledge of the flavor  
 32 dependence of TMD PDFs will reduce an important theoretical uncertainty in the LHC  
 33  $W$  boson mass measurement [122–124]. These measurements will stimulate theoretical  
 34 developments to accurately compute QCD and electroweak radiative contributions, as well  
 35 as their interplay, in a consistent framework applying to both the EIC and LHC.

36 **Semi-inclusive DIS, hadron fragmentation, and jet formation:** The large range  
 37 of beam energies available at the EIC, combined with the fine resolution and particle identifi-  
 38 cation of the EIC detector, opens a unique venue for exploring formation of hadronic jets,  
 39 especially the interplay of perturbative QCD radiation and nonperturbative hadronization.  
 40 The process of semi-inclusive production of hadronic states in DIS will measure in detail  
 41 the flavor composition of the initial hadronic states as a function of the parton’s momentum  
 42 fraction  $x$  and fragmentation of partons into various hadrons as a function of the momentum  
 43 fraction  $z$ . At the EIC, it will be possible to study the multiplicity and angular distributions  
 44 of final hadronic states as a function of the variable center-of-mass energy of lepton-hadron  
 45 scattering events [125]. These observations will offer unique insights about the formation of

1 final-state jets, jet substructure and jet angularity, and they will test universality of under-  
2 lying perturbative and nonperturbative QCD mechanisms. In turn, production of hadronic  
3 jets accompanied by the relevant theoretical advancements will offer novel channels to probe  
4 the flavor and spin composition of the EIC initial states ranging from nucleons to heavy  
5 nuclei. EIC studies of jet formation and jet properties go hand-in-hand with the LHC jet  
6 physics program, by focusing on aspects of nonperturbative hadronization that are difficult  
7 to access in the complex LHC environment. These observations will guide the development  
8 of advanced parton shower algorithms for event generators used by LHC experiments.

9 **Heavy-flavor production:** At the EIC, heavy-flavor production will play an important  
10 role and will elucidate QCD factorization formalisms ("factorization schemes") for processes  
11 with massive quarks, as well as the nonperturbative aspects of heavy-quark scattering dy-  
12 namics [126]. Advanced capabilities for detection of jets containing charmed particles will  
13 open avenues for unique measurements, like the determination of the strangeness content  
14 of the (polarized) nucleons and nuclei at momentum fractions  $x > 0.1$  [127]. Hypothetical  
15 dynamical mechanisms for massive quark scattering such as "intrinsic charm" [128] will be  
16 constrained. As an example of unique synergistic capabilities, the construction of a multi-  
17 purpose Forward Physics Facility (FPF) is proposed in the next 5-10 years in a cavern in  
18 a far-forward region of ATLAS to carry out diverse searches for long-lived particles such as  
19 neutrinos and dark bosons [129]. Production of forward neutrinos in the ATLAS collision  
20 point and their detection in the FPF will proceed through interactions of weak bosons with  
21 charm quarks in a proton or a heavy nucleus, in a similar kinematic region as the one ac-  
22 cessed at the EIC. Studies of charm-quark production at large momentum fractions at the  
23 EIC thus can provide essential theoretical inputs for the LHC FPF program, by measuring  
24 the "intrinsic charm" and other production mechanisms.

25 **Electroweak precision and BSM physics:** The combination of high luminosity, the  
26 range of accessible energies, and beam polarization at the EIC opens unique opportunities  
27 for precision tests of the SM and searches for new BSM physics [130]. Section 2.5 discusses  
28 several measurements and BSM channels that are accessible at the EIC, ranging from the  
29  $Q^2$  dependence of  $\sin \theta_W$  to tests of charged lepton flavor violation and searches for heavy  
30 photons and axions. In addition to these topics, searches for indirect signatures of new  
31 physics in the framework of the Standard Model Effective Field Theory (SMEFT) will  
32 be complementary to those at the LHC. The EIC, with its polarizable beams, will likely  
33 constrain dimension-6 SMEFT operators from new physics that cannot be easily accessed  
34 at the LHC. "Combined fits of LHC and projected EIC data can lead to much stronger  
35 constraints than either experiment alone." [130]

36 **Saturation and diffractive effects:** The intermediate energy of the EIC will allow one  
37 to examine power-suppressed hadronic contributions and their dependence on the nuclear  
38 target. A large part of the EIC program will be dedicated to the structure of nuclei probed  
39 in high-energy collisions, including shadowing or saturation effects predicted by QCD for  
40 the scattering of high-density partonic systems.

41 **Neutrino Physics:** The accurate characterization of the structure of nucleons and  
42 nuclei provided by the EIC program can directly benefit neutrino physics. Massive nuclear  
43 targets are typically required in neutrino experiments to collect sizable statistics, but they  
44 also introduce uncertainties related to nuclear effects [131]. Since the energy of the incoming  
45 neutrino is unknown on an event-by-event basis, it must be inferred from the detected

final-state particles, which are affected by a substantial nuclear smearing. The latter is present even for an ideal detector since the initial momentum of the bound nucleon is not known and hadrons produced in the primary interactions can be absorbed or re-interact within the nucleus. Target nuclei commonly used in neutrino experiments include C, O, Ar, Fe, Pb. Understanding the impact of nuclear effects on the measured cross sections and event distributions is particularly critical for the next-generation long-baseline neutrino oscillation experiments like DUNE [132] and Hyper-Kamiokande [133], which are looking for CP violation via tiny differences between neutrino and antineutrino interactions off Ar and H<sub>2</sub>O targets, respectively. The kinematic coverage of the EIC has overlap with the region accessible at the Long-Baseline Neutrino Facility (LBNF), which is dominated by inelastic interactions. In addition to the default energy spectrum optimized for the neutrino oscillation measurements in DUNE — in which more than 54% of the events have  $W > 1.4 \text{ GeV}$  — a high-energy beam option is available with energies in the 10 – 20 GeV range.

**Cosmic Rays :** Cosmic-ray air showers occur when a high-energy proton or heavier nucleus strikes the atmosphere, producing a shower of millions to trillions of particles. Cosmic rays with energies above about  $10^{15} \text{ eV}$  are rare enough so that they can only be studied with ground-based detectors. These detectors sample the shower particles that reach the ground, measuring their density and lateral spread. Cosmic-ray physicists use these indirect data to determine the energy spectrum and nuclear composition of cosmic-rays. The energy can be determined largely from the overall particle density. The composition is often inferred from the muonic content of the shower. The muons are mostly from the decays of charged pions and kaons and neutral kaons, while photons and electrons come from photons from  $\pi^0$  decays. Strangeness production models thus play a large role in inferring the composition from muon data. A hadronic interaction model is required to quantify these relationships, and to infer event energies and composition. Cosmic-ray physicists use a number of different models, for this, with SIBYLL, QGSJet and EPOS being the most common. These models use pQCD to model hard interactions, with a Pomeron inspired phenomenology to simulate the soft interactions that account for most of the produced particles. They are tied, to varying degrees, to RHIC and LHC data, but still vary significantly in their predictions [134].

Since cosmic-rays essentially follow a fixed-target geometry, measurements in the far forward region are critical to track energy flow downward through the atmosphere. Although the TOTEM [135] and LHCf & RHICf [136] experiments have made some cross-section and forward multiplicity measurements, this phase space has not been well studied at colliders. The EIC will have excellent forward and far-forward instrumentation, allowing for accurate studies in the target fragmentation region. In particular, a knowledge of the inelasticity of struck protons in hadronic collisions is a vital input to hadronic models. Electron-proton collisions are not the same as  $pp$ , but they will help constrain the models.

These models are receiving attention because the energy spectra measured by the two very large (area more than 1,000 km<sup>2</sup>) experiments, Auger [137] and Telescope Array (TA) [138] are in tension. A joint working group could not resolve this disagreement [139]. The difference may be due to physically different cosmic-ray spectra in the Northern and Southern hemispheres [140]. This would be a very important discovery, pointing to the existence of a few local cosmic-ray sources. However, before reaching that conclusion, we

need to exclude other possibilities. The two experiments use somewhat different detection techniques - water Cherenkov detectors for Auger, scintillator for TA, so inaccuracies in hadronic models could lead to differences in energy calibration. EIC data could significantly help to reduce these uncertainties, by providing high-accuracy measurements of hadronic particle production to tune the models, especially in the forward region, and, for high  $p_T$  muon analyses, by pinning down parton distributions at low  $x$ . If it is observed, saturation could also explain some of the inflection points seen in the composition distributions. Data from oxygen and/or nitrogen targets is of particular value, to match the air-shower targets.

### 3.4 Synergy with Lattice QCD and QCD Phenomenology

The synergy with **lattice QCD** (LQCD) will be absolutely critical for EIC. Lattice calculations have become mature by now, thanks to improvements in algorithms, increased computer power and conceptual breakthroughs. An example of the latter are the new space-like parton correlators [24, 25] employing which, for the first time, the  $x$ -dependence of PDFs and related quantities can be computed directly in lattice QCD. Lattice calculations can be used to interpret data from the EIC. Moreover, combining information from lattice QCD with EIC data will considerably increase our knowledge about the structure of strongly interacting systems.

Modern LQCD can provide us with the information on the partonic structure of hadrons through the PDFs and their generalizations (GPDs and TMDs). These parton distributions are defined through operators on the light-cone, which is inaccessible in LQCD as it is formulated in Euclidean space. Limited information on those quantities may be accessed through their Mellin moments, which have been extensively studied in LQCD for the PDFs and GPDs. However, a systematic calculation of moments beyond the third nontrivial moment is obstructed due to the decaying statistical signal and power-law mixing between operators. A new field has emerged in recent years, the so-called quasi-PDFs approach [24], which connects lattice-calculable matrix elements to light-cone PDFs via a perturbative matching procedure in the so-called Large Momentum Effective Theory (LaMET) [141, 142]. Other ways to extract the  $x$ -dependence of distribution functions have been proposed earlier that are based on the hadronic tensor [143–145], as well as auxiliary quark field approaches [146, 147]. Following the work on the quasi-PDFs, a number of other methods have been developed, such as the current-current correlator approach [148–150], the pseudo-PDFs [151], and a method based on the operator product expansion [152]. These approaches are now widely applied in LQCD, for the study of proton PDFs, GPDs and more recently TMDs. They have also been extended to other particles, such as the pion and kaon, mostly for the distribution amplitudes. Improvements in these calculations will complement the experimental efforts at the EIC.

The range of beam energies and kinematic coverage of the EIC is ideally suited for extracting PDFs and the corresponding Mellin moments, and comparing them with LQCD [121]. Moreover, lattice data are now beginning to be incorporated into global analyses on similar footing as the experimental data sets. This is not new, lattice data with heavy quarks already provided the tightest low-energy constraint to the running of the strong coupling constant in the early 2000s [153]; albeit with too optimistic lattice uncertainty estimates at the time. More recently, inclusion of lattice data led to improved estimates of

1 PDFs, particularly in regions where the experimental data are either sparse, imprecise, or  
 2 non-existing. Synergy between phenomenology and LQCD already led to better estimates  
 3 of the transversity PDFs by using lattice results for the tensor charge [154]. Lattice data  
 4 on the helicity PDFs were also included within the JAM global analysis framework [155].  
 5 Along similar lines, further possibilities for synergy between LQCD and global QCD fits  
 6 exists for a variety of other quantities, such as the ( $x$ -dependent) transversity PDF, twist-3  
 7 PDFs, GPDs and TMDs. Exploratory studies within LQCD exist for the aforementioned  
 8 quantities [156–161].

9 The EIC will provide a unique tool with which to probe the modification of the partonic  
 10 structure of the nucleon in nuclei. Along with precise studies of nuclear modification of  
 11 the unpolarized PDFs through the  $F_2$  structure function at moderate  $x$ , the famous EMC  
 12 effect [162–165], it will also provide access to its polarized analog [166–169]. LQCD calcu-  
 13 lations of moments of parton distributions in light nuclei are just beginning [170] and in  
 14 the coming years will improve significantly. It is expected that LQCD predictions for the  
 15 spin and flavor dependence of EMC-like effects will be available before EIC begins taking  
 16 data. Additionally, the EIC will enable studies of double-helicity-flip structure functions of  
 17 nuclei with spin  $J > 1/2$ ; these distributions isolate contributions of exotic nuclear gluons  
 18 that cannot be localized to the individual constituent nucleons. First attempts to access  
 19 moments of this distribution for the deuteron have been made [171] and will be improved  
 20 upon in the coming years.

21 LQCD can also play an important role in tests of electroweak and beyond-Standard-  
 22 Model physics at the EIC. As one example, the polarization asymmetry in  $eD$  scattering  
 23 provides a method for extracting the weak mixing angle,  $\theta_W$  [172]. In the limit that charge  
 24 symmetry violation is neglected (up quarks in the proton are the same as down quarks in  
 25 the neutron) and sea-quark effects are negligible ( $\bar{s} - s = 0$ ), the asymmetry is independent  
 26 of hadron structure for  $Q^2 \rightarrow \infty$  [173]. However, in reality these approximations limit the  
 27 precision with which  $\theta_W$  can be extracted, and even rudimentary LQCD calculations of  
 28  $u_p - d_n$  or  $\bar{s} - s$  or their moments will enable a better determination of  $\theta_W$ .



# <sup>1</sup> Chapter 4

## <sup>2</sup> Detectors

### <sup>3</sup> 4.1 Introduction - Detector Requirements

<sup>4</sup> EIC detector design and concepts are essential to reach the physics goals described in  
<sup>5</sup> earlier sections. The detector development efforts profit from a wealth of experience gained  
<sup>6</sup> at the first  $e+p$  collider facility HERA at DESY, Germany, and the enormous development  
<sup>7</sup> of novel detector concepts over the last several decades, as documented in part by the  
<sup>8</sup> Yellow Report publication of the EIC Users Group [8]. In parallel with a nearly two-  
<sup>9</sup> decade-long community effort of EIC science development and refinement and experimental  
<sup>10</sup> equipment conceptualization, BNL, in association with TJNAF and the DOE Office of  
<sup>11</sup> Nuclear Physics, established in 2011 a highly successful generic EIC-related detector R&D  
<sup>12</sup> program. This program built bridges between various domestic and international research  
<sup>13</sup> groups and scientific communities. Many supported projects are now integral parts of  
<sup>14</sup> existing detector concepts or are considered potential alternatives. Due to this longstanding  
<sup>15</sup> generic EIC-related detector R&D program and further support from Laboratory Directed  
<sup>16</sup> Research & Development (LDRD) Programs within the US national laboratories and many  
<sup>17</sup> university groups both inside and outside the US, the detector technologies to implement  
<sup>18</sup> a successful comprehensive Day-One EIC Science program exist with (at least one) general  
<sup>19</sup> purpose EIC detector.

<sup>20</sup> The first general-purpose EIC detector will be a sophisticated experimental instrument  
<sup>21</sup> designed and constructed by the multi-institutional international EPIC collaboration. The  
<sup>22</sup> EPIC detector is required to fit into the constraints of the interaction region. It will include  
<sup>23</sup> instrumentation for forward and backward regions and have multiple hermetic functionalities  
<sup>24</sup> (precision energy measurement and particle tracking and identification) to determine  
<sup>25</sup> the energy-momentum four-vector of final-state particles over an extensive range of ener-  
<sup>26</sup> gies,  $\sim 100$  MeV to  $\sim 50$  GeV. Throughout this document, the beams' directions follow the  
<sup>27</sup> convention used at the HERA collider at DESY: the hadron beam travels in the positive  
<sup>28</sup>  $z$ -direction/pseudorapidity. It is said to be going "forward." The electron beam travels  
<sup>29</sup> in the negative  $z$ -direction/pseudorapidity and is said to be going "backward" or in the  
<sup>30</sup> "rear" direction. In addition to the detector suit developed by the EPIC collaboration for  
<sup>31</sup> the primary interaction region, other sophisticated instruments will aid the EIC scientific  
<sup>32</sup> program: luminosity monitors, electron and ion beam polarimeters, etc.

<sup>33</sup> The design of the EPIC detector for the EIC is centered around a solenoidal super-

1 conducting magnet at 1.8 T. This configuration naturally leads to tracking and vertexing,  
 2 particle identification, and calorimetry systems organized in a configuration with barrel and  
 3 endcap detectors. In contrast to symmetric  $e^+e^-$  and  $p+p$  colliders, the asymmetric nature  
 4 of collisions at the EIC leads to unique detector requirements. For example, the hadron  
 5 endcap, barrel, and electron endcap detector systems see very different particle distribu-  
 6 tions, reflected in different detector requirements for the track, vertex, energy resolution,  
 7 and particle identification at different angles. These detector requirements in each kine-  
 8 matic region were informed by physics program needs with many specific measurements in  
 9 mind. They were evaluated in the context of the major research thrusts of the EIC. Prelimi-  
 10 nary investigations were put forward in the EIC White Paper [6] and later advanced by the  
 11 Yellow Report EIC Users Group community effort [8]. Three basic types of DIS processes  
 12 organized recent studies of the physics-driven detector requirements: inclusive DIS both  
 13 in neutral and charged current mode, semi-inclusive DIS, and exclusive DIS. Those basic  
 14 processes are shown below:

- 15 • **Neutral-current Inclusive DIS:**  $e + p/A \rightarrow e' + X$ ; for this process, it is essential  
 16 to detect the scattered electron,  $e'$ , with high precision. All other final state particles  
 17 ( $X$ ) are ignored. The scattered electron is critical for all processes to determine the  
 18 event kinematics.
- 19 • **Charged-current Inclusive DIS:**  $e + p/A \rightarrow \nu + X$ ; at high enough momentum  
 20 transfer  $Q^2$ , the electron-quark interaction is mediated by the exchange of a  $W^\pm$   
 21 gauge boson instead of the virtual photon. In this case, the event kinematic cannot  
 22 be reconstructed from the scattered electron but needs to be reconstructed from the  
 23 final state particles.
- 24 • **Semi-inclusive DIS:**  $e + p/A \rightarrow e' + h^{\pm,0} + X$ , which requires measurement of *at*  
 25 *least one* identified hadron in coincidence with the scattered electron.
- 26 • **Exclusive DIS:**  $e + p/A \rightarrow e' + p'/A' + \gamma/h^{\pm,0}/VM$ , which require the measurement  
 27 of *all* particles in the event with high precision.

28 Special attention was also given to evaluating detector requirements for measurements of  
 29 processes involving jets, jet substructure, and heavy-flavor hadrons.

30 All physics processes to be measured at an EIC require having the event and particle  
 31 kinematics ( $x, Q^2, y, W, p_t, z, \phi, \theta$ ) reconstructed with high precision. Kinematic variables  
 32 such as  $x, Q^2, y$ , and  $W$  can be determined from the scattered electron, the hadronic final  
 33 state, or a combination of both. To access the entire  $x - Q^2$  plane at different center-of-  
 34 mass energies and for strongly asymmetric beam-energy combinations, the detector must  
 35 be able to reconstruct events over a wide span in polar angle ( $\theta$ ) and pseudorapidity ( $\eta$ ).  
 36 This imposes stringent requirements on detector acceptance and the resolution of measured  
 37 quantities, such as the energy and polar angle in the electron-method case. The EIC detector  
 38 requirements developed by the Yellow Report initiative are summarized below:

- 39 • The EIC program requires a  $4\pi$  hermetic detector with low mass inner tracking.

- 1     • The primary general-purpose detector must cover the range of  $-4 < \eta < 4$  for the  
2 measurement of electrons, photons, hadrons, and jets. It will need to be augmented  
3 by auxiliary detectors like low- $Q^2$  tagger in the far backward region and proton and  
4 neutron detection in the far forward region.
- 5     • Compared to LHC detectors, the various subsystems of an EIC detector have moderate  
6 radiation hardness requirements.
- 7     • While many EIC detector subdetectors will have moderate occupancy, specific compo-  
8 nents close to the beam line might see higher occupancies depending on the machine  
9 background level and should have a good tolerance for high occupancy.
- 10    • Excellent momentum resolution in the central detector ( $\sigma_{p_T}/p_T(\%) = 0.05p_T \oplus 0.5$ ).
- 11    • Good momentum resolution in the backward region with low multiple-scattering terms  
12 ( $\sigma_{p_T}/p_T(\%) \approx 0.1p_T \oplus 0.5$ ).
- 13    • Good momentum resolution at forward rapidities ( $\sigma_{p_T}/p_T(\%) \approx 0.1p_T \oplus (1 - 2)$ ).
- 14    • Good impact parameter resolution for heavy flavor measurements ( $\sigma_{xy} \sim 20/p_T \oplus$   
15  $5 \mu\text{m}$ ).
- 16    • Good electromagnetic calorimeter resolution in the central detector ( $\sigma(E)/E \approx 10\%/\sqrt{E} \oplus$   
17  $(1 - 3)\%$  at midrapidity).
- 18    • Excellent electromagnetic calorimeter resolution at backward rapidities ( $\sigma(E)/E \approx$   
19  $2\%/\sqrt{E} \oplus (1 - 3)\%$ ).
- 20    • Good hadronic resolution in the forward region ( $\sigma(E)/E \approx 50\%/\sqrt{E} \oplus 10\%$ ).
- 21    • Excellent PID for  $3 \sigma \pi/K/p$  separation up to  $50 \text{ GeV}/c$  in the forward region, up to  
22  $10 \text{ GeV}/c$  in the central detector region, and up to  $7 \text{ GeV}/c$  in the backward region.

23       The following section will describe the current design motivation and status of the  
24 primary subsystems in the EPIC detector.

## 25    **4.2 The EPIC Detector**

### 26    **4.2.1 Vertex and Tracking Detector**

27       The EPIC vertex and tracking detector is being optimised for best performance in terms  
28 of primary and displaced vertex reconstruction and momentum resolution of reconstructed  
29 tracks in the pseudorapidity region of  $|\eta| < 3.5$ . It will deploy Monolithic Active Pixel  
30 Sensor (MAPS) silicon detectors near the interaction point and Micro-Pattern Gaseous  
31 Detectors (MPGDs) farther out. This configuration is chosen to design an overall cost  
32 effective detector system with high precision, low material budget and large lever arm. The  
33 current geometry of the EPIC vertex and tracking detector for the first simulation campaign  
34 (Oct. 2022) is illustrated in figure 4.1.

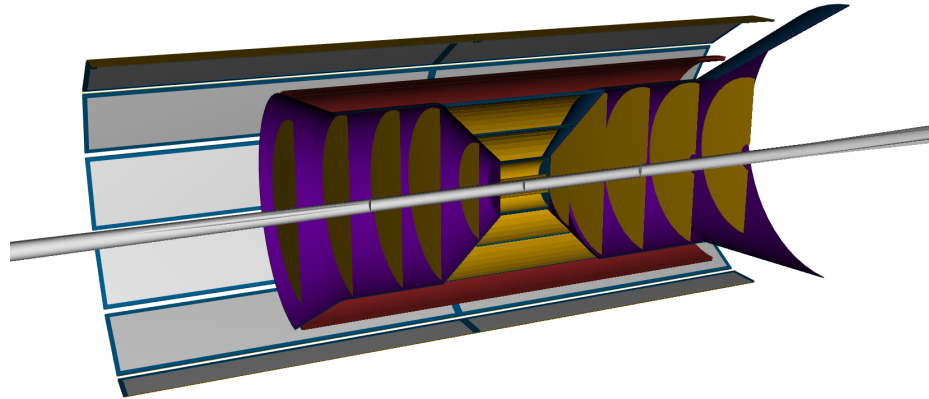


Figure 4.1: EPIC vertex and tracking detector implementation for the first simulation campaign (Oct. 2022) comprising of silicon vertex and barrel layers and forward/backward silicon disks, complemented by large-area Micro-Pattern Gaseous Detectors in the outer barrel layers. Two layers of MPGD are shown, one before and one after the hpDIRC (in red and grey respectively). The hpDIRC and the barrel time-of-flight detectors are not shown. Some support structures are included in the figure (in purple). [Figure may be updated](#)

The silicon part consists of five barrel layers in the central region and five disks per endcap region. In the central region, the three innermost layers are used primarily for vertex reconstruction. The first and second vertex layers are located at radii of 3.6 cm and 4.8 cm to satisfy the constraints from beam pipe bake out and sensor size, while providing a first point for track reconstruction as close as possible to the beam pipe, and a distance between the first two layers adequate for the required vertex resolution. The third vertex layer is placed at a radius of 12 cm to contribute to the momentum resolution. The vertex layers are equipped with stitched, wafer-scale sensors, thinned and bent around the beam pipe. They are 27 cm long with services foreseen on one side only to reduce material in the electron going direction. Two sagitta layers are placed at radii of 27 cm and 42 cm with a length 54 cm and 84 cm respectively. They consist of traditional stave support structures equipped with smaller stitched sensors. The disks in the forward and backward region occupy the entire space available to increase lever arm at large pseudorapidity. Whether the silicon detector configuration with five disks per side can provide sufficient number of hits per track is under investigation and will be studied with simulation including the relevant EIC backgrounds. The innermost disk on both sides is placed at 25 cm from the interaction point, with the last disks placed at 135 cm in the forward region and at 115 cm in the backward region. The inner radii are determined by the divergence of the beam pipe. The maximum outer radius of the disks is approximately 43 cm. Disks use the same sensor technology as the vertex and sagitta layers, with stitched sensor size optimized for maximum acceptance at the innermost and outermost radii.

In the central pseudo-rapidity region, the Si barrel layers will be complemented, at larger radii, by a set of large-area low-material-budget cylindrical MPGD layers. Simulations

with embedded backgrounds from synchrotron radiation and beam gas interactions will be used to determine the optimal number and locations of MPGD layers that allow for an efficient track finding and reconstruction. These layers will be installed in the radial space between the last silicon sagitta layer and the time-of-flight detector, covering the pseudo-rapidity range  $|\eta| < 1.5$  (Check!). An additional MPGD layer is being considered for the improvement of the hpDIRC detector. This layer will be located after the hpDIRC detector and it will provide a precise space point to improve the angular resolution inside the radiator material for better ring reconstruction. Similarly an MPGD disk layer behind the dRICH in the hadron end cap is been investigate to help with the Cerenkov ring seeding as well as additional hit point at large lever-arm to enhance the tracking performance in the forward region.

## Technology choice

The technology chosen for the silicon detector is a new generation 65 nm MAPS sensor being developed by the ALICE collaboration for the upgrade of the experiment inner tracking system at the HL-LHC, the so called ITS3 detector. This technology has been identified as the best candidate to satisfy the EIC requirements. The ITS3 sensor features a pixel pitch down to  $10\text{ }\mu\text{m}$  and a power consumption as low as  $20\text{ mW cm}^{-2}$ . The EPIC vertex layers will use the ITS3 sensor and detector concept, with stitched, wafer-scale devices, thinned below  $50\text{ }\mu\text{m}$  and bent around the beam pipe. This configuration requires only minimal mechanical support in the active area of the detector. As the length of each layer is covered by one sensor only, there are no services in the active area. These features, coupled with air cooling made possible by the sensor low power consumption, give a total thickness per layer of only  $0.05\% X/X_0$ . In the sagitta barrel layers and disks, the same sensor will be used with a size optimised for cost effective large area coverage. Sensors will be mounted flat onto stave and disk structures with integrated cooling and electrical interfaces for services, giving a material budget estimate of  $0.25\% X/X_0$  and  $0.55\% X/X_0$  for the first and second sagitta layer respectively and  $0.24\% X/X_0$  for the disks. The development of the EPIC silicon vertex and tracking detector is being carried out by the EIC Silicon Consortium within the framework of the eRD104, eRD111 and eRD113 projects.

MPGDs are gaseous devices with a high granularity strip or pad readouts to provide good 2D space point resolution ( $< 100\text{ }\mu\text{m}$ ), fast signals ( $\approx 10\text{ ns}$ ), high rate capability (up to  $1\text{ MHz cm}^{-2}$ ), low material budget, radiation hardness and large area coverage. Micromegas and  $\mu$ RWELL technologies have been identified as best candidates for the EPIC detector. Low material budget cylindrical Micromegas have been in use since many years in the CLAS12 experiment at JLab and the ASACUSA experiment at CERN.  $\mu$ RWELL is being actively developed and large area detector are being built for experiments at JLab and CERN. Through the EIC generic and targeted detector R&D program (eRD3/eRD6/eRD108) advancements towards low material and large-area MPGD detectors with low channel counts 2D readout structures have been made.

### 4.2.2 Particle Identification Detector Systems

The ability to identify hadrons in the final state is a key requirement for the physics program of the EIC. Being able to tag the flavor of the struck quark in semi-inclusive DIS can, for

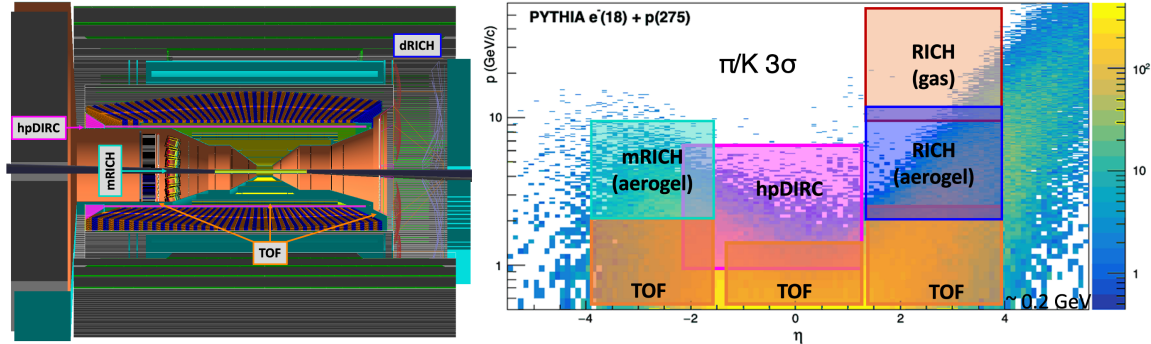


Figure 4.2: Left: RICH-based and TOF PID detectors in the full EPIC detector simulation. Right: Expected 3 s.d.  $\pi/K$  separation coverage for the EPIC PID systems as a function of the particle momentum and pseudo-rapidity. Full coverage is achieved by making use of the veto mode of the Cherenkov detectors, complementing the TOF PID in the low momentum region.

1 instance, provide valuable information about the transverse momentum distributions (and  
 2 potentially orbital angular momentum) of the strange sea quark, while open charm (with  
 3 subsequent decays into kaons) is important for probing the distribution of gluons in protons  
 4 and nuclei.

5 Charged hadron PID in the EPIC detector can be achieved for particle momenta  $1 <$   
 6  $p_{\text{hadron}} < 60 \text{ GeV}$  with a combination of gaseous and solid-radiator ring-imaging Cherenkov  
 7 (RICH) systems. The measurement of the emission angle of Cherenkov photons is a powerful  
 8 particle identification (PID) technique that allows for a tunable dynamic range in hadron  
 9 momentum. The ring-shaped image created by photons on the detector plane is used to  
 10 reconstruct the the Cherenkov emission angle which, in combination with the momentum  
 11 information, is used to determine the particle species.

12 The selection of RICH technology types for EPIC is carefully tuned to the required  
 13 physics and unique aspects of the EPIC detector design. Because the momentum range  
 14 needs for PID vary significantly with  $\eta$  it is necessary to tune the radiator index differently  
 15 in three regions: electron endcap, barrel, and hadron endcap.

16 The choice of Cherenkov based PID technologies for the EPIC detector is in line with  
 17 the baseline EIC reference detector design. It follows recommendations of DPAP review,  
 18 reference detector concept established in the Yellow Report (YR) [8], and the outcome of the  
 19 EIC generic R&D program, started in 2011. The longitudinally compact, modular RICH  
 20 (mRICH), the radially thin high-performance DIRC (hpDIRC), and the dual-radiator RICH  
 21 (dRICH), provide excellent PID over a wide momentum range. The geometries of all PID  
 22 detectors were optimized to fit the EPIC baseline design while maintaining the required  
 23 performance.

24 Figure 4.2 shows the four PID technologies in a Geant4 simulation framework and their  
 25 coverage as a function of momenta and pseudo-rapidity for a sample of physics event.  
 26 Realistic EPIC PID detectors have been implemented and studied in standalone Geant4  
 27 simulation packages. The expected PID performance of the three EPIC Cherenkov detectors  
 28 is summarized in Table 4.1. The Cherenkov system performance is further separated into the

<sup>1</sup> nominal “Ring Imaging” mode of operation, which provides positive ID of the particle type,  
<sup>2</sup> and the so-called “threshold mode” or “veto mode”, which uses the number of Cherenkov  
<sup>3</sup> photons in excess of the expected background to differentiate between particle types above  
<sup>4</sup> or below the threshold for Cherenkov light emission.

Table 4.1: Summary of the PID performance of the EPIC Cherenkov systems (momentum coverage in  $\text{GeV}/c$ ).

PID	Mode	mRICH	hpDIRC	dRICH	
				aerogel	gas
$\pi/K$	Ring Imaging	2 – 9	1 – 7	2 – 13	12 – 60
	Threshold	0.6 – 2	0.3 – 1	0.7 – 2	3.5 – 12
$e/\pi$	Ring Imaging	0.6 – 2.5	< 1.2	0.6 – 13	3.5 – 15
	Threshold	< 0.6	–	< 0.6	< 3.5

<sup>5</sup> The Cherenkov systems provide, in addition to hadron PID, a significant contribution to  
<sup>6</sup> the  $e/\pi$  identification. When combined with the electromagnetic calorimeter, the mRICH  
<sup>7</sup> and hpDIRC will provide excellent suppression of the low-momentum charged-pion back-  
<sup>8</sup> grounds, which otherwise limit the ability of the EMCAL to measure the scattered electron  
<sup>9</sup> in kinematics where it loses most of its energy.

## <sup>10</sup> dRICH

<sup>11</sup> The dual-radiator Ring Imaging Cherenkov (dRICH) detector is designed to provide continuous  
<sup>12</sup> full hadron identification (pion-kaon separation better than  $3\sigma$  apart) from  $\sim 3 \text{ GeV}/c$   
<sup>13</sup> to around  $\sim 60 \text{ GeV}/c$  in the (outgoing) ion-side endcap of the EPIC detector. It also of-  
<sup>14</sup> fers a remarkable electron and positron identification ( $e^\pm/\pi$  separation) from few hundred  
<sup>15</sup> MeV up to about  $15 \text{ GeV}/c$ . The proposed geometry covers polar angles from  $\sim 5^\circ$  up to  
<sup>16</sup>  $25^\circ$ . Achieving such a momentum coverage in the ion-side region is a key requirement for  
<sup>17</sup> the EIC physics program. The dRICH is the only available option to provide continuous  
<sup>18</sup> coverage in RICH mode over the full momentum range required for the forward endcap.  
<sup>19</sup> The dRICH concept was inspired by the HERMES and LHCb (RICH1) dual-radiator RICH  
<sup>20</sup> detectors. The dRICH configuration for EPIC consists of six identical, transversely open  
<sup>21</sup> sectors. Each contains two radiators (aerogel and  $\text{C}_2\text{F}_6$  gas), sharing the same outward  
<sup>22</sup> focusing mirror and readout planes, which are instrumented with highly segmented photo-  
<sup>23</sup> sensors (3 mm  $\times$  3 mm pixels), located outside of charged particle acceptance. The focal  
<sup>24</sup> plane is moved to a lower radiation zone. This helps not only in the level of background hits  
<sup>25</sup> that can interfere with the photon ring, but also may allow the use of emerging technology  
<sup>26</sup> such as SiPM detectors to be used for the readout. The photosensor tiles are arranged on  
<sup>27</sup> a curved surface to compensate for aberrations. Due to the open geometry of the dRICH  
<sup>28</sup> sectors, photons from a Cherenkov cone may split over two or more sectors.

<sup>29</sup> As is true for most modern gas Cherenkov detectors, the dRICH utilizes the superior  
<sup>30</sup> performance of perfluorocarbon radiator gas ( $\text{C}_2\text{F}_6$ ). Future environmental concerns studies  
<sup>31</sup> for an alternative environmentally friendly gas at high pressure.

**1 hpDIRC**

2 A radially-compact detector based on the DIRC (Detection of Internally Reflected Cherenkov  
 3 light) principle, is a special kind of RICH counter using solid rectangular-shaped radiators  
 4 made of synthetic fused silica that are utilized also to guide Cherenkov photons to the  
 5 readout section, placed on the side where the photons are recorded by an array of pixelated  
 6 photon sensors. Thanks to the excellent optical finish of the optics the emission angle of  
 7 Cherenkov photons, in respect to the particle track, is maintained during the photon trans-  
 8 port via the total internal reflection and can be reconstructed from the measured position  
 9 of the photon on the detector surface and the arrival time of each photon.

10 The high-performance DIRC (hpDIRC) concept was developed as part of the generic  
 11 R&D program performed by the EIC PID collaboration (eRD14) with the focus on extend-  
 12 ing the momentum coverage well beyond the DIRC counter state-of-the-art to 3 standard  
 13 deviations or more separation of  $\pi/K$  up to 6 GeV/c,  $p/K$  up to 10 GeV/c, and  $e/\pi$  up to  
 14 1.2 GeV/c momentum.

15 The radiation-hard 3-layer spherical focusing lens is an innovative component of the  
 16 hpDIRC and crucial in reaching the required PID performance, together with small (3 mm  $\times$  3 mm)  
 17 pixel MCP-PMTs, and fast readout electronics providing the 100ps single photon timing  
 18 precision. The design of hpDIRC is flexible, the radius and length of the bars can be  
 19 modified without impact on the PID performance and the shape of the expansion volume  
 20 prism can be selected for optimum position of the sensors in the magnetic field. It has low  
 21 demands on the detector infrastructure (no cryogenic cooling, no flammable gases) and is  
 22 easy to operate.

**23 mRICH**

24 A modular RICH (mRICH) is an aerogel-based compact Cherenkov detector developed  
 25 with a goal to meet the EIC physics requirements for  $K/\pi$  separation in momentum range  
 26 from 3 to 9 GeV/c and the geometrical constraints of the EPIC detector. It also provides  
 27 excellent  $e/\pi$  for momentum below 2 GeV/c. A unique feature of this technology is the use  
 28 of a Fresnel lens to make a focused ring, thereby significantly improving the performance  
 29 without a need of large expansion volume as compared to a “proximity focused” detector  
 30 which is more common in aerogel applications. A pixelated optical sensor is located in the  
 31 focal plane, and flat mirrors form the sides of each mRICH module. The mirrors along the  
 32 sides of the device allow it to collect light which is not initially directed to the photocathode  
 33 found at the detector exit.

34 The projective array design of mRICH allows to fill the allocated space, maximize the  
 35 acceptance, remove the track polar-angle impact on performance, and reduce the material  
 36 budget. The center of each module is projected toward the interaction point (IP) and the  
 37 dead region between the mRICH modules is minimized using optimized thin module walls  
 38 and mirrors.

39 A proximity focusing RICH (pfRICH) is being developed as a potential alternative  
 40 solution for the electron side of EPIC detector.

<sup>1</sup> **Time-of-Flight**

<sup>2</sup> The physics program of the EIC requires hermetic particle identification spanning a wide  
<sup>3</sup> momentum range. At relatively low momenta, the direct measurement of a particle's velocity  
<sup>4</sup> provides an excellent means for such particle identification. Substantial advancements  
<sup>5</sup> in the precision by which detector devices can measure the time of passage of a particle  
<sup>6</sup> have led to silicon-based detectors that can be made relatively thin, measured both by ra-  
<sup>7</sup> diation length and physical dimension. Moreover, silicon-based technologies such as Low  
<sup>8</sup> Gain Avalanche Detectors (LGADs) are intrinsically insensitive to magnetic fields.

<sup>9</sup> A time-of-flight (TOF) detector system consisting of a central barrel and a forward  
<sup>10</sup> endcap detector is designed to extend particle identification into the low end of the mo-  
<sup>11</sup> mentum spectra. The central TOF system is situated between the barrel silicon tracker  
<sup>12</sup> and electromagnetic calorimeter at a radius between 63 and 66 cm and an acceptance of  
<sup>13</sup>  $|\eta| < 1.4$ . The forward TOF system is mounted in front of the dRICH system at a distance  
<sup>14</sup> between 1.80 and 1.95 m from the center of the detector. Its pseudorapidity coverage is  
<sup>15</sup>  $1.75 < \eta < 4.0$ . Both are based on AC-coupled LGAD technology, which can yield single-  
<sup>16</sup> hit timing resolutions of 25 ps. Such a time resolution will allow the barrel and endcap TOF  
<sup>17</sup> systems to separate pions and kaons at a  $3\sigma$  level for  $p_T < 1.5$  GeV/c and  $p < 2.0$  GeV/c,  
<sup>18</sup> respectively. Additionally, spatial points from these detectors, combining high timing and  
<sup>19</sup> position resolution, will allow "4D" track reconstruction and background rejection.

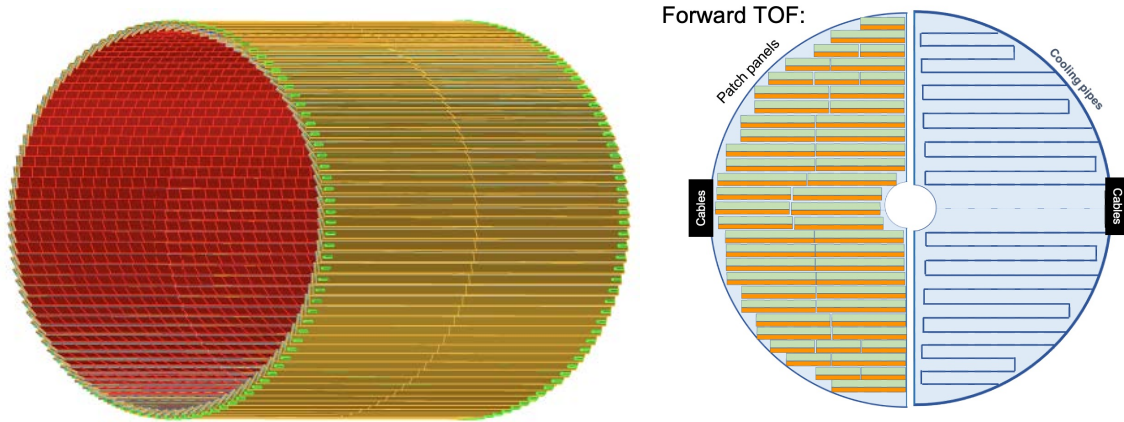


Figure 4.3: Layout of the EPIC AC-LGAD TTL detectors in the barrel (left) and endcap regions (right).

<sup>20</sup> The design of the barrel TOF follows that of the STAR Intermediate Silicon Tracker  
<sup>21</sup> [174], while the endcap TOF design is based on the Endcap Timing Layer of the CMS  
<sup>22</sup> MIP Timing Detector [175]. The layout of the EPIC TOF detectors is shown in Fig. 4.3.  
<sup>23</sup> The barrel TOF is made from a single layer of tilted stave modules with a total length  
<sup>24</sup> of about 240 cm. AC-LGAD strip sensors are wire-bonded to front-end readout ASICs  
<sup>25</sup> and mounted on low-mass flexible Kapton circuit boards. These boards are glued onto  
<sup>26</sup> lightweight structures made from Carbon-Fiber (CF) composite materials and bring low  
<sup>27</sup> voltage, high voltage, and input/output signals to the AC-LGAD sensors and ASICs<sup>1</sup>. The

<sup>1</sup> Application Specific Integrated Circuits

heat generated by the ASICs is removed by an embedded aluminum cooling tube in the CF structure. The material budget of the barrel TOF is about 1%  $X_0$ . The tilted design provides full azimuthal coverage, while the longitudinal range can be more than 95%. With a radius between 8 and 67 cm, the endcap TOF is based on detector modules that consist of AC-LGAD pixel sensors bump-bonded to front-end ASICs. The modules are mounted from both sides onto a thermally conductive supporting disk with embedded liquid cooling lines. A total material budget of about 8%  $X_0$  is assumed for the endcap TOF. As the design matures, the forward coverage will follow from an optimization of the layout with modules that serve different numbers of ASICs.

#### 4.2.3 Calorimeter Detector Systems

The EIC physics program imposes strong detector performance requirements on the calorimeter systems. While single inclusive DIS, jets and heavy quark reconstruction require an excellent energy resolution for the electromagnetic and hadronic calorimeters, further requirements for  $\pi / e$  separation at the  $3\sigma$  level are imposed, for example, by spin asymmetry measurements, TMD evolution, and  $XYZ$  spectroscopy. To probe the broadest possible kinematic range of all these processes, a nearly hermetic coverage is required in particular for the electromagnetic calorimeters with a superb energy resolution in particular at backward and mid-rapidity to detect the scattered electron. Driven by these concerns, homogeneous electromagnetic calorimeters (ECals) for the electron end cap and the barrel region are selected, while a highly granular tungsten scintillating fiber (W/SciFi) calorimeter is chosen in the hadron going direction, see Fig. 4.4. The homogeneous calorimeter in the electron going direction is a classical PbWO<sub>4</sub> crystal calorimeter, while the barrel calorimeter is constructed out of scintillating glass (SciGlass). For the barrel region a silicon pixel based imaging calorimeter together with a lead scintillating fiber sampling calorimeter is being considered as an alternative solution. The gaps between these calorimeters in  $\eta$  are minimized by reducing the support structures for the inner most detectors and even adopting a projective design for the barrel SciGlass ECal.

Due to the asymmetric collision system at the EIC most of the hadronic particles are

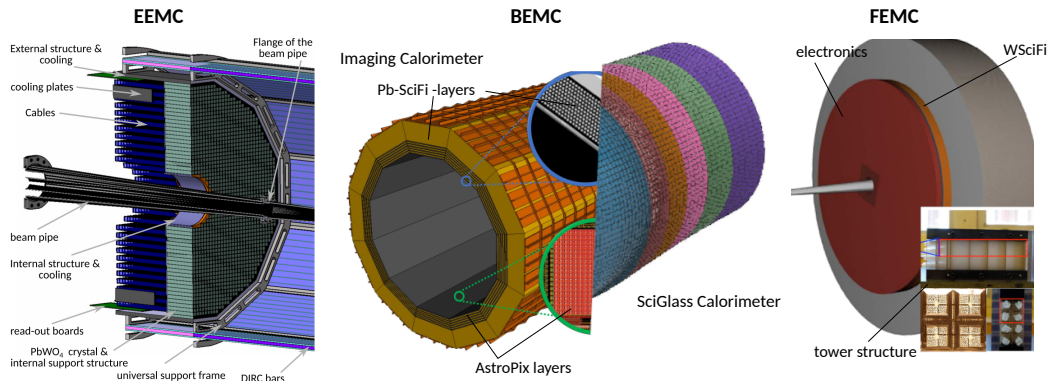


Figure 4.4: Illustration of EPIC electromagnetic calorimeter designs: homogeneous PbWO<sub>4</sub> crystal calorimeter (left), imaging calorimeter (middle left), homogeneous SciGlass calorimeter (middle right) and WSciFi calorimeter (right).

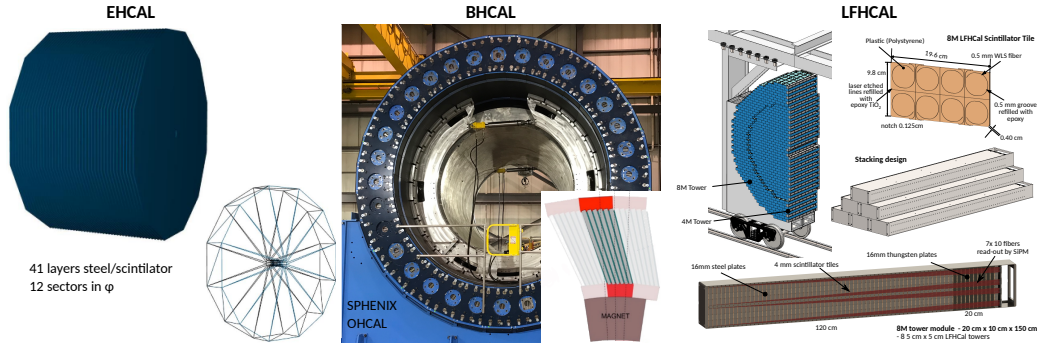


Figure 4.5: Illustration of EPIC hadronic calorimeter designs: electron-going Steel-Scintillator HCal (left), barrel Steel-Scintillator HCal reused from sPHENIX (middle), longitudinally separated forward Steel-Tungsten-Scintillator HCal (right).

1 emitted at mid- or forward rapidity, with the most energetic particles and jets flying towards  
 2 the forward end-cap. With the tracking system designed to provide excellent momentum  
 3 resolution for charged particles at low momenta the hadronic calorimeters are designed to  
 4 detect neutral hadrons and complement the tracking with a sufficient energy and position  
 5 resolution in particular at high momenta. The baseline design of the hadronic calorimeters  
 6 for the EPIC experiment foresees a re-purposing of the outer HCal of the sPHENIX exper-  
 7 iment [176] and a new longitudinally separated forward hadronic calorimeter, see Fig. 4.5.  
 8 A hadronic calorimeter in the electron going direction is envisioned as a future upgrade.  
 9 All of the three calorimeters are steel-scintillator calorimeters in various geometrical setups  
 10 and granularities. In order to improve the energy resolution of the forward calorimeter the  
 11 last longitudinal segment is made of tungsten and serves as tail catcher.

12 The performance of the above described calorimeters strongly depends on the material  
 13 budget of the inner detectors, as early material interactions can deteriorate the reconstruc-  
 14 tion performance significantly in particular for the electromagnetic calorimeters. Thus, the  
 15 material of all inner detector systems and support frames in the EPIC experiment has  
 16 been greatly minimized by design, resulting in a material budget of only  $0.2 - 1X/X_0$  in  
 17 the barrel and approximately  $0.15X/X_0$  in the forward and backward direction with slight  
 18 modulations depending on  $\eta$ . All calorimeters will be read out using SiPMs in different  
 19 configurations.

## 20 Electromagnetic Calorimeters

21 The electron-end-cap electromagnetic calorimeter (EEMC) will cover a dynamic energy  
 22 range of  $0.1 - 18$  GeV in order to detect the scattered electrons even at the highest possible  
 23 collision energies as well as final-state photons being emitted in the electron-going region. Its  
 24 baseline design is based on an array of approximately 3000 lead tungsten crystals ( $\text{PbWO}_4$ )  
 25  $2 \times 2 \times 20$  cm $^3$  in size, which correspond to approximately  $20 X/X_0$  longitudinally and a  
 26 transverse size equal to the  $\text{PbWO}_4$  Molière radius. The light yield of the  $\text{PbWO}_4$  crystals  
 27 ranges from 15 to 25 photo-electrons per MeV, providing an excellent energy resolution of  
 28  $\sigma_E/E \approx 2\%/\sqrt{E} \oplus 1\%$  [177,178] within a very compact design. With a density of 8.28 g/cm $^3$ ,  
 29 and a mass of 0.6624 kg per crystal the total weight of the EEMC is slightly more than two

metric tons which is embedded with its cooling structures and mechanical support in the universal support frame, which also houses the DIRC. It covers a pseudorapidity rapidity region of  $-3.4 < \eta < -1.5$  and will be installed at  $Z = -175$  cm. The EEMC can reject pions between 2 and 7 GeV with a rejection factor better than  $10^4$ .

The barrel electromagnetic calorimeter is optimized simultaneously for the scattered electron detection and identification as well as the reconstruction of low energetic electromagnetic jet fragments. It covers the central detector region ( $-1.72 < \eta < 1.31$ ) and is embedded within the solenoid magnet after the DIRC detector at a radius of about 85 cm. The homogeneous barrel electromagnetic calorimeter consists of 8960 towers made out of scintillating glass (SciGlass), which are organized in 128 towers per  $\varphi$  slice and 70 blocks in the  $\eta$  direction. It is designed with offset projectivity in  $\eta$  and  $\varphi$  in order to avoid channeling of particles produced in the collision within the passive material between the towers. All towers currently have an inner size of  $4 \times 4 \text{ cm}^2$  and a length of 45.5 cm, which corresponds to approximately  $16 X/X_0$ , yielding an energy resolution of about  $2.5\%/\sqrt{E} + 1.6\%$  and a pion rejection of better than 100 over the full kinematic range.

The alternatively proposed hybrid imaging calorimeter, following the GlueX design [179], using light-collecting calorimetry based on SciFi embedded in Pb and imaging calorimetry based on AstroPix monolithic silicon sensors would be situated at the same radius. It is composed of six layers of silicon sensors interleaved with five Pb/SciFi layers, followed by a thick layer of Pb/SciFi calorimeter resulting in a total radiation thickness of about 20  $X_0$ . The calorimeter is arranged in 12  $\varphi$  segments which are read out on the ends. This hybrid design offers precise measurements of both energy and position of the incident particle's cascade in 3D and through utilization of AI techniques a pion rejection better than traditional sampling calorimeters.

EPIC's forward end-cap will be equipped with a compact W/SciFi calorimeter made of W powder with embedded scintillating fibers with a transverse tower size of  $2.5 \times 2.5 \text{ cm}^2$  and depth of 17 cm. Following an improved design of the sPHENIX ECal [180, 181] it should reach and  $e/h \sim 1$  and an energy resolution of  $\sim 10\%/\sqrt{E} + 2\%$ .

## Hadronic Calorimeters

The barrel hadronic calorimeter (BHCAL) will be reused from the sPHENIX HCal [182], which instruments the large steel-based barrel flux return of the magnet. Its absorber plates are tilted in the radial direction and thus allow for more uniform sampling in azimuth and offer some information on the longitudinal development of the shower. Extruded tiles of plastic scintillator with an embedded wavelength shifting fiber are interspersed between the absorber plates and read out at the outer radius with SiPMs. The detector consists of 32 modules, which are wedge-shaped sectors containing 2 towers in  $\varphi$  and 24 towers in  $\eta$  equipped with SiPM sensors, preamplifiers, and cables carrying the differential output of the preamplifiers to the digitizer system on the floor and upper platform of the detector. The BHCAL is only 4 hadronic interaction length deep and consequently only has an expected energy resolution of about  $75\%/\sqrt{E} + 15\%$  which suffices in combination with the excellent tracking capabilities of the EPIC detector for the barrel region to reconstruct jets up to approximately 50 GeV with the desired accuracy.

The longitudinally separated forward HCal (LFHCAL) is a Steel-Tungsten-Scintillator

1 calorimeter and was designed to handle single particle energies up to 150 GeV with jets  
 2 up to 200 GeV. It is based on PSD calorimeter employed in the forward direction for the  
 3 NA61/SHINE experiment [183], but it has been extensively modified to meet the desired  
 4 physics performance laid out in the Yellow Report [8, 184]. This longitudinally separated  
 5 HCal is positioned after the tracking and PID detectors at  $z = 3.60\text{m}$  from the center of  
 6 the detector and is made up of two half disks with a radius of about 2.6m.

7 Its comprised of six 20 cm long segments of alternating steel and scintillator followed by a  
 8 10 cm deep tungsten/scintillator segment serving as a tail catcher, corresponding to about  
 9 6.7 interaction length. Each tower consists of 65 layers with alternating 1.6 cm absorber and  
 10 0.4 cm scintillator material with embedded wavelength shifting fibers and has transverse  
 11 dimensions of  $5 \times 5 \text{ cm}^2$ . The towers are constructed in units of 8-, 4-, 2- and 1-tower  
 12 modules to ease the construction and to reduce the dead space between the towers. Current  
 13 simulations indicate an expected energy resolution of  $30 - 40\%/\sqrt{E} + 10\%$ .

14 In a future upgrade the electron-end cap might be equipped with a coarse Steel-scintillator  
 15 calorimeter following closely the STAR endcap ECal design [185] with a depth of 3-4  $\lambda$ . This  
 16 detector mainly serves to tag events with a significant neutral hadronic energy fraction in  
 17 the electron going direction or events with muons being emitted in the same direction.

#### 18 **4.2.4 Far-Forward Detector Systems**

19 The EIC physics program includes final-states in which charged or neutral particles emerge  
 20 from the collision with rapidities  $> 4.5$  - so-called “far-forward” rapidities. These final states  
 21 are of prime importance for partonic imaging and all exclusive + diffractive final states at  
 22 the EIC. The high rapidities observed for these final states motivate the need for sub-systems  
 23 integrated within and alongside the accelerator beam line, creating unique challenges both  
 24 for detector acceptance and for reconstruction of kinematic quantities. Four subsystems are  
 25 needed for maximum coverage of the available phase space: 1) the B0 spectrometer, which  
 26 consists of a silicon tracking system and photon EM calorimetry, 2) the Off-Momentum  
 27 Detector (OMD) which is responsible for fully reconstructing the momentum of charged  
 28 particles from nuclear breakup, 3) the Roman Pots (RP), which enable the tagging and  
 29 reconstruction of protons (or coherent light nuclear final states) with magnetic rigidity  $>$   
 30 60%, and 4) the Zero-Degree Calorimeter (ZDC), which is responsible for reconstructing  
 31 photons and neutrons. A full 3D layout of the FF region can be found in Fig. 4.6. The  
 32 technologies chosen for each detector are described below, and in the EIC Yellow Report [8].

#### 33 **Technology Choices**

34 The choice of detector technologies was driven by the performance requirements estimated  
 35 by the physics working groups and the desire to reduce schedule risk by maximizing overlap  
 36 with other systems at the EIC and LHC.

37 The B0 spectrometer relies on both silicon layers with precise spatial resolution ( $\sim$   
 38  $5 - 20\mu\text{m}$ ), and a system for reconstructing photons. For the silicon tracking system,  
 39 we propose use of two technologies, namely, ITS3 MAPS and AC-LGADs, which provide  
 40 both the needed spatial resolution (MAPS), as well as very precise timing information  
 41 ( $\sim 20 - 30\text{ps}$ ; AC-LGADs). Such a timing resolution will help reject background and  
 42 will reduce the effect of vertex smearing from the crab cavity rotation of the bunches.

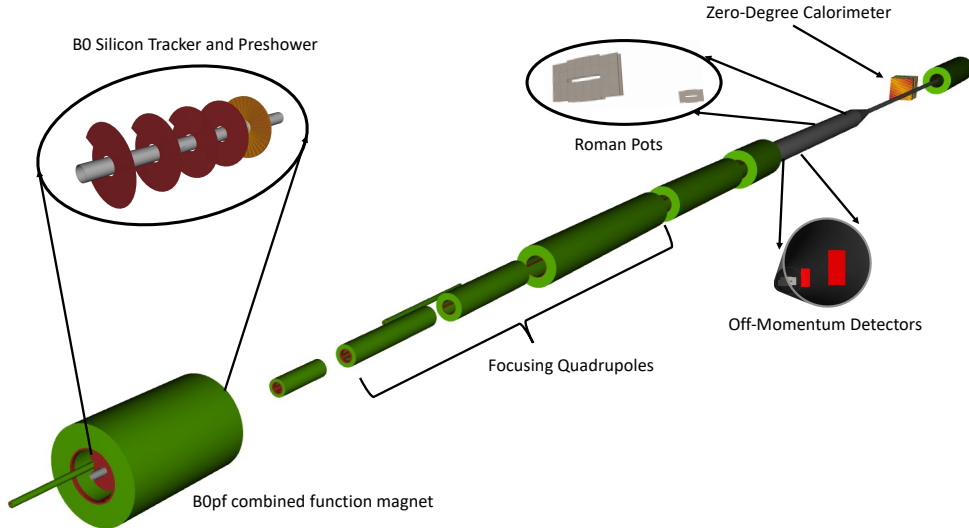


Figure 4.6: A birds eye view of the Far-Forward region of IP6 with the proposed EPIC detector instrumentation. This rendering was produced using the DD4HEP simulation framework.

1 For Photons, a short  $\text{PbWO}_4$  array is ideal, but spatial constraints may preclude this.  
 2 In that case, a silicon pre-shower + shower-maximum detector will be installed to enable  
 3 reconstruction of photons from conversion lepton pairs. The silicon preshower will rely on  
 4  $\sim 2X_0$  of lead as a converter layer for photons, and two layers of silicon for reconstructing  
 5 the produced lepton pair.

6 The Roman Pots consist of two stations separated by 2 meters, with each station con-  
 7 sisting of two active layers. The AC-LGAD technology would be ideal for this application  
 8 because of its ability to provide both spatial and timing information. We propose to insert  
 9 the silicon planes directly into the beam pipe vacuum (i.e. roman pots style detectors with  
 10 no "pots") to maximize acceptance. The off-momentum detector system follows the same  
 11 design philosophy, with a modified geometric orientation for maximal coverage of spectator  
 12 nucleons from nuclear breakup.

13 The EIC Zero-Degree Calorimeter detector system is based on the ALICE FoCAL de-  
 14 sign, and consists of a layer of 10cm  $\text{PbWO}_4$  crystals, 12 layers of W+Silicon for EMCAL  
 15 imaging, 22 layers of Pb/Silicon for imaging of hadronic showers, and finally 30 layers of  
 16 Pb/Sci for sampling hadronic calorimetry. This configuration meets the requirement for  
 17 hadronic energy resolution of  $\frac{\sigma_E}{E} = \frac{50\%}{\sqrt{E}} \oplus 5\%$ , and significantly outperforms the spec for  
 18 electromagnetic calorimetry of  $\frac{\sigma_E}{E} < \frac{30\%}{\sqrt{E}}$ . Angular resolution is required to be  $\frac{\sigma_\theta}{\theta} < \frac{3\text{mrad}}{\sqrt{E}}$ ,  
 19 which is still under investigation via the imaging system.

## 20 Detector Performance and acceptance

21 The momentum resolutions in each detector are driven by different considerations, with  
 22 effects coming from intrinsic detector limitations (e.g. pixel size), and effects coming from

the hadron beam (e.g. angular divergence). In general, the beam effects dominate the momentum reconstruction and are the limiting factor in analyses using the far-forward detectors. For the tracking silicon detectors, resolutions from full GEANT4 simulations have been found to be between 2 and 10% for 3 momentum, and 5 and 25% for transverse momentum. The resolutions are worse in the low momentum region where beam effects have a larger impact. Table 4.2 summarizes the acceptance of the four detector systems.

Detector	$\theta$ accep. [mrad]	Rigidity accep.
B0 tracker	5.5–20.0	N/A
Off-Momentum	0.0–5.0	45%–65%
Roman Pots	0.0–5.0	60%–95%
Zero-Degree Calorim.	0.0–4.0	N/A

Table 4.2: Summary of the geometric acceptance for far-forward protons and neutrons in polar angle  $\theta$  and magnetic rigidity percentage provided by the baseline EIC far-forward detector design. The Roman Pots acceptance at high values of rigidity depends on the optics choice for the machine (high-rigidity means closer to the beam momentum). In all cases, the upper bound of the acceptance is driven by the magnet apertures.

#### 4.2.5 Far-Backward Detector Systems

The Far Backward region hosts detector systems that are critical for the precise absolute and relative luminosity determination needed for cross section and asymmetry measurements. For this, the bremsstrahlung process is used as it has a large, precisely known QED cross-section, resulting in negligible statistical uncertainty and minimizing theoretical uncertainty. The absolute and relative luminosity determination is obtained by the direct and indirect measurement of bremsstrahlung photons, with complimentary measurements used to reduce and control systematic effects that would typically dominate the measurement uncertainty. Three detector systems provides the necessary information to calibrate, verify, and precisely determine the absolute and relative luminosity. The direct photon detector, the pair spectrometer, and the low- $Q^2$  taggers are discussed in more detail below.

##### Direct photon detector

The direct photon detector system is placed on the zero-degree line in the far backward region. This system allows the direct determination of the number of bremsstrahlung photons utilizing a calorimeter. The calorimeter is also exposed to the direct synchrotron radiation fan and must thus be shielded, which degrades the energy resolution. At an EIC luminosity of  $10^{33} \text{ cm}^{-2}\text{s}^{-1}$ , the mean number of such photons per bunch crossing is over 20 for electron-proton scattering and increases with  $Z^2$  of the target for nuclear beams. The per-bunch energy distributions are broad, with a mean proportional to the number of photons per bunch crossing. The counting of bremsstrahlung photons is therefore effectively an energy measurement in the photon calorimeter with all of the related systematic uncertainties (e.g. gain stability) of such a measurement.

**<sup>1</sup> Pair spectrometer**

<sup>2</sup> The pair spectrometer provides a complimentary measurement of luminosity that is outside  
<sup>3</sup> the primary synchrotron radiation fan and is operated in a reduced rate environment. A  
<sup>4</sup> small fraction of the bremsstrahlung photons are converted into  $e^+e^-$  pairs in the vacuum  
<sup>5</sup> chamber exit window. A dipole magnet splits the pairs vertically and each particle hits  
<sup>6</sup> a separate calorimeter adjacent to the unconverted photon path. The spectrometer rate  
<sup>7</sup> is directly proportional to the fraction of photons which convert into  $e^+e^-$  pairs, placing  
<sup>8</sup> stringent requirements on the photon exit window. It must have a precisely known material  
<sup>9</sup> composition, and a precisely measured and uniform thickness along the photon direction.  
<sup>10</sup> Alternative designs that utilize a sweeping magnet after the initial exit window and pair  
<sup>11</sup> converters of various thicknesses allow us to overcome challenges in the design of the exit  
<sup>12</sup> window and provide a robust handle on systematics related with the converter characteris-  
<sup>13</sup> tics.

<sup>14</sup> The pair spectrometer is composed of calorimeters as well as tracking detectors for the  
<sup>15</sup> precise determination of the opening angle of the  $e^+e^-$  pair, which allows the reconstruction  
<sup>16</sup> of the converted photon positions. The distribution of photon positions is required to correct  
<sup>17</sup> for the lost photons falling outside the photon aperture and detector acceptances.

**<sup>18</sup> Low  $Q^2$  taggers**

<sup>19</sup> The low- $Q^2$  taggers enable the detection of bremsstrahlung electrons, as well as final state  
<sup>20</sup> electrons which participated in quasi-real ( $Q^2 \approx 0$ ) photoproduction reactions. The final  
<sup>21</sup> state bremsstrahlung electrons provide a powerful tool for calibrating and verifying the  
<sup>22</sup> luminosity measurement with photons. Tagging bremsstrahlung electrons and counting  
<sup>23</sup> corresponding photons in the photon detectors provides a direct measure of the lumino-  
<sup>24</sup> sity detector acceptance in the tagged energy range. This is of paramount importance to  
<sup>25</sup> precisely determine the pair conversion probability for the luminosity spectrometer, which  
<sup>26</sup> depends on the exit window composition and thickness. Such measurements will require  
<sup>27</sup> special runs with low bunch currents to ensure that there is only one bremsstrahlung elec-  
<sup>28</sup> tron/photon pair in the system per bunch crossing.

<sup>29</sup> Tagging of low- $Q^2$  processes provides an extension of the kinematic range of DIS pro-  
<sup>30</sup> cesses measured with electrons in the central detector. It crosses the transition from DIS  
<sup>31</sup> to hadronic reactions with quasi-real photons. Taggers provide useful acceptance in the  
<sup>32</sup> range  $Q^2 < 10^{-2}$  GeV $^2$ . Application of the electron taggers for low- $Q^2$  physics will face a  
<sup>33</sup> challenge from the high rate of bremsstrahlung electrons, which can be addressed by tagger  
<sup>34</sup> design and correlation with information from the central detector.

**<sup>35</sup> 4.3 Electron Polarimetry**

<sup>36</sup> Rapid, precise polarization measurement of the electron beam is crucial for meeting the  
<sup>37</sup> goals of the EIC physics program and facilitating the setup of the accelerator. The mea-  
<sup>38</sup> surement needs to be non-destructive with minimal impact on the beam lifetime. The  
<sup>39</sup> precision of the measurement needs to be 1% or better. Both longitudinal and transverse  
<sup>40</sup> components of the polarization need to be measured for each bunch. The most commonly

1 used technique for measuring electron beam polarization in rings and colliders is Compton  
2 polarimetry, in which the polarized electrons scatter from 100% circularly polarized laser  
3 photons. The asymmetry from this reaction is measured via the scattered electrons or high-  
4 energy backscattered photons. Plans for electron polarimetry at EIC include a Compton  
5 polarimeter in the Electron Storage Ring (ESR), a Compton polarimeter for the Rapid  
6 Cycling Synchrotron (RCS), and two Mott polarimeters at the source. The Compton po-  
7 larimeters for RCS and ESR have similarities but will operate in different modes: ESR in  
8 single photon/counting mode and RCS in multi-photon/integrating mode.

9 For the electron storage ring (ESR), the Compton polarimeter is proposed to be located  
10 on the upstream of IR6. The laser interaction point is in front of the quadrupole magnet  
11  $Q6EF\_6$  and is about 72 m away from IP6. The photon detector is placed in front of the  
12  $Q3EF\_6$ . The distance between the photon detector and the laser interaction point is 29m.  
13 The electron detector is placed before  $Q4EF\_6$ . Open midplane or a hole in the return yoke  
14 (hole radius about 2 cm ) is required for  $Q4EF\_6$  to allow the clearance for the photon cone.  
15 By carefully designing the coils, we can make the space for this requirement. An exit window  
16 is needed for the scattered photons near the dipole after the laser interaction point. It is  
17 perpendicular to the scattered photons. Geant4 simulation indicates that high acceptance  
18 of scattered photons can be achieved by using 1 mm thickness Beryllium exit window. For  
19 the photon detector, a homogeneous calorimeter with preshower detector is planned. The  
20 preshower is made of two planes of lead followed by silicon sensors and the segmentation of  
21 the silicon sensor on the order of 100-400  $\mu m$  is required. PbWO4 is a possible candidate,  
22 but the slow component may be an issue. A fiber-tungsten or lead sampling calorimeter is  
23 another (perhaps safer) option, but would likely result in reduced precision for the energy  
24 resolution on the photon side. For the electron detector, a diamond strip detector similar  
25 to Jefferson Lab Hall C diamond detector is being considered. Diamond detectors are  
26 extremely radiation hard and are fast enough to have response times sufficient to resolve  
27 the minimum bunch spacing (10 ns) at EIC.

28 A laser system based on the gain-switched diode lasers used in the injector at Jefferson  
29 Lab can provide all of the requirements we need for the Compton polarimeters. The pro-  
30 posed system will make use of a gain-switched diode laser at 1064 nm, amplified to high  
31 average power (10-20 W) via a fiber amplifier, and then frequency doubled to 532 nm using  
32 a PPLN or LBO crystal. The repetition rate of the laser is dictated by an applied RF signal  
33 and can be readily varied. We will employ the "back-reflection" technique similar to that  
34 used at Jefferson Lab for the laser polarization setup.

35 Backgrounds are an important consideration for Compton polarimetry as well. The  
36 primary processes of interest are Bremsstrahlung and synchrotron radiation. We are still  
37 going through initial studies of synchrotron radiation. As expected these photons will have  
38 a very small impact on the electron detector but will travel toward the photon detector. The  
39 study for the dipole before the laser IP is ongoing. Bremsstrahlung and other beam-related  
40 backgrounds will be handled by making measurements with the laser off.

41 In addition to measurements in the EIC electron ring, it is important to be able to  
42 determine the electron beam polarization in the RCS. In the RCS, electron bunches of  
43 approximately 28 nC are accelerated from 400 MeV to the nominal beam energy (5, 10, or  
44 18 GeV) in about 100 ms. Compton polarimetry can also be used for the measurement of  
45 polarization in RCS. It is proposed to be located at the IR6. Measurements will be averaged

1 over several bunches. The short bunch lifetime would require measurements in multiphoton  
 2 mode ( 1000 backscattered photons/crossing). Assuming 28 nC electron bunches at 2 Hz,  
 3 the backscattered photon rate is about 240 kHz and the measurement time would be on the  
 4 order of a few seconds.

## 5 4.4 Hadron Polarimetry

6 For hadron polarimetry at the EIC, the natural starting point is the system used successfully  
 7 for polarized proton beams at RHIC for two decades. The system has two components. A  
 8 low rate absolute polarimeter provides a measure of the polarization scale, but with coarse  
 9 grained, infrequent measurements. The absolute polarization measurements are used to  
 10 normalize the measurements from high rate relative polarimeters. Their high rate allows  
 11 measurement of finer grained polarization details, including time dependence of the beam  
 12 polarization. Additionally, local polarization measurements at the experimental collision  
 13 points are made, primarily to provide verification of the beam spin direction.

14 The absolute polarimeter at RHIC (Hjet) passes a polarized atomic hydrogen jet across  
 15 the proton beam path. The jet polarization is precisely measured with standard laboratory  
 16 techniques, and the polarization state is regularly reversed. Recoil protons from beam-  
 17 jet scattering are detected in silicon detectors around the interaction point. The Hjet  
 18 polarimeter is self-calibrating. The azimuthal asymmetry of recoil protons with respect to  
 19 the jet spin state, with known polarization, determines the asymmetry-polarization relation  
 20 for the apparatus. With this relation, the asymmetry with respect to the beam spin state  
 21 determines the beam polarization. This self-calibration procedure is only valid for elastic  
 22 scattering,  $pp \rightarrow pp$ . The energy and angle resolution of recoil protons are adequate to  
 23 distinguish the elastic proton final state from the lowest lying inelastic final state,  $N\pi$ .

24 The Hjet polarimeter will be installed in the EIC hadron storage ring. Operation for  
 25 polarized protons will be largely unchanged from RHIC, although an improved data acqui-  
 26 sition system will be required to accommodate the higher bunch crossing frequency.

27 For polarized  $^3\text{He}$  beams at the EIC, a polarized  $^3\text{He}$  target would allow absolute po-  
 28 larimetry as performed at RHIC. Alternatively, an unpolarized hydrogen jet target can be  
 29 used; in this arrangement, absolute  $^3\text{He}$  polarimetry would require a special calibration  
 30 procedure with a proton beam on a polarized  $^3\text{He}$  target at the same center of mass energy.  
 31 In either case, elastic beam-target scattering is required for the absolute polarization mea-  
 32 surement. The lowest lying breakup states of the  $^3\text{He}$  beam are  $pd$  and  $npp$ ; at only a few  
 33 MeV/c<sup>2</sup> above the  $^3\text{He}$  mass, the breakup states cannot be resolved with the target recoil  
 34 measurement. Inelastic events will need to be identified by tagging the breakup fragments.  
 35 A suitable location in the EIC hadron storage ring for the Hjet polarimeter with taggers  
 36 has been identified by the straight section design group.

37 The relative polarimeters at RHIC (pC) sweep a thin carbon ribbon target across the  
 38 proton beam. Recoil carbon nuclei from beam-target scattering are detected in silicon de-  
 39 tectors arranged azimuthally around the interaction point. The azimuthal asymmetry of  
 40 the carbon nuclei provides a measure of the beam polarization; an ensemble of pC measure-  
 41 ments is normalized to the concurrent Hjet measurements to set the absolute polarization  
 42 scale. The azimuthal spacing of the detectors also allows a measurement of the transverse  
 43 component of the beam spin direction. The high rate from a solid target allows statistically

1 significant measurement of the polarization in a few seconds; several pC measurements  
2 over the hours-long RHIC stores provide the polarization lifetime. The carbon target is  
3  $\sim 10\mu\text{m}$  wide, significantly smaller than the transverse size of the beam. As the carbon  
4 target is swept across the beam, the pC polarimeters are thus able to measure the transverse  
5 polarization profile, required for spin measurements with colliding beams.

6 The principle of the pC polarimeters is directly applicable for proton beams at the EIC.  
7 The asymmetry for polarized  $^3\text{He}$ -C scattering is expected to be similar in magnitude to  
8 that for polarized p-p scattering, so the pC polarimeters should also be capable of  $^3\text{He}$   
9 polarimetry. However, the total proton beam current at the EIC will be over an order of  
10 magnitude higher than at RHIC. Simulations indicate that the carbon ribbon targets will  
11 break after a few seconds in the beam, allowing only a few measurements. The targets would  
12 require frequent replacement, leading to unacceptable interruptions in beam operation. An  
13 alternative to the carbon ribbon technology is under investigation.

14 Local polarimetry at RHIC is provided by the empirically observed azimuthal asymmetry  
15 of neutrons from the reaction  $pp \rightarrow nX$ . The neutrons are measured in the collider  
16 experiments zero degree calorimeters. No analogous  $ep$  or  $e^3\text{He}$  process exists for local  
17 polarimetry at the EIC. Instead, it is planned to install pC polarimeters immediately adjacent  
18 to the collider experiments, where the spin direction is the same as at the collision  
19 point. They will be operated primarily to measure spin direction and to ensure vanishing  
20 transverse components for longitudinal spin operation.

## 21 **4.5 The Need for Two Detectors**

22 The EIC is a monumental effort, a unique accelerator that will enable nuclear matter studies  
23 with unprecedented precision. Being built as a true discovery machine, the EIC is required  
24 to address fundamental open questions in nuclear science, such as the origin of mass and  
25 spin of hadrons, and to probe the "glue" that binds protons and neutrons, for the first time  
26 detailing the nature of very dense gluon systems in nuclei. A sophisticated set of detectors  
27 must be designed and constructed to capitalize on the investment in the accelerator facility  
28 for extracting the physics signals.

29 Historically, projects of similar scientific impact and scope were designed to include two  
30 or more complementary detectors. Multiple detectors expand scientific opportunities, draw  
31 a more vivid and complete picture of the science, and provide independent confirmation for  
32 discovery measurements, thus mitigating potential risks when entering uncharted territories.  
33 The nuclear physics community behind the EIC project has emphasized the need for at  
34 least two detectors for many years. Several community reports, such as the 2007 and 2015  
35 U.S. Long Range Plan reports for Nuclear Science, reference "as many as four interaction  
36 points" or the need for collisions "at two interaction points." This notion is echoed in the  
37 2018 National Academies of Sciences, Engineering, and Medicine report on an Assessment  
38 of U.S.-Based Electron-Ion Collider Science. At the moment, design on the first detector  
39 are well underway by the collective effort of EIC Project and EPIC collaboration. The EIC  
40 community is actively exploring the design options and opportunities for a second detector  
41 to capitalize on the investments into the new collider facility.

**1 Risk management** Large-scale scientific endeavors like the EIC are tremendously exciting but also inherently risky. History holds numerous examples of scientific dead ends, seemingly apparent signals for new phenomena resulting from misinterpretation. Many historical examples illustrate that the capability of near-simultaneous discovery by multiple detectors was essential for establishing the validity of the newly emerging paradigm. The scientific community can only become truly convinced of discovery if independent cross-checks by at least two different experiments (with different setups and/or approaches) are available for such critical new measurements. The delivery of a sufficiently diverse experimental input of the highest quality and precision is critical for EIC to justify the financial and intellectual investment and to realize its discovery potential fully. Only if the scientific question is illuminated from multiple angles does our understanding of nature tend asymptotically to an ever-more accurate description.

**13 Detector redundancy and complementarity** The ongoing detector design for the world's only Electron-Ion Collider facility has several years of construction lead time. It is only natural that each subsystem will explore multiple performance optimization routes and push for the most advanced, state-of-the-art technologies. Varying design decisions and technology choices between the two complementary detector concepts will ensure the necessary redundancy and mitigate risk associated with the possible failure of individual detector subcomponents.

**20** Alternative technology choices would also allow each experiment to optimize for different measurements while still preserving the ability to perform independent cross-checks. Possible optimization areas include consideration of different magnetic field strengths and associated trade-offs in the central part of the detector between particle identification capabilities and tracking performance at high particle momenta. These design choices impact the precision with which different physics can be accessed. The complementarity of multiple detectors enhances the science scope and ultimately leads to higher scientific impact. Having a second EIC detector with complementary sub-detector technologies and/or different coverage, and optimizations will ensure redundancy, cross-calibration, and independent validation of the most important results, providing higher-impact science for this significant investment.

**31** The clear conclusion is that the best way to optimize the science output is through building more than one detector, with complementarity in detector acceptance and systematic effects and added benefits due to technology redundancy. Existing studies already suggest the opportunity to optimize the overall physics output of the EIC in terms of precision and kinematic range through careful complementary choices of two general-purpose detectors.

**36 Taking advantage of the existing layout** The scientific mission of the Electron-Ion Collider includes a diverse set of open physics questions about the nature of the matter in our universe. Answering these questions requires a state-of-the-art experimental apparatus that ideally detect all the particles produced in electron-ion collisions. This functionality demands an onion-like structure composed of multiple layers that can be used to determine the type of particles produced and reconstruct their momenta and energy.

**42** Compared to existing collider experiments, the design of an EIC detector presents unique challenges. The device must cover a large area, from very close to the incoming beamlines

1 to the central region, where the remnants from the most energetic collisions are scattered.  
 2 The EIC will repurpose the existing Relativistic Heavy Ion Collider layout, which currently  
 3 weaves the beams in different directions at the two possible interaction points. These  
 4 constraints provide an opportunity to optimize the complementarity of the two detectors  
 5 so that the necessary gaps in coverage occur in different regions, allowing one detector  
 6 to see particles where the other is blind. It is also possible to tune the beam optics for  
 7 each detector to emphasize different physics processes, satisfying what would otherwise be  
 8 mutually exclusive demands. The flexibility will allow, for example, the inclusion into the  
 9 mainstream program of rare scattering processes, which are critical for imaging the deep  
 10 internal structure of nucleons and nuclei. This potential is further illustrated in figures 4.7  
 11 and 4.8. The science reach of the EIC will be significantly enhanced by leveraging the  
 12 beamline optics and interaction region.

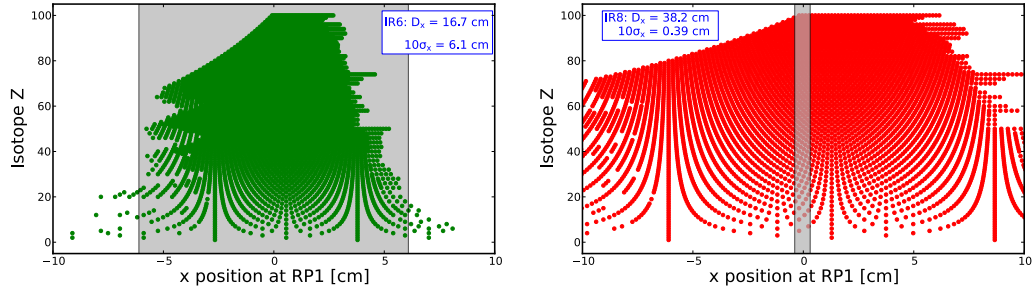


Figure 4.7: Isotope Z vs. hit position in the best Roman pot (RP) in IR-6 (left) and IR-8 (right). The gray box on each plot shows the  $10\sigma$  beam size, which prevents detection. This exclusion is much smaller in IR-8 due to the secondary focus in the beam optics. The larger horizontal spacing in IR-8 is due to a larger dispersion. The isotopes shown assume a  $^{238}\text{U}$  beam but are representative for all heavy ions. The exceptional ability of IR-8 to detect fragments with magnetic rigidities very close to that of the beam is also indicative of the acceptance for recoil protons and nuclei that emerge from exclusive reactions with a low transverse momentum  $p_T$  with respect to the beam, enabling a detailed science program of imaging the spatial and momentum distributions in nuclei, from light to heavy nuclei.

13 **Independent confirmation of science need** BNL and JLab management as host lab-  
 14 oratories for the EIC science program charged in 2021 a blue-ribbon Detector Proposal  
 15 Advisory Panel composed of renowned high-energy and nuclear physicists worldwide to  
 16 advise on the optimal approach to realize the EIC physics program. Their first priority  
 17 was identifying the approach for realizing the first EIC detector system, which is now mor-  
 18 phed into the EPIC detector. In addition, the Panel was asked to assess options for an  
 19 additional detector system that could address science beyond the EIC White Paper and  
 20 the 2018 National Academies of Sciences, Engineering, and Medicine report and/or enable  
 21 some complementarity to the first detector. The Panel concluded that "A strong case for  
 22 two complementary general-purpose detectors has been made during the panel review" and  
 23 that "it is essential to have two detectors with a sufficient degree of complementarity in

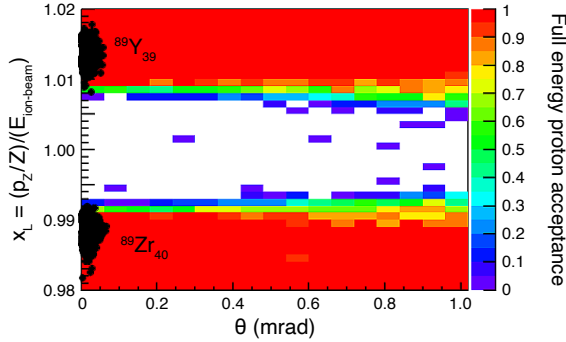


Figure 4.8: The acceptance fraction in longitudinal momentum fraction  $x_L$  with respect to the incident ion beam energy versus the forward scattering angle  $\theta$  near the ion beam direction. The figure illustrates the full detection capability for  $A - 1$  particles following the electro-induced  $J/\Psi$  production for diffractive scattering off the doubly closed-shell  $^{90}\text{Zr}$  beam, as enabled by the existence of a secondary focus in the beam optics.

<sup>1</sup> layout and detector technologies.” In particular, the Panel pointed to ”a convincing case  
<sup>2</sup> for the significant gain in physics reach achievable with a secondary focus:

- <sup>3</sup> • increased acceptance in the invariant momentum transfer  $t$  of the scattered proton in  
<sup>4</sup>  $e+p$  collisions, which directly translates into an increased resolution power for imaging  
<sup>5</sup> partons in the transverse plane,
- <sup>6</sup> • significantly improved abilities to detect nuclear breakup in exclusive and diffractive  
<sup>7</sup> scattering on light and heavy nuclei. The distinction between coherent and incoherent  
<sup>8</sup> scattering is essential for the physics interpretation of these processes,
- <sup>9</sup> • prospects for a program of low-background  $\gamma$  gamma spectroscopy with rare isotopes  
<sup>10</sup> in the beam fragments.”

<sup>11</sup> The Panel further pointed out: ”Furthermore, the additional R&D required for a second  
<sup>12</sup> detector will bring additional benefits in developing technologies and in training the associated  
<sup>13</sup> workforce.” The DOE Office of Nuclear Physics has followed up on this and restarted  
<sup>14</sup> a generic EIC-related detector R&D program.

<sup>15</sup> **A gateway to innovation and international cooperation** The EIC project has generated  
<sup>16</sup> immense interest and support from the international community. The current size  
<sup>17</sup> of the EIC Users Group has surpassed 1300 scientists, quickly achieving the critical mass  
<sup>18</sup> of physicists and engineers needed for a highly active and successful detector collaboration  
<sup>19</sup> at this scale. The growth of this community shows no sign of slowing and could perhaps  
<sup>20</sup> double by the start of data collection in 2030. The fact that the EIC project continues to  
<sup>21</sup> attract scientists, many of them leaders in their fields, reflects the EIC effort’s substantial  
<sup>22</sup> scope and physics potential. Establishing two detector collaborations at two beam collision  
<sup>23</sup> points allows for harnessing this growth while efficiently using the talent and resources the  
<sup>24</sup> community has to offer. Two collaborations will also expand the opportunities for a new  
<sup>25</sup> generation of scientists, providing avenues for the best amongst them to contribute and

1 develop into the next generation of scientific leaders. Having two detectors at the EIC will  
2 also broaden and strengthen the scientific workforce worldwide.

3 **Path for scientific innovations** In addition to developing the scientific workforce, two  
4 detectors will foster a natural and healthy competition between the collaborations, which  
5 will, in turn, encourage innovation and drive technological development. A case in point is  
6 the design of the two EIC interaction regions, which are not identical but housed in halls  
7 of different dimensions and with beams colliding at different angles. Unique constraints  
8 require unique solutions, which often manifest in the form of new technologies designed to  
9 specifically address the challenges presented by these two different interaction regions.

10 The concurrent development of complementary technologies for the two detectors is an  
11 asset: it broadens the opportunities for the societal impact of the EIC, allows for the verifi-  
12 cation of measurements in two truly independent ways, and provides the scope to capitalize  
13 on the complementary strengths of different solutions. Most importantly, friendly com-  
14 petition perhaps provides the most fertile ground for the emergence of the best new ideas.  
15 The existence of two collaborations opens a natural dialogue and encourages critical assess-  
16 ment of methods and solutions by the most qualified and uniquely invested audience. The  
17 healthy discussion and questioning of approaches provide objectivity and drive the desire to  
18 improve. The different needs and focus of the detectors may also lead to a cross-fertilization  
19 of ideas, as they usually do in similar cases, to the mutual benefit of both collaborations, the  
20 scientific community, and the EIC project at large. In the end, having two collaborations  
21 to include and develop new ideas and improve technologies will simultaneously lead to a  
22 faster path for further technology development to meet societal needs.

23 **A long-term investment in national vitality** It is broadly acknowledged that Nuclear  
24 Physics has produced and continues to produce many significant applications that directly  
25 benefit society. Highly reliable, small accelerators are central to advances in cancer treat-  
26 ment and industry (e.g., for studying and manufacturing new materials, including computer  
27 chips, electronics, batteries, and pharmaceuticals). They already constitute a multibillion-  
28 dollar enterprise with more than 30,000 installations worldwide. It is imperative to grow a  
29 highly qualified workforce trained in nuclear science for the vitality of the nation’s health,  
30 economy, and security (including nuclear weapons control and counterterrorism). In addi-  
31 tion to fundamental research positions, nuclear physicists serve in governments worldwide  
32 in leadership positions that address these critical issues. Financial organizations and private  
33 companies in all sectors seek out scientists trained in nuclear science for their quantitative  
34 skills, expertise in big data analysis, and creative problem-solving abilities. The EIC will  
35 play a crucial role in inspiring and training the next generation of highly skilled sci-  
36 entists and engineers required to meet future challenges in the coming decades. Advances in  
37 technology are inevitable when we gain a better understanding of nuclear matter’s inner-  
38 most structures at sub-femtometer scales. Ensuring this future implies that the time for  
39 decision-making is now because of the long timescale of operations.



# <sup>1</sup> Chapter 5

## <sup>2</sup> Wider Impact

### <sup>3</sup> 5.1 Accelerator Science and Technology

<sup>4</sup> The EIC must collide electrons with protons and other atomic nuclei (ions) over a range of  
<sup>5</sup> energies. There must be enough collisions for the experiment to gather adequate data to  
<sup>6</sup> elucidate or settle the known physics questions, and other questions that may emerge, in  
<sup>7</sup> a reasonable time. A collider's ability to squeeze many particles of two beams into a tiny  
<sup>8</sup> volume where they collide defines its luminosity. The luminosity ultimately required of the  
<sup>9</sup> EIC is comparable to those of the highest performing colliders built to date, such as the  
<sup>10</sup> Large Hadron Collider (LHC) at CERN and the B-meson factories at SLAC and KEK.

<sup>11</sup> Furthermore, given the crucial role of spin, there must be the capability to polarize both  
<sup>12</sup> electron and proton (or to achieve information on neutrons, light ion) beams. That is to  
<sup>13</sup> say, the spins of the individual particles in each beam must be made to line up with each  
<sup>14</sup> other, overcoming their natural tendency to point “every which way” at random.

<sup>15</sup> To achieve these goals, a host of techniques in accelerator physics and technology must  
<sup>16</sup> be brought to bear. Only a few are mentioned here. State-of-the-art superconducting  
<sup>17</sup> radio-frequency (SRF) cavities will accelerate high-intensity beams efficiently. Further spe-  
<sup>18</sup> cialized RF “crab” cavities will rotate the beams as they collide to optimize their overlap.  
<sup>19</sup> Elaborate interaction region designs must squeeze two very different beams simultaneously  
<sup>20</sup> into tiny spot sizes using advanced superconducting magnet designs. The hadron beams  
<sup>21</sup> must be compressed in volume by sophisticated new “beam cooling” techniques that in-  
<sup>22</sup> volve subtle interaction with yet other electron beams. Polarized beams require polarized  
<sup>23</sup> particle sources, special magnets, and a further level of mastery of beam physics to pre-  
<sup>24</sup> serve the polarization through the acceleration process to the collisions. Polarized colliding  
<sup>25</sup> stored beams have been achieved before only at HERA (polarized positrons or electrons on  
<sup>26</sup> unpolarized protons) and at RHIC (both colliding proton beams polarized).

<sup>27</sup> EIC accelerator requirements are by and large pushing the current technology and their  
<sup>28</sup> realization requires significant research and development (R&D). Indeed, an important el-  
<sup>29</sup> ement of the scientific justification for a U.S. electron-ion facility is that it drives advances  
<sup>30</sup> in accelerator science and technology, which in turn will benefit other fields of accelerator-  
<sup>31</sup> based science and society.

<sup>32</sup> The three primary areas that require significant accelerator science and technology R&D  
<sup>33</sup> are energy, luminosity, and polarization. The extensive energy variability and elaborate

1 interaction region of an EIC require advanced superconducting magnet designs that are  
2 challenging. To attain the highest luminosities demanded by the science, cooling of the  
3 hadron beam is essential. Accelerating the high intensity, electron beam produced by a  
4 state-of-the art electron gun for cooling of the hadron beam can only be achieved in an  
5 economic manner by recovering the accelerating energy in an energy recovery linac (ERL),  
6 a special type of recirculating linac. To optimize the overlap of the colliding beams at the  
7 interaction point, specialized superconducting radio frequency (SRF) crab cavities rotate  
8 the beams as they collide. Polarized beams require optimized polarized particle sources,  
9 use of special snake magnets, and a further level of mastery of beam physics to preserve the  
10 polarization through the acceleration process to the collisions.

11 To reach the performance goals of the EIC, a number of accelerator science and tech-  
12 nology advances are required. In the following paragraphs we will expand a bit more on  
13 these advances, needed to achieve the energy versatility, luminosity and polarization that  
14 underpin the EIC.

15 Development of magnet technologies are required to validate the magnet designs as-  
16 sociated with high-acceptance interaction points. In order to attain the high luminosity  
17 required, the final focus quadrupole magnets must be in close proximity to the interac-  
18 tion point. Large magnet apertures are required to maximize acceptance by the detectors.  
19 The first spectrometer dipoles must also have large apertures for detector acceptance and  
20 accommodating the close proximity of the adjacent electron beam pipe.

21 Cooling of hadron beams is essential to achieving the highest luminosities demanded by  
22 the EIC science. Use of an energy recovery linac presently offer the only credible concept for  
23 electron cooling of high-energy, colliding hadron beams. This takes advantage of both the  
24 expertise gained at Jefferson Lab with the development of the worldwide first ERL in the  
25 10-100 MeV scale in support of research for the U.S. Navy, and one of the most remarkable  
26 innovations at the Relativistic Heavy-Ion Collider at BNL: the implementation of bunched-  
27 beam stochastic cooling of the heavy-ion beams at full energy in collision. In addition, a  
28 recent collaboration of BNL with Cornell University successfully built a high-intensity multi-  
29 pass 150 MeV test energy recovery linac (ERL) taking advantage of non-scaling fixed-field  
30 alternating gradient magnets.

31 To reach the ultimate luminosity goals, the EIC design requires “crab crossing.” In a  
32 storage ring collider with beams crossing at an angle, much luminosity is lost because the  
33 colliding bunches do not overlap well. A crab crossing scheme counteracts this by means  
34 of transverse RF deflectors placed at symmetric locations around the IP. These tilt the  
35 bunches in the crossing plane, by half the crossing angle, so that they collide head-on (in  
36 a frame moving transversely) at the IP without loss of luminosity. After the collision,  
37 the tilt angle is reversed by the crab cavities installed at the opposite side of the IP. To  
38 date, the only operational implementation of crab crossing has been at the electron-positron  
39 collider (KEKB) at the High Energy Accelerator Research Organization (KEK) in Japan.  
40 Crab crossing was until recently never demonstrated in a hadron machine, but supported  
41 by the U.S. LHC Accelerator Research Program (LARP) program, intense research and  
42 development of crab cavities for the High-Luminosity Large Hadron Collider (HL-LHC)  
43 has been successfully ongoing at BNL and at Old Dominion University (ODU), near JLab,  
44 and was subsequently successfully tested for high-energy but small crab crossing angles at  
45 CERN.

1 A further essential element is the development of new and adaptation of existing simulation  
2 tools that can validate the many novel concepts of the EIC, and assist efforts towards operability and commissioning. The EIC accelerator requires electron beam parameters  
3 that are similar to a B-factory, and hadron beam parameters that are a factor of three more  
4 intense than at RHIC, but with a flat emittance. The operational modes are thus a significant  
5 extrapolation and have never been demonstrated experimentally. To establish the  
6 feasibility of these concepts, validation through self-consistent, start-to-end simulations is  
7 essential. In turn, the simulation codes should be validated through benchmarking against  
8 experimental data. Specific modes of operation which require the development of new  
9 simulation codes include beam-beam interactions with crabbed beams in asymmetric e-p  
10 collisions and bunch-by-bunch swap out injections of high-intensity electron bunches during  
11 the collision process. The development of a central simulation toolbox can be broadly  
12 applicable to other accelerator designs.

14 Development of an EIC will advance accelerator science and technology in nuclear science,  
15 but it would benefit other fields of accelerator-based science and society. The accelerator  
16 physics and technology advances required for an EIC will, importantly, have the potential to extend the capabilities of many particle accelerators built for other purposes,  
17 from medicine through materials science to elementary particle physics. Construction and  
18 future operations of an EIC including an appropriate program of dedicated accelerator test  
19 experiments would sustain and develop this precious national asset and help the United  
20 States to maintain a leading role in international accelerator-based science.

## 22 **5.2 Detector Technology**

23 The detector requirements that are imposed by the rich physics program of an EIC are  
24 demanding and unique among collider detectors: hermetic coverage in tracking, calorimetry and particle ID within a wide pseudorapidity range, substantial angular and momentum  
25 acceptance in the hadron-going direction, as well as high quality calorimetry. In the electron-going direction, electromagnetic calorimetry providing high-precision and hermetic  
26 detection of the scattered electron is required: in the very backward region for electron  
27 kinematics measurements and in the backward and barrel region for clean electron identification.  
28 Precision measurements require high momentum resolution, high efficiency, several  
29  $\sigma$  of PID separation, and most of all low material budget. These requirements drives detector  
30 technologies with often different demands than those in high-energy and particle  
31 physics.

34 The need for detector R&D was realized early by the community and involved laboratories and in January 2011 BNL, in association with TJNAF and the DOE Office of Nuclear  
35 Physics, created a generic detector R&D program [186] to address the scientific requirements  
36 for measurements at an EIC. The original goals of this program were to develop  
37 detector concepts and technologies that have particular importance to experiments in an  
38 EIC environment and to help ensure that the techniques and resources for implementing  
39 these technologies are well established within the EIC user community. It was also meant to  
40 stimulate the formation of user groups and collaborations that will be essential for the ultimate  
41 design effort and construction of the EIC experiments. This program was open to the

whole international EIC community. Many of the supported projects developed technologies that are now integral parts of existing detector concepts or are regarded as potential alternatives. The original generic detector R&D program ended in 2021 and was superseded by the EIC Project R&D program in 2022 [187]. The aim of the latter is to ensure that the respective detector technologies reach a viable state of maturity for construction readiness and minimal risks. In Summer 2022 the generic R&D program was reinstated [188] and now focuses on potential upgrades of the current EIC detector EPIC, as well as on technologies for a potential second EIC detector.

A variety of additional sources of support for R&D relevant for an EIC detector have been available to the community. For example, several National Laboratories, among them BNL, JLab, ANL, ORNL, and LANL, supported EIC detector R&D through Laboratory Directed Research & Development Programs (LDRDs) and many university groups in and outside of the US, active in the many R&D projects received support from their respective department and/or funding agencies. The EIC also benefited substantially from R&D conducted for many HEP and NP experiments such as ALICE and LHCb at CERN, Panda at GSI and Belle-II at KEK.

Several R&D projects also engaged successfully in the Small Business Innovation Research (SBIR) and Small Business Technology Transfer (STTR) programs, highly competitive programs that encourage domestic small businesses to engage in R&D with the potential for commercialization. Central to the STTR program is the partnership between small businesses and universities and laboratories. Examples are the development of SciGlass for calorimetry and the optimization of LAPPDs.

In the following paragraph we review the R&D consortia and projects that have been supported over the last 10 years. The vertex detector R&D consortium aims to develop new improved Monolithic Active Pixel Sensors (MAPS) to meet the requirements demanded by the EIC requirements. Various Micro-Pattern Gas Detector (MPGD) technologies, such as Gaseous Electron Multiplier (GEM), Micromegas, and  $\mu$ RWELL, have been pursued for low material tracking in barrel and forward regions as well as Time-Projection Chamber (TPC) readouts. New concepts like miniTPCs and integrated Cherenkov-TPCs had been developed and tested. R&D efforts within the calorimetry consortium have been dedicated to the development of several electromagnetic, and recently, hadronic calorimetry technologies. From this grew the Tungsten-Scintillating Fiber (W-SciFi) calorimeter, scintillating fibers embedded in a W-powder composite absorber. In parallel, novel scintillating glasses (SciGlass) have been developed with unprecedented quality as cost-effective alternative to lead-tungstate ( $PbWO_4$ ) crystals. The particle identification consortium is pursuing various technologies, such as Direct-Internally Reflected Cherenkov light (DIRC) detectors, modular and Dual Ring-Imaging Cherenkov (RICH) detectors, with Fresnel lens focalization in the former and with gas and aerogel radiators in the latter. New coating materials like nano-diamonds to replace Cesium-Iodide (CsI) for RICH photo sensors are also under investigation. Time-of-Flight detectors, as well as Roman Pots for forward proton detection, require highly segmented AC-coupled Low-Gas Avalanche Detector (AC-LGAD) sensors whose development has just started to get support from the program. Besides hardware R&D the program has supported various vital projects such as machine background studies and simulation software developments to enable more accurate definition of the physics' requirements. Sartre and Beagle are two examples of Monte-Carlo event generators whose

1 development was substantially boosted by the program.

2 New opportunities have emerged since the beginning of the first detector R&D for EIC.  
3 These are in part driven by pursuing alternative detector technologies for a complementary  
4 second fully integrated EIC detector and Interaction Region. With regard to the first  
5 detector, and as soon as its design and construction phase, the need for new technology  
6 capabilities for enhanced access as well as future cost-effective upgrades for access to new  
7 nuclear physics opportunities may arise. Furthermore, the EIC will be a multi-decade  
8 nuclear physics facility after its construction is completed and will in this period likely  
9 require detector upgrades driven by its science findings.

10 Thus, many opportunities for detector technology in the near and intermediate term  
11 exist within the overarching nuclear physics areas in the EIC design, construction, and  
12 science operations era. These can best be considered in detector functionality areas such  
13 as particle identification, calorimetry, tracking, and readout electronics, to address how one  
14 can enhance the performance of the EIC detector(s) with target R&D projects in a year or  
15 more.

16 Examples of such detector opportunities include, but are not limited to, the follow-  
17 ing: material minimization in a possible all-Silicon tracker, particle identification reach at  
18 mid rapidity and at higher momenta, cost-effectiveness of readout of particle identification  
19 detectors by improvements to Silicon Photomultipliers (SiPMs) or to Large-Area Picosec-  
20 ond Photo-detectors (LAPPDs). Furthermore, improvement of the achievable hadronic  
21 calorimetry resolutions, large-scale production and low-energy photon detection efficiency  
22 of possible glass-based electromagnetic calorimetry, new Application-Specific Integrated Cir-  
23 cuit (ASIC) and front-end readout board needs required for streaming readout modes, or  
24 improved spatial and/or timing resolution of Zero-Degree Calorimeters driven by the imag-  
25 ing and diffractive science programs. It is crucial that some of this research for enhanced  
26 detector functionality continues and is recognized as driven by Nuclear Physics needs.

### 27 **5.3 Advanced Computing**

28 In parallel with these detector opportunities, unique opportunities exist to directly *integrate*  
29 modern computing and data analysis methods in the experiment. These range from opera-  
30 tion of accelerator and scientific instruments and autonomous control and experimentation  
31 to data reduction and extracting information from large complex data sets, as well as, the  
32 intersections between real-time machine learning and control and optimization of accelera-  
33 tor systems operation and detector design. Efforts are underway to develop methods and  
34 production systems to establish a near real-time high-level nuclear physics analysis based  
35 on modern statistical methods. This requires a self-calibrated matrix of detector raw data  
36 synchronized to a reference time and would remove intermediate data storage requirements.  
37 This takes direct advantage of advances in micro-electronics and computing, and of artificial  
38 intelligence (AI) methods.

39 Micro-electronics and computing technologies have made order-of-magnitude advances  
40 in the last decades. Combined with modern statistical methods, it is now possible to analyze  
41 scientific data to rapidly expose correlations of data patterns and compare with advanced  
42 theoretical expectations. While many existing nuclear physics and high-energy physics ex-  
43 periments are taking advantage of these developments by upgrading their existing triggered

1 data acquisition to a streaming readout model (where detectors are read out continuously),  
 2 these experiments do not have the opportunity of implementing integrated systems from  
 3 data acquisition through analysis, such as the EIC has. Hence, we aim to merge the sep-  
 4 aration of data readout and analysis altogether, taking advantage of modern electronics,  
 5 computing and analysis techniques in order to build the next generation computing model  
 6 that will be essential for probing the femto-scale science accessible at the EIC.

7 An integrated whole-experiment approach to detector readout and analysis towards sci-  
 8 entific output will take advantage of multiple existing and emerging technologies. Amongst  
 9 these are: streaming readout, continuous data quality control and calibration, task-based  
 10 high performance local computing, distributed bulk data processing at supercomputer cen-  
 11 ters, modern statistical methods that can detect differences among groups of data or as-  
 12 sociations among variables even under very small departures from normal behavior, and  
 13 systematic use of artificial intelligence methods at various stages.

14 To further elaborate on the latter, AI is becoming ubiquitous in all disciplines of Nuclear  
 15 Physics [189]. EIC could be one of the first large-scale collider-based programs where  
 16 AI is systematically employed from the start. An AI4EIC Working Group <sup>1</sup> with annual  
 17 workshops, the most recent one in 2022, community events such as hackathons, and a  
 18 series of regular topical meetings has been included in the as part of the EIC Software  
 19 Working group. With the EIC detector design ongoing and opportunities for two detectors  
 20 at the EIC, AI can be gainfully used for the design optimization process of the large and  
 21 complex EIC detector systems that are based on computationally intensive simulations, for  
 22 the optimization of the individual detector systems, and even the optimization of materials  
 23 used within detectors for improved performance. Indeed, AI-based optimization strategies  
 24 have already been systematically exploited during the design and R&D phase of the EIC  
 25 detector [8, 190].

26 In detector design, Bayesian Optimization has gained popularity because it offers a  
 27 derivative-free principled approach to global optimization of noisy and computationally ex-  
 28 pensive black-box functions. An automated, highly-parallelized, and self-consistent proce-  
 29 dure has been developed and tested for a dual-radiator Ring Imaging Cherenkov (d-RICH)  
 30 design [191], which has been considered as a case study. Gaussian processes have been  
 31 used for regression, and a surrogate model has been reconstructed. These studies not only  
 32 resulted in a statistically significant improvement in the PID performance compared to an  
 33 existing baseline design, but they also shed light on the relevance of different features of  
 34 the detector for the overall performance. Multi-Objective Optimization has been used to  
 35 assist the design of the ECCE detector; this approach dealt with a multidimensional design  
 36 space driven by multiple objectives that encode the detector performance, while satisfying  
 37 several mechanical constraints.

38 Supported by modern electronics able to continuously convert the analog detector sig-  
 39 nals, streaming readout can further the convergence of online and offline analysis: here the  
 40 incorporation of high-level AI algorithms in the analysis pipeline can lead to better data  
 41 quality control during data taking and shorter analysis cycles. Indeed, AI could foster in the  
 42 next years significant advances in the crucial area of fast calibration/alignment of detectors,  
 43 greatly facilitating a data streaming readout approach.

---

<sup>1</sup><https://eic.ai/>

1 For example, the CLAS12 experiment at Jefferson Lab tested a prototype streaming  
2 readout system successfully under beam conditions [192]. An unsupervised hierarchical  
3 cluster algorithm was utilized in real-time with real data taken in streaming readout mode  
4 to combine the time, position, and energy information at the hit level, and associate each hit  
5 with a cluster membership and an outlier score. The implementation allows to successfully  
6 reject noise hits and to identify clusters for diverse topologies and large hit multiplicities.

7 For charged-particle tracking, where in nuclear physics experiments typically most of the  
8 computing cycles are spent in propagating the particles through inhomogeneous magnetic  
9 fields and material maps, AI can contribute to determine the optimal initial track parameters  
10 allowing to decrease the number of iterations needed. Particle identification, crucial for  
11 Nuclear Physics experiments, has recently seen a large growth of applications. For example,  
12 for imaging Cherenkov detectors, AI is expected to play an important role in speeding up  
13 compute intensive simulations and help in the classification of complex patterns of hits [193].

14 AI at the EIC is also expected to play a role in high-level physics analysis such as  
15 searches for rare signatures which necessitates advanced techniques making strong use of  
16 machine learning to filter out events, the utilization of jets to empower taggers for boosted  
17 jets and quark flavors within the jets, and in the aid for construction of higher-level Wigner  
18 distributions from sparse and missing data. As an example, Machine Learning techniques  
19 were recently applied to H1 data to correct for detector effects enabling the simultaneous  
20 and unbinned unfolding of the target observables [194].

## 21 **5.4 International and Domestic Interest**

22 The EIC Users Group (EICUG) has served as an entryway into the international EIC  
23 community since the founding in 2016. As of this writing it is composed of 1363 members  
24 from 267 institutions located in 36 countries around the world (see Fig. 5.1). The EICUG  
25 strives to represent the entire community that will contribute to a successful EIC. In addition  
26 to experimental nuclear physics, the users group includes nuclear and particle theorists  
27 (25%), accelerator physicists (10%) and computer scientists (< 1%). This unique mix of  
28 expertise has contributed greatly to the rapid rate of progress in the EIC project.

29 The early career members in the EICUG are passionate and engaged in nearly all levels  
30 of the EIC project, including detector design, software development and directing physics  
31 studies. They have self-organized, applied for and been awarded funds to host dedicated  
32 early career meetings that precede the annual EICUG meetings. These workshops provide  
33 early career members a dedicated time to network, present and discuss their work and  
34 socialize. The training and support of these early career members is integral to the success  
35 of the future EIC and the users group will continue to promote their scientific work and  
36 community building efforts.

37 The EICUG membership has tripled in size in the past six years, and continues to  
38 grow. U.S. institutions currently make up 35% of the users group. The location of these  
39 institutions, shown in Figure 5.2, is spread broadly across the country, indicating there is  
40 support and potential resources from 29 states/territories. The EICUG has always been  
41 strongly supported by the international community as well, evidenced by the large fraction  
42 of institutions in Europe (30%) and Asia(25%). The international nature of the users group  
43 is reflected in the leadership of our working group conveners as well as the structure of the



Figure 5.1: World map with locations of EICUG member institutions



Figure 5.2: United States map with locations of EICUG member institutions

- <sup>1</sup> Steering Committee, where two elected seats are dedicated to European and Asian members.
- <sup>2</sup> The annual EICUG meetings alternate between a U.S. site and a non-U.S. destination, for example Trieste, Paris and Warsaw planned for 2023. While several strong groups from
- <sup>3</sup> South America, Oceania and Africa have joined the EIC effort, these regions remain areas
- <sup>4</sup> of opportunity and potential growth. If the rate of growth remains steady, then the users
- <sup>5</sup> group could have 3000 members by the time EIC operations start.
- <sup>6</sup>

# References

- [1] R. Alarcon, et al., Opportunities in Nuclear Science: A Long-Range Plan for the Next Decade., DOE/NSF Nuclear Science Advisory Panel Report (2002).  
URL <https://science.osti.gov/np/nsac/Reports/Reports-Archive#2002>
- [2] D. Bryman, et al., The Frontiers of Nuclear Science, A Long Range Plan, DOE/NSF Nuclear Science Advisory Panel Report (2007).  
URL <https://science.osti.gov/np/nsac/Reports/Reports-Archive#2007>
- [3] A. Aprahamian, et al., Reaching for the horizon: The 2015 long range plan for nuclear science, DOE/NSF Nuclear Science Advisory Panel Report (2015).  
URL <http://www.osti.gov/biblio/1296778>
- [4] A High Luminosity, High Energy Electron-Ion-Collider : A new experimental quest to study the glue that binds us all , [http://web.mit.edu/eicc/DOCUMENTS/EIC\\_LRP-20070424.pdf](http://web.mit.edu/eicc/DOCUMENTS/EIC_LRP-20070424.pdf) (2007).
- [5] D. Boer, et al., Gluons and the quark sea at high energies: Distributions, polarization, tomography (2011). [arXiv:1108.1713](https://arxiv.org/abs/1108.1713).
- [6] A. Accardi, et al., Electron Ion Collider: The Next QCD Frontier: Understanding the glue that binds us all, Eur. Phys. J. A 52 (2016) 268. [arXiv:1212.1701](https://arxiv.org/abs/1212.1701), doi: [10.1140/epja/i2016-16268-9](https://doi.org/10.1140/epja/i2016-16268-9).
- [7] National Academies of Sciences, Engineering, and Medicine, An Assessment of U.S.-Based Electron-Ion Collider Science, The National Academies Press, Washington, DC, 2018. doi: [10.17226/25171](https://doi.org/10.17226/25171).
- [8] R. Abdul Khalek, et al., Science Requirements and Detector Concepts for the Electron-Ion Collider: EIC Yellow Report, Nucl. Phys. A 1026 (2022) 122447. [arXiv:2103.05419](https://arxiv.org/abs/2103.05419), doi: [10.1016/j.nuclphysa.2022.122447](https://doi.org/10.1016/j.nuclphysa.2022.122447).
- [9] R. L. Jaffe, A. Manohar, The G(1) problem: fact and fantasy on the spin of the proton, Nucl. Phys. B 337 (1990) 509–546. doi: [10.1016/0550-3213\(90\)90506-9](https://doi.org/10.1016/0550-3213(90)90506-9).
- [10] X.-D. Ji, Gauge invariant decomposition of nucleon spin, Phys. Rev. Lett. 78 (1997) 610–613. [arXiv:hep-ph/9603249](https://arxiv.org/abs/hep-ph/9603249), doi: [10.1103/PhysRevLett.78.610](https://doi.org/10.1103/PhysRevLett.78.610).
- [11] D. de Florian, R. Sassot, M. Stratmann, W. Vogelsang, Evidence for polarization of gluons in the proton, Phys. Rev. Lett. 113 (1) (2014) 012001. [arXiv:1404.4293](https://arxiv.org/abs/1404.4293), doi: [10.1103/PhysRevLett.113.012001](https://doi.org/10.1103/PhysRevLett.113.012001).

- [12] D. De Florian, G. A. Lucero, R. Sassot, M. Stratmann, W. Vogelsang, Monte Carlo sampling variant of the DSSV14 set of helicity parton densities, Phys. Rev. D 100 (11) (2019) 114027. [arXiv:1902.10548](https://arxiv.org/abs/1902.10548), doi:10.1103/PhysRevD.100.114027.
- [13] E. R. Nocera, R. D. Ball, S. Forte, G. Ridolfi, J. Rojo, A first unbiased global determination of polarized PDFs and their uncertainties, Nucl. Phys. B 887 (2014) 276–308. [arXiv:1406.5539](https://arxiv.org/abs/1406.5539), doi:10.1016/j.nuclphysb.2014.08.008.
- [14] Y. Zhou, N. Sato, W. Melnitchouk, How well do we know the gluon polarization in the proton?, Phys. Rev. D 105 (7) (2022) 074022. [arXiv:2201.02075](https://arxiv.org/abs/2201.02075), doi:10.1103/PhysRevD.105.074022.
- [15] I. Borsa, G. Lucero, R. Sassot, E. C. Aschenauer, A. S. Nunes, Revisiting helicity parton distributions at a future electron-ion collider, Phys. Rev. D 102 (9) (2020) 094018. [arXiv:2007.08300](https://arxiv.org/abs/2007.08300), doi:10.1103/PhysRevD.102.094018.
- [16] E. C. Aschenauer, R. Sassot, M. Stratmann, Unveiling the proton spin decomposition at a future Electron-Ion Collider, Phys. Rev. D 92 (2015) 094030. [arXiv:1509.06489](https://arxiv.org/abs/1509.06489), doi:10.1103/PhysRevD.92.094030.
- [17] E. C. Aschenauer, S. Fazio, J. H. Lee, H. Mantysaari, B. S. Page, B. Schenke, T. Ullrich, R. Venugopalan, P. Zurita, The Electron-Ion Collider: Assessing the energy dependence of key measurements, Rept. Prog. Phys. 82 (2019) 024301. [arXiv:1708.01527](https://arxiv.org/abs/1708.01527), doi:10.1088/1361-6633/aaf216.
- [18] J. Bartels, B. I. Ermolaev, M. G. Ryskin, Flavor singlet contribution to the structure function  $G(1)$  at small  $x$ , Z. Phys. C 72 (1996) 627–635. [arXiv:hep-ph/9603204](https://arxiv.org/abs/hep-ph/9603204), doi:10.1007/BF02909194.
- [19] Y. V. Kovchegov, D. Pitonyak, M. D. Sievert, Helicity Evolution at Small- $x$ , JHEP 01 (2016) 072, [Erratum: JHEP 10, 148 (2016)]. [arXiv:1511.06737](https://arxiv.org/abs/1511.06737), doi:10.1007/JHEP01(2016)072.
- [20] Y. Hatta, Y. Nakagawa, F. Yuan, Y. Zhao, B. Xiao, Gluon orbital angular momentum at small- $x$ , Phys. Rev. D 95 (11) (2017) 114032. [arXiv:1612.02445](https://arxiv.org/abs/1612.02445), doi:10.1103/PhysRevD.95.114032.
- [21] G. A. Chirilli, High-energy operator product expansion at sub-eikonal level, JHEP 06 (2021) 096. [arXiv:2101.12744](https://arxiv.org/abs/2101.12744), doi:10.1007/JHEP06(2021)096.
- [22] F. Cougoulic, Y. V. Kovchegov, A. Tarasov, Y. Tawabutr, Quark and gluon helicity evolution at small  $x$ : revised and updated, JHEP 07 (2022) 095. [arXiv:2204.11898](https://arxiv.org/abs/2204.11898), doi:10.1007/JHEP07(2022)095.
- [23] S. Bhattacharya, R. Boussarie, Y. Hatta, Signature of the Gluon Orbital Angular Momentum, Phys. Rev. Lett. 128 (18) (2022) 182002. [arXiv:2201.08709](https://arxiv.org/abs/2201.08709), doi:10.1103/PhysRevLett.128.182002.
- [24] X. Ji, Parton Physics on a Euclidean Lattice, Phys. Rev. Lett. 110 (2013) 262002. [arXiv:1305.1539](https://arxiv.org/abs/1305.1539), doi:10.1103/PhysRevLett.110.262002.

- [25] A. V. Radyushkin, Quasi-parton distribution functions, momentum distributions, and pseudo-parton distribution functions, Phys. Rev. D 96 (3) (2017) 034025. [arXiv:1705.01488](#), [doi:10.1103/PhysRevD.96.034025](#).
- [26] C. Alexandrou, M. Constantinou, K. Hadjyiannakou, K. Jansen, F. Manigrasso, Flavor decomposition for the proton helicity parton distribution functions, Phys. Rev. Lett. 126 (10) (2021) 102003. [arXiv:2009.13061](#), [doi:10.1103/PhysRevLett.126.102003](#).
- [27] G. Wang, Y.-B. Yang, J. Liang, T. Draper, K.-F. Liu, Proton momentum and angular momentum decompositions with overlap fermions, Phys. Rev. D 106 (1) (2022) 014512. [arXiv:2111.09329](#), [doi:10.1103/PhysRevD.106.014512](#).
- [28] C. Alexandrou, M. Constantinou, K. Hadjyiannakou, K. Jansen, C. Kallidonis, G. Koutsou, A. Vaquero Avilés-Casco, C. Wiese, Nucleon Spin and Momentum Decomposition Using Lattice QCD Simulations, Phys. Rev. Lett. 119 (14) (2017) 142002. [arXiv:1706.02973](#), [doi:10.1103/PhysRevLett.119.142002](#).
- [29] C. Cocuzza, W. Melnitchouk, A. Metz, N. Sato, Polarized antimatter in the proton from a global QCD analysis, Phys. Rev. D 106 (3) (2022) L031502. [arXiv:2202.03372](#), [doi:10.1103/PhysRevD.106.L031502](#).
- [30] D. Adamiak, Y. V. Kovchegov, W. Melnitchouk, D. Pitonyak, N. Sato, M. D. Sievert, First analysis of world polarized dis data with small- $x$  helicity evolution, Phys. Rev. D 104 (2021) L031501. [doi:10.1103/PhysRevD.104.L031501](#). URL <https://link.aps.org/doi/10.1103/PhysRevD.104.L031501>
- [31] I. Borsa, G. Lucero, R. Sassot, E. C. Aschenauer, A. S. Nunes, Revisiting helicity parton distributions at a future electron-ion collider, Phys. Rev. D 102 (9) (2020) 094018. [arXiv:2007.08300](#), [doi:10.1103/PhysRevD.102.094018](#).
- [32] X.-D. Ji, A QCD analysis of the mass structure of the nucleon, Phys. Rev. Lett. 74 (1995) 1071–1074. [arXiv:hep-ph/9410274](#), [doi:10.1103/PhysRevLett.74.1071](#).
- [33] C. Lorcé, On the hadron mass decomposition, Eur. Phys. J. C 78 (2) (2018) 120. [arXiv:1706.05853](#), [doi:10.1140/epjc/s10052-018-5561-2](#).
- [34] Y. Hatta, A. Rajan, K. Tanaka, Quark and gluon contributions to the QCD trace anomaly, JHEP 12 (2018) 008. [arXiv:1810.05116](#), [doi:10.1007/JHEP12\(2018\)008](#).
- [35] A. Metz, B. Pasquini, S. Rodini, Revisiting the proton mass decomposition, Phys. Rev. D 102 (11) (2021) 114042. [arXiv:2006.11171](#), [doi:10.1103/PhysRevD.102.114042](#).
- [36] A. C. Aguilar, et al., Pion and Kaon Structure at the Electron-Ion Collider, Eur. Phys. J. A 55 (10) (2019) 190. [arXiv:1907.08218](#), [doi:10.1140/epja/i2019-12885-0](#).
- [37] D. W. Sivers, Single Spin Production Asymmetries from the Hard Scattering of Point-Like Constituents, Phys. Rev. D 41 (1990) 83. [doi:10.1103/PhysRevD.41.83](#).

- [38] D. W. Sivers, Hard scattering scaling laws for single spin production asymmetries, Phys. Rev. D43 (1991) 261–263. [doi:10.1103/PhysRevD.43.261](https://doi.org/10.1103/PhysRevD.43.261).
- [39] D. Boer, P. J. Mulders, Time reversal odd distribution functions in lepto-production, Phys. Rev. D57 (1998) 5780–5786. [arXiv:hep-ph/9711485](https://arxiv.org/abs/hep-ph/9711485), [doi:10.1103/PhysRevD.57.5780](https://doi.org/10.1103/PhysRevD.57.5780).
- [40] Femtoscale Imaging of Nuclei using Exascale Platforms, QUAntum chromodynamics Nuclear TOMography Collaboration, <https://www.anl.gov/phy/quantom> (2022).
- [41] D. Müller, D. Robaschik, B. Geyer, F. M. Dittes, J. Hořejši, Wave functions, evolution equations and evolution kernels from light ray operators of QCD, Fortsch. Phys. 42 (1994) 101–141. [arXiv:hep-ph/9812448](https://arxiv.org/abs/hep-ph/9812448), [doi:10.1002/prop.2190420202](https://doi.org/10.1002/prop.2190420202).
- [42] A. V. Radyushkin, Scaling limit of deeply virtual Compton scattering, Phys. Lett. B380 (1996) 417–425. [arXiv:hep-ph/9604317](https://arxiv.org/abs/hep-ph/9604317), [doi:10.1016/0370-2693\(96\)00528-X](https://doi.org/10.1016/0370-2693(96)00528-X).
- [43] X.-D. Ji, Deeply virtual Compton scattering, Phys. Rev. D55 (1997) 7114–7125. [arXiv:hep-ph/9609381](https://arxiv.org/abs/hep-ph/9609381), [doi:10.1103/PhysRevD.55.7114](https://doi.org/10.1103/PhysRevD.55.7114).
- [44] M. Burkardt, Impact parameter space interpretation for generalized parton distributions, Int. J. Mod. Phys. A18 (2003) 173–208. [arXiv:hep-ph/0207047](https://arxiv.org/abs/hep-ph/0207047), [doi:10.1142/S0217751X03012370](https://doi.org/10.1142/S0217751X03012370).
- [45] M. Polyakov, Generalized parton distributions and strong forces inside nucleons and nuclei, Phys. Lett. B 555 (2003) 57–62. [arXiv:hep-ph/0210165](https://arxiv.org/abs/hep-ph/0210165), [doi:10.1016/S0370-2693\(03\)00036-4](https://doi.org/10.1016/S0370-2693(03)00036-4).
- [46] E.-C. Aschenauer, S. Fazio, K. Kumericki, D. Mueller, Deeply Virtual Compton Scattering at a Proposed High-Luminosity Electron-Ion Collider, JHEP 09 (2013) 093. [arXiv:1304.0077](https://arxiv.org/abs/1304.0077), [doi:10.1007/JHEP09\(2013\)093](https://doi.org/10.1007/JHEP09(2013)093).
- [47] J. C. Collins, D. E. Soper, Parton Distribution and Decay Functions, Nucl. Phys. B 194 (1982) 445–492. [doi:10.1016/0550-3213\(82\)90021-9](https://doi.org/10.1016/0550-3213(82)90021-9).
- [48] J. C. Collins, D. E. Soper, Back-To-Back Jets in QCD, Nucl. Phys. B 193 (1981) 381, [Erratum: Nucl.Phys.B 213, 545 (1983)]. [doi:10.1016/0550-3213\(81\)90339-4](https://doi.org/10.1016/0550-3213(81)90339-4).
- [49] J. C. Collins, D. E. Soper, Back-To-Back Jets: Fourier Transform from B to K-Transverse, Nucl. Phys. B 197 (1982) 446–476. [doi:10.1016/0550-3213\(82\)90453-9](https://doi.org/10.1016/0550-3213(82)90453-9).
- [50] J. C. Collins, D. E. Soper, G. F. Sterman, Transverse Momentum Distribution in Drell-Yan Pair and W and Z Boson Production, Nucl. Phys. B 250 (1985) 199–224. [doi:10.1016/0550-3213\(85\)90479-1](https://doi.org/10.1016/0550-3213(85)90479-1).
- [51] J. C. Collins, D. E. Soper, G. F. Sterman, Factorization of Hard Processes in QCD, Adv. Ser. Direct. High Energy Phys. 5 (1989) 1–91. [arXiv:hep-ph/0409313](https://arxiv.org/abs/hep-ph/0409313), [doi:10.1142/9789814503266\\_0001](https://doi.org/10.1142/9789814503266_0001).

- [52] J. C. Collins, Leading twist single transverse-spin asymmetries: Drell-Yan and deep inelastic scattering, Phys. Lett. B 536 (2002) 43–48. [arXiv:hep-ph/0204004](https://arxiv.org/abs/hep-ph/0204004), doi: [10.1016/S0370-2693\(02\)01819-1](https://doi.org/10.1016/S0370-2693(02)01819-1).
- [53] S. J. Brodsky, D. S. Hwang, I. Schmidt, Initial state interactions and single spin asymmetries in Drell-Yan processes, Nucl. Phys. B 642 (2002) 344–356. [arXiv:hep-ph/0206259](https://arxiv.org/abs/hep-ph/0206259), doi: [10.1016/S0550-3213\(02\)00617-X](https://doi.org/10.1016/S0550-3213(02)00617-X).
- [54] L. Zheng, E. C. Aschenauer, J. H. Lee, B.-W. Xiao, Z.-B. Yin, Accessing the gluon Sivers function at a future electron-ion collider, Phys. Rev. D 98 (3) (2018) 034011. [arXiv:1805.05290](https://arxiv.org/abs/1805.05290), doi: [10.1103/PhysRevD.98.034011](https://doi.org/10.1103/PhysRevD.98.034011).
- [55] V. N. Gribov, L. N. Lipatov, Deep inelastic e p scattering in perturbation theory, Sov. J. Nucl. Phys. 15 (1972) 438–450.
- [56] G. Altarelli, G. Parisi, Asymptotic Freedom in Parton Language, Nucl. Phys. B 126 (1977) 298–318. doi: [10.1016/0550-3213\(77\)90384-4](https://doi.org/10.1016/0550-3213(77)90384-4).
- [57] Y. L. Dokshitzer, Calculation of the Structure Functions for Deep Inelastic Scattering and e+ e- Annihilation by Perturbation Theory in Quantum Chromodynamics., Sov. Phys. JETP 46 (1977) 641–653.
- [58] E. A. Kuraev, L. N. Lipatov, V. S. Fadin, The Pomeranchuk Singularity in Nonabelian Gauge Theories, Sov. Phys. JETP 45 (1977) 199–204.
- [59] I. I. Balitsky, L. N. Lipatov, The Pomeranchuk Singularity in Quantum Chromodynamics, Sov. J. Nucl. Phys. 28 (1978) 822–829.
- [60] L. V. Gribov, E. M. Levin, M. G. Ryskin, Semihard Processes in QCD, Phys. Rept. 100 (1983) 1–150. doi: [10.1016/0370-1573\(83\)90022-4](https://doi.org/10.1016/0370-1573(83)90022-4).
- [61] E. Iancu, R. Venugopalan, The Color glass condensate and high-energy scattering in QCD, 2003, pp. 249–3363. [arXiv:hep-ph/0303204](https://arxiv.org/abs/hep-ph/0303204), doi: [10.1142/9789812795533\\_0005](https://doi.org/10.1142/9789812795533_0005).
- [62] H. Weigert, Evolution at small x(bj): The Color glass condensate, Prog. Part. Nucl. Phys. 55 (2005) 461–565. [arXiv:hep-ph/0501087](https://arxiv.org/abs/hep-ph/0501087), doi: [10.1016/j.ppnp.2005.01.029](https://doi.org/10.1016/j.ppnp.2005.01.029).
- [63] J. Jalilian-Marian, Y. V. Kovchegov, Saturation physics and deuteron-Gold collisions at RHIC, Prog. Part. Nucl. Phys. 56 (2006) 104–231. [arXiv:hep-ph/0505052](https://arxiv.org/abs/hep-ph/0505052), doi: [10.1016/j.ppnp.2005.07.002](https://doi.org/10.1016/j.ppnp.2005.07.002).
- [64] F. Gelis, E. Iancu, J. Jalilian-Marian, R. Venugopalan, The Color Glass Condensate, Ann. Rev. Nucl. Part. Sci. 60 (2010) 463–489. [arXiv:1002.0333](https://arxiv.org/abs/1002.0333), doi: [10.1146/annurev.nucl.010909.083629](https://doi.org/10.1146/annurev.nucl.010909.083629).
- [65] J. L. Albacete, C. Marquet, Gluon saturation and initial conditions for relativistic heavy ion collisions, Prog. Part. Nucl. Phys. 76 (2014) 1–42. [arXiv:1401.4866](https://arxiv.org/abs/1401.4866), doi: [10.1016/j.ppnp.2014.01.004](https://doi.org/10.1016/j.ppnp.2014.01.004).

- [66] Y. V. Kovchegov, E. Levin, Quantum chromodynamics at high energy, Vol. 33, Cambridge University Press, 2012. [doi:10.1017/CBO9781139022187](https://doi.org/10.1017/CBO9781139022187).
- [67] A. Morreale, F. Salazar, Mining for Gluon Saturation at Colliders, Universe 7 (8) (2021) 312. [arXiv:2108.08254](https://arxiv.org/abs/2108.08254), [doi:10.3390/universe7080312](https://doi.org/10.3390/universe7080312).
- [68] I. Balitsky, Operator expansion for high-energy scattering, Nucl. Phys. B 463 (1996) 99–160. [arXiv:hep-ph/9509348](https://arxiv.org/abs/hep-ph/9509348), [doi:10.1016/0550-3213\(95\)00638-9](https://doi.org/10.1016/0550-3213(95)00638-9).
- [69] I. Balitsky, Factorization and high-energy effective action, Phys. Rev. D 60 (1999) 014020. [arXiv:hep-ph/9812311](https://arxiv.org/abs/hep-ph/9812311), [doi:10.1103/PhysRevD.60.014020](https://doi.org/10.1103/PhysRevD.60.014020).
- [70] Y. V. Kovchegov, Small  $x$   $F(2)$  structure function of a nucleus including multiple pomeron exchanges, Phys. Rev. D 60 (1999) 034008. [arXiv:hep-ph/9901281](https://arxiv.org/abs/hep-ph/9901281), [doi:10.1103/PhysRevD.60.034008](https://doi.org/10.1103/PhysRevD.60.034008).
- [71] Y. V. Kovchegov, Unitarization of the BFKL pomeron on a nucleus, Phys. Rev. D 61 (2000) 074018. [arXiv:hep-ph/9905214](https://arxiv.org/abs/hep-ph/9905214), [doi:10.1103/PhysRevD.61.074018](https://doi.org/10.1103/PhysRevD.61.074018).
- [72] J. Jalilian-Marian, A. Kovner, A. Leonidov, H. Weigert, The Wilson renormalization group for low  $x$  physics: Towards the high density regime, Phys. Rev. D 59 (1998) 014014. [arXiv:hep-ph/9706377](https://arxiv.org/abs/hep-ph/9706377), [doi:10.1103/PhysRevD.59.014014](https://doi.org/10.1103/PhysRevD.59.014014).
- [73] J. Jalilian-Marian, A. Kovner, A. Leonidov, H. Weigert, The BFKL equation from the Wilson renormalization group, Nucl. Phys. B 504 (1997) 415–431. [arXiv:hep-ph/9701284](https://arxiv.org/abs/hep-ph/9701284), [doi:10.1016/S0550-3213\(97\)00440-9](https://doi.org/10.1016/S0550-3213(97)00440-9).
- [74] H. Weigert, Unitarity at small Bjorken  $x$ , Nucl. Phys. A 703 (2002) 823–860. [arXiv:hep-ph/0004044](https://arxiv.org/abs/hep-ph/0004044), [doi:10.1016/S0375-9474\(01\)01668-2](https://doi.org/10.1016/S0375-9474(01)01668-2).
- [75] E. Iancu, A. Leonidov, L. D. McLerran, The Renormalization group equation for the color glass condensate, Phys. Lett. B 510 (2001) 133–144. [arXiv:hep-ph/0102009](https://arxiv.org/abs/hep-ph/0102009), [doi:10.1016/S0370-2693\(01\)00524-X](https://doi.org/10.1016/S0370-2693(01)00524-X).
- [76] E. Iancu, A. Leonidov, L. D. McLerran, Nonlinear gluon evolution in the color glass condensate. 1., Nucl. Phys. A 692 (2001) 583–645. [arXiv:hep-ph/0011241](https://arxiv.org/abs/hep-ph/0011241), [doi:10.1016/S0375-9474\(01\)00642-X](https://doi.org/10.1016/S0375-9474(01)00642-X).
- [77] E. Ferreiro, E. Iancu, A. Leonidov, L. McLerran, Nonlinear gluon evolution in the color glass condensate. 2., Nucl. Phys. A 703 (2002) 489–538. [arXiv:hep-ph/0109115](https://arxiv.org/abs/hep-ph/0109115), [doi:10.1016/S0375-9474\(01\)01329-X](https://doi.org/10.1016/S0375-9474(01)01329-X).
- [78] A. H. Mueller, Small  $x$  Behavior and Parton Saturation: A QCD Model, Nucl. Phys. B 335 (1990) 115–137. [doi:10.1016/0550-3213\(90\)90173-B](https://doi.org/10.1016/0550-3213(90)90173-B).
- [79] L. D. McLerran, R. Venugopalan, Computing quark and gluon distribution functions for very large nuclei, Phys. Rev. D 49 (1994) 2233–2241. [arXiv:hep-ph/9309289](https://arxiv.org/abs/hep-ph/9309289), [doi:10.1103/PhysRevD.49.2233](https://doi.org/10.1103/PhysRevD.49.2233).

- [80] L. D. McLerran, R. Venugopalan, Gluon distribution functions for very large nuclei at small transverse momentum, Phys. Rev. D 49 (1994) 3352–3355. [arXiv:hep-ph/9311205](https://arxiv.org/abs/hep-ph/9311205), [doi:10.1103/PhysRevD.49.3352](https://doi.org/10.1103/PhysRevD.49.3352).
- [81] L. D. McLerran, R. Venugopalan, Green's functions in the color field of a large nucleus, Phys. Rev. D 50 (1994) 2225–2233. [arXiv:hep-ph/9402335](https://arxiv.org/abs/hep-ph/9402335), [doi:10.1103/PhysRevD.50.2225](https://doi.org/10.1103/PhysRevD.50.2225).
- [82] M. Arratia, Y. Song, F. Ringer, B. Jacak, Jets as precision probes in electron-nucleus collisions at the Electron-Ion Collider, Phys. Rev. C 101 (6) (2020) 065204. [arXiv:1912.05931](https://arxiv.org/abs/1912.05931), [doi:10.1103/PhysRevC.101.065204](https://doi.org/10.1103/PhysRevC.101.065204).
- [83] X. Liu, F. Ringer, W. Vogelsang, F. Yuan, Lepton-jet Correlations in Deep Inelastic Scattering at the Electron-Ion Collider, Phys. Rev. Lett. 122 (19) (2019) 192003. [arXiv:1812.08077](https://arxiv.org/abs/1812.08077), [doi:10.1103/PhysRevLett.122.192003](https://doi.org/10.1103/PhysRevLett.122.192003).
- [84] H. T. Li, Z. L. Liu, I. Vitev, Nuclear matter effects on jet production at electron-ion colliders, SciPost Phys. Proc. 8 (2022) 134. [arXiv:2110.04858](https://arxiv.org/abs/2110.04858), [doi:10.21468/SciPostPhysProc.8.134](https://doi.org/10.21468/SciPostPhysProc.8.134).
- [85] K. J. Eskola, P. Paakkinen, H. Paukkunen, C. A. Salgado, EPPS16: Nuclear parton distributions with LHC data, Eur. Phys. J. C77 (2017) 163. [arXiv:1612.05741](https://arxiv.org/abs/1612.05741), [doi:10.1140/epjc/s10052-017-4725-9](https://doi.org/10.1140/epjc/s10052-017-4725-9).
- [86] X. Chu, E.-C. Aschenauer, J.-H. Lee, L. Zheng, Photon structure studied at an Electron Ion Collider, Phys. Rev. D 96 (7) (2017) 074035. [arXiv:1705.08831](https://arxiv.org/abs/1705.08831), [doi:10.1103/PhysRevD.96.074035](https://doi.org/10.1103/PhysRevD.96.074035).
- [87] R. A. Khalek, U. D'Alesio, M. Arratia, A. Bacchetta, M. Battaglieri, M. Begel, M. Boglione, R. Boughezal, R. Boussarie, G. Bozzi, S. V. Chekanov, F. G. Celiberto, G. Chirilli, T. Cridge, R. Cruz-Torres, R. Corliss, C. Cotton, H. Davoudiasl, A. Deshpande, X. Dong, A. Emmert, S. Fazio, S. Forte, Y. Furletova, C. Gal, C. Gwenlan, V. Guzey, L. A. Harland-Lang, I. Helenius, M. Hentschinski, T. J. Hobbs, S. Hoeche, T. J. Hou, Y. Ji, X. Jing, M. Kelsey, M. Klasen, Z. B. Kang, Y. V. Kovchegov, K. S. Kumar, T. Lappi, K. Lee, Y. J. Lee, H. T. Li, X. Li, H. W. Lin, H. Liu, Z. L. Liu, S. Liuti, C. Lorce, E. Lunghi, R. Marcarelli, S. Magill, Y. Makris, S. Mantry, W. Melnitchouk, C. Mezrag, S. Moch, H. Moutarde, S. Mukherjee, F. Muriglia, B. Nachman, P. M. Nadolsky, J. D. Nam, D. Neill, E. T. Neill, E. Nocera, M. Nycz, F. Olness, F. Petriello, D. Pitonyak, S. Platzer, S. Prestel, A. Prokudin, J. Qiu, M. Radici, S. Radhakrishnan, A. Sadofyev, J. Rojo, F. Ringer, F. Salazar, N. Sato, B. Schenke, S. Schlichting, P. Schweitzer, S. J. Sekula, D. Y. Shao, N. Sherrill, E. Sichtermann, A. Signori, K. Simsek, A. Simonelli, P. Sznajder, K. Tezgin, R. S. Thorne, A. Tricoli, R. Venugopalan, A. Vladimirov, A. Vicini, I. Vitev, D. Wiegand, C. P. Wong, K. Xie, M. Zaccheddu, Y. Zhao, J. Zhang, X. Zheng, P. Zurita, **Snowmass 2021 white paper: Electron ion collider for high energy physics** (2022). [doi:10.48550/ARXIV.2203.13199](https://doi.org/10.48550/ARXIV.2203.13199).  
URL <https://arxiv.org/abs/2203.13199>

- <sup>1</sup> [88] A. Filippi, M. De Napoli, Searching in the dark: the hunt for the dark photon, Rev. Phys. 5 (2020) 100042. [arXiv:2006.04640](https://arxiv.org/abs/2006.04640), doi:10.1016/j.revip.2020.100042.
- <sup>2</sup>
- <sup>3</sup> [89] M. Fabbrichesi, E. Gabrielli, G. Lanfranchi, The Dark Photon (2020). [arXiv:2005.01515](https://arxiv.org/abs/2005.01515).
- <sup>4</sup>
- <sup>5</sup> [90] C. Collaboration, Search for a narrow resonance decaying to a pair of muons in proton-proton collisions at 13 TeV, Tech. rep., CERN (2019).
- <sup>6</sup>
- <sup>7</sup> [91] D. Colladay, V. A. Kostelecky, Lorentz violating extension of the standard model, Phys. Rev. D 58 (1998) 116002. [arXiv:hep-ph/9809521](https://arxiv.org/abs/hep-ph/9809521), doi:10.1103/PhysRevD.58.116002.
- <sup>8</sup>
- <sup>9</sup>
- <sup>10</sup> [92] V. A. Kostelecky, Gravity, Lorentz violation, and the standard model, Phys. Rev. D 69 (2004) 105009. [arXiv:hep-th/0312310](https://arxiv.org/abs/hep-th/0312310), doi:10.1103/PhysRevD.69.105009.
- <sup>11</sup>
- <sup>12</sup> [93] D. Colladay, V. A. Kostelecky, CPT violation and the standard model, Phys. Rev. D 55 (1997) 6760–6774. [arXiv:hep-ph/9703464](https://arxiv.org/abs/hep-ph/9703464), doi:10.1103/PhysRevD.55.6760.
- <sup>13</sup>
- <sup>14</sup> [94] E. Lunghi, Lorentz Violation in Deep Inelastic Electron-Proton Scattering, in: 7th Meeting on CPT and Lorentz Symmetry, 2017, pp. 165–168. [arXiv:1610.09318](https://arxiv.org/abs/1610.09318), doi:10.1142/9789813148505\_0042.
- <sup>15</sup>
- <sup>16</sup>
- <sup>17</sup> [95] E. Lunghi, N. Sherrill, Lorentz violation and the electron-ion collider, Phys. Rev. D 98 (11) (2018) 115018. [arXiv:1805.11684](https://arxiv.org/abs/1805.11684), doi:10.1103/PhysRevD.98.115018.
- <sup>18</sup>
- <sup>19</sup> [96] V. A. Kostelecký, E. Lunghi, N. Sherrill, A. R. Vieira, Lorentz and CPT Violation in Partons, JHEP 04 (2020) 143. [arXiv:1911.04002](https://arxiv.org/abs/1911.04002), doi:10.1007/JHEP04(2020)143.
- <sup>20</sup>
- <sup>21</sup> [97] E. C. Aschenauer, S. Fazio, M. A. C. Lamont, H. Paukkunen, P. Zurita, Nuclear Structure Functions at a Future Electron-Ion Collider, Phys. Rev. D96 (11) (2017) 114005. [arXiv:1708.05654](https://arxiv.org/abs/1708.05654), doi:10.1103/PhysRevD.96.114005.
- <sup>22</sup>
- <sup>23</sup>
- <sup>24</sup> [98] R. Abdul Khalek, J. J. Ethier, J. Rojo, Nuclear parton distributions from lepton-nucleus scattering and the impact of an electron-ion collider, Eur. Phys. J. C 79 (6) (2019) 471. [arXiv:1904.00018](https://arxiv.org/abs/1904.00018), doi:10.1140/epjc/s10052-019-6983-1.
- <sup>25</sup>
- <sup>26</sup>
- <sup>27</sup> [99] R. Aaij, et al., Study of prompt  $D^0$  meson production in  $p\text{Pb}$  collisions at  $\sqrt{s_{\text{NN}}} = 5$  TeV, JHEP 10 (2017) 090. [arXiv:1707.02750](https://arxiv.org/abs/1707.02750), doi:10.1007/JHEP10(2017)090.
- <sup>28</sup>
- <sup>29</sup> [100] A. Collaboration, Letter of Intent: A Forward Calorimeter (FoCal) in the ALICE experiment, Tech. rep., CERN (2020).
- <sup>30</sup>
- <sup>31</sup> [101] H. Mäntysaari, Review of proton and nuclear shape fluctuations at high energy, Rept. Prog. Phys. 83 (8) (2020) 082201. [arXiv:2001.10705](https://arxiv.org/abs/2001.10705), doi:10.1088/1361-6633/aba347.
- <sup>32</sup>
- <sup>33</sup>
- <sup>34</sup> [102] A. Dumitru, F. Gelis, L. McLerran, R. Venugopalan, Glasma flux tubes and the near side ridge phenomenon at RHIC, Nucl. Phys. A 810 (2008) 91–108. [arXiv:0804.3858](https://arxiv.org/abs/0804.3858), doi:10.1016/j.nuclphysa.2008.06.012.
- <sup>35</sup>
- <sup>36</sup>

- [103] A. Dumitru, J. Jalilian-Marian, Two-particle correlations in high energy collisions and the gluon four-point function, Phys. Rev. D 81 (2010) 094015. [arXiv:1001.4820](https://arxiv.org/abs/1001.4820), [doi:10.1103/PhysRevD.81.094015](https://doi.org/10.1103/PhysRevD.81.094015).
- [104] A. Kovner, M. Lublinsky, Angular Correlations in Gluon Production at High Energy, Phys. Rev. D 83 (2011) 034017. [arXiv:1012.3398](https://arxiv.org/abs/1012.3398), [doi:10.1103/PhysRevD.83.034017](https://doi.org/10.1103/PhysRevD.83.034017).
- [105] Y. V. Kovchegov, D. E. Wertepny, Long-Range Rapidity Correlations in Heavy-Light Ion Collisions, Nucl. Phys. A 906 (2013) 50–83. [arXiv:1212.1195](https://arxiv.org/abs/1212.1195), [doi:10.1016/j.nuclphysa.2013.03.006](https://doi.org/10.1016/j.nuclphysa.2013.03.006).
- [106] S. Schlichting, P. Tribedy, Collectivity in Small Collision Systems: An Initial-State Perspective, Adv. High Energy Phys. 2016 (2016) 8460349. [arXiv:1611.00329](https://arxiv.org/abs/1611.00329), [doi:10.1155/2016/8460349](https://doi.org/10.1155/2016/8460349).
- [107] T. Altinoluk, N. Armesto, Particle correlations from the initial state, Eur. Phys. J. A 56 (8) (2020) 215. [arXiv:2004.08185](https://arxiv.org/abs/2004.08185), [doi:10.1140/epja/s10050-020-00225-6](https://doi.org/10.1140/epja/s10050-020-00225-6).
- [108] A. Dumitru, T. Lappi, V. Skokov, Distribution of Linearly Polarized Gluons and Elliptic Azimuthal Anisotropy in Deep Inelastic Scattering Dijet Production at High Energy, Phys. Rev. Lett. 115 (25) (2015) 252301. [arXiv:1508.04438](https://arxiv.org/abs/1508.04438), [doi:10.1103/PhysRevLett.115.252301](https://doi.org/10.1103/PhysRevLett.115.252301).
- [109] C. Marquet, E. Petreska, C. Roiesnel, Transverse-momentum-dependent gluon distributions from JIMWLK evolution, JHEP 10 (2016) 065. [arXiv:1608.02577](https://arxiv.org/abs/1608.02577), [doi:10.1007/JHEP10\(2016\)065](https://doi.org/10.1007/JHEP10(2016)065).
- [110] G. Aad, et al., Centrality and rapidity dependence of inclusive jet production in  $\sqrt{s_{NN}} = 5.02$  TeV proton-lead collisions with the ATLAS detector, Phys. Lett. B 748 (2015) 392–413. [arXiv:1412.4092](https://arxiv.org/abs/1412.4092), [doi:10.1016/j.physletb.2015.07.023](https://doi.org/10.1016/j.physletb.2015.07.023).
- [111] I. Vitev, Non-Abelian energy loss in cold nuclear matter, Phys. Rev. C 75 (2007) 064906. [arXiv:hep-ph/0703002](https://arxiv.org/abs/hep-ph/0703002), [doi:10.1103/PhysRevC.75.064906](https://doi.org/10.1103/PhysRevC.75.064906).
- [112] R. B. Neufeld, I. Vitev, B.-W. Zhang, A possible determination of the quark radiation length in cold nuclear matter, Phys. Lett. B 704 (2011) 590–595. [arXiv:1010.3708](https://arxiv.org/abs/1010.3708), [doi:10.1016/j.physletb.2011.09.045](https://doi.org/10.1016/j.physletb.2011.09.045).
- [113] H. Xing, Y. Guo, E. Wang, X.-N. Wang, Parton Energy Loss and Modified Beam Quark Distribution Functions in Drell-Yan Process in p+A Collisions, Nucl. Phys. A 879 (2012) 77–106. [arXiv:1110.1903](https://arxiv.org/abs/1110.1903), [doi:10.1016/j.nuclphysa.2012.01.012](https://doi.org/10.1016/j.nuclphysa.2012.01.012).
- [114] F. Arleo, S. Peigne,  $J/\psi$  suppression in p-A collisions from parton energy loss in cold QCD matter, Phys. Rev. Lett. 109 (2012) 122301. [arXiv:1204.4609](https://arxiv.org/abs/1204.4609), [doi:10.1103/PhysRevLett.109.122301](https://doi.org/10.1103/PhysRevLett.109.122301).
- [115] Z.-B. Kang, I. Vitev, H. Xing, Effects of cold nuclear matter energy loss on inclusive jet production in p+A collisions at energies available at the BNL Relativistic Heavy

- 1 Ion Collider and the CERN Large Hadron Collider, Phys. Rev. C 92 (5) (2015) 054911.  
2 [arXiv:1507.05987](https://arxiv.org/abs/1507.05987), doi:10.1103/PhysRevC.92.054911.
- 3 [116] Y.-T. Chien, I. Vitev, Towards the understanding of jet shapes and cross sections in  
4 heavy ion collisions using soft-collinear effective theory, JHEP 05 (2016) 023. [arXiv:1509.07257](https://arxiv.org/abs/1509.07257), doi:10.1007/JHEP05(2016)023.
- 6 [117] I. Vitev, Jet quenching at intermediate RHIC energies, Phys. Lett. B 606 (2005)  
7 303–312. [arXiv:nucl-th/0404052](https://arxiv.org/abs/nucl-th/0404052), doi:10.1016/j.physletb.2004.12.013.
- 8 [118] J.-w. Qiu, I. Vitev, Transverse momentum diffusion and broadening of the back-  
9 to-back dihadron correlation function, Phys. Lett. B 570 (2003) 161–170. [arXiv:nucl-th/0306039](https://arxiv.org/abs/nucl-th/0306039), doi:10.1016/j.physletb.2003.08.009.
- 11 [119] S. Fazio, et al., Hadronic Tomography at the EIC and the Energy Frontier,  
12 [https://www.snowmass21.org/docs/files/summaries/EF/SNOWMASS21-EF6\\_EF7-TF5\\_TF7-CompF2\\_CompF3\\_Hobbs-205.pdf](https://www.snowmass21.org/docs/files/summaries/EF/SNOWMASS21-EF6_EF7-TF5_TF7-CompF2_CompF3_Hobbs-205.pdf), Letter of Interest submitted to the  
14 Snowmass 2021 Theory Frontier (2020).
- 15 [120] T.-J. Hou, et al., New CTEQ global analysis of quantum chromodynamics with high-  
16 precision data from the LHC, Phys. Rev. D 103 (1) (2021) 014013. [arXiv:1912.10053](https://arxiv.org/abs/1912.10053),  
17 doi:10.1103/PhysRevD.103.014013.
- 18 [121] T. J. Hobbs, B.-T. Wang, P. M. Nadolsky, F. I. Olness, Charting the coming synergy  
19 between lattice QCD and high-energy phenomenology, Phys. Rev. D 100 (9) (2019)  
20 094040. [arXiv:1904.00022](https://arxiv.org/abs/1904.00022), doi:10.1103/PhysRevD.100.094040.
- 21 [122] A. Bacchetta, G. Bozzi, M. Radici, M. Ritzmann, A. Signori, Effect of Flavor-  
22 Dependent Partonic Transverse Momentum on the Determination of the  $W$  Boson  
23 Mass in Hadronic Collisions, Phys. Lett. B 788 (2019) 542–545. [arXiv:1807.02101](https://arxiv.org/abs/1807.02101),  
24 doi:10.1016/j.physletb.2018.11.002.
- 25 [123] G. Bozzi, A. Signori, Nonperturbative Uncertainties on the Transverse Momentum  
26 Distribution of Electroweak Bosons and on the Determination of the Boson Mass at  
27 the LHC, Adv. High Energy Phys. 2019 (2019) 2526897. [arXiv:1901.01162](https://arxiv.org/abs/1901.01162), doi:  
28 10.1155/2019/2526897.
- 29 [124] A. Bacchetta, V. Bertone, C. Bissolotti, G. Bozzi, F. Delcarro, F. Piacenza, M. Radici,  
30 Transverse-momentum-dependent parton distributions up to  $N^3LL$  from Drell-Yan  
31 data, JHEP 07 (2020) 117. [arXiv:1912.07550](https://arxiv.org/abs/1912.07550), doi:10.1007/JHEP07(2020)117.
- 32 [125] M. Arratia, et al., Jet Physics at the Electron Ion Collider, [https://www.snowmass21.org/docs/files/summaries/EF/SNOWMASS21-EF6\\_EF7-TF2\\_TF6-CompF3\\_CompF2-153.pdf](https://www.snowmass21.org/docs/files/summaries/EF/SNOWMASS21-EF6_EF7-TF2_TF6-CompF3_CompF2-153.pdf), Letter of Interest submitted to the Snowmass 2021  
33 Theory Frontier (2020).
- 36 [126] M. Abdolmaleki, et al., Heavy flavors at the EIC, [https://www.snowmass21.org/docs/files/summaries/EF/SNOWMASS21-EF6\\_EF7-TF2\\_TF7-CompF2\\_CompF0\\_Ivan\\_Vitev-068.pdf](https://www.snowmass21.org/docs/files/summaries/EF/SNOWMASS21-EF6_EF7-TF2_TF7-CompF2_CompF0_Ivan_Vitev-068.pdf), Letter of Interest submitted to the Snowmass 2021 Theory Frontier  
37 (2020).

- [127] M. Arratia, Y. Furletova, T. J. Hobbs, F. Olness, S. J. Sekula, Charm jets as a probe for strangeness at the future Electron-Ion Collider (2020). [arXiv:2006.12520](https://arxiv.org/abs/2006.12520).
- [128] S. J. Brodsky, P. Hoyer, C. Peterson, N. Sakai, The Intrinsic Charm of the Proton, Phys. Lett. B 93 (1980) 451–455. [doi:10.1016/0370-2693\(80\)90364-0](https://doi.org/10.1016/0370-2693(80)90364-0).
- [129] R. Abraham, et al., Forward Physics Facility, Letter of Interest submitted to the Snowmass 2021 Theory Frontier (2020). [doi:https://doi.org/10.5281/zenodo.4009640](https://doi.org/10.5281/zenodo.4009640).
- [130] M. Arratia, et al., EW and BSM physics at EIC, [https://www.snowmass21.org/docs/files/summaries/EF/SNOWMASS21-EF5\\_EF9-210.pdf](https://www.snowmass21.org/docs/files/summaries/EF/SNOWMASS21-EF5_EF9-210.pdf), letter of Interest submitted to the Snowmass 2021 Theory Frontier (2020).
- [131] L. Alvarez-Ruso, et al., NuSTEC White Paper: Status and challenges of neutrino–nucleus scattering, Prog. Part. Nucl. Phys. 100 (2018) 1–68. [arXiv:1706.03621](https://arxiv.org/abs/1706.03621), [doi:10.1016/j.ppnp.2018.01.006](https://doi.org/10.1016/j.ppnp.2018.01.006).
- [132] B. Abi, et al., Deep Underground Neutrino Experiment (DUNE), Far Detector Technical Design Report, Volume II DUNE Physics (2020). [arXiv:2002.03005](https://arxiv.org/abs/2002.03005).
- [133] K. Abe, et al., Hyper-Kamiokande Design Report (2018). [arXiv:1805.04163](https://arxiv.org/abs/1805.04163).
- [134] H. P. Dembinski, et al., Report on Tests and Measurements of Hadronic Interaction Properties with Air Showers, EPJ Web Conf. 210 (2019) 02004. [arXiv:1902.08124](https://arxiv.org/abs/1902.08124), [doi:10.1051/epjconf/201921002004](https://doi.org/10.1051/epjconf/201921002004).
- [135] C. Royon, Recent results from the TOTEM collaboration at the LHC, in: Workshop of QCD and Forward Physics at the the LHC, the future Electron Ion Collider and Cosmic Ray Physics, University of Kansas Libraries, Lawrence, 2020, pp. 131–138. [arXiv:2006.15220](https://arxiv.org/abs/2006.15220).
- [136] T. Sako, Recent status and prospects of LHCf and RHICf Takashi Sako for the LHCf and RHICf Collaborations, in: Workshop of QCD and Forward Physics at the the LHC, the future Electron Ion Collider and Cosmic Ray Physics, University of Kansas Libraries, Lawrence, 2020, pp. 147–155.
- [137] F. Fenu, The cosmic ray energy spectrum measured using the Pierre Auger Observatory, PoS ICRC2017 (2018) 486. [doi:10.22323/1.301.0486](https://doi.org/10.22323/1.301.0486).
- [138] D. Ivanov, Energy Spectrum Measured by the Telescope Array, PoS ICRC2019 (2020) 298. [doi:10.22323/1.358.0298](https://doi.org/10.22323/1.358.0298).
- [139] D. Ivanov, Report of the Telescope Array - Pierre Auger Observatory Working Group on Energy Spectrum, PoS ICRC2017 (2018) 498. [doi:10.22323/1.301.0498](https://doi.org/10.22323/1.301.0498).
- [140] A. di Matteo, et al., Full-sky searches for anisotropies in UHECR arrival directions with the Pierre Auger Observatory and the Telescope Array, PoS ICRC2019 (2020) 439. [arXiv:2001.01864](https://arxiv.org/abs/2001.01864), [doi:10.22323/1.358.0439](https://doi.org/10.22323/1.358.0439).

- <sup>1</sup> [141] X. Ji, Parton Physics from Large-Momentum Effective Field Theory, *Sci. China Phys. Mech. Astron.* 57 (2014) 1407–1412. [arXiv:1404.6680](https://arxiv.org/abs/1404.6680), doi:10.1007/s11433-014-5492-3.
- <sup>4</sup> [142] X. Ji, Y.-S. Liu, Y. Liu, J.-H. Zhang, Y. Zhao, Large-Momentum Effective Theory (2020). [arXiv:2004.03543](https://arxiv.org/abs/2004.03543).
- <sup>6</sup> [143] K.-F. Liu, S.-J. Dong, Origin of difference between anti-d and anti-u partons in the nucleon, *Phys. Rev. Lett.* 72 (1994) 1790–1793. [arXiv:hep-ph/9306299](https://arxiv.org/abs/hep-ph/9306299), doi:10.1103/PhysRevLett.72.1790.
- <sup>9</sup> [144] K. F. Liu, S. J. Dong, T. Draper, D. Leinweber, J. H. Sloan, W. Wilcox, R. M. Woloshyn, Valence QCD: Connecting QCD to the quark model, *Phys. Rev. D* 59 (1999) 112001. [arXiv:hep-ph/9806491](https://arxiv.org/abs/hep-ph/9806491), doi:10.1103/PhysRevD.59.112001.
- <sup>12</sup> [145] K.-F. Liu, Parton degrees of freedom from the path integral formalism, *Phys. Rev. D* 62 (2000) 074501. [arXiv:hep-ph/9910306](https://arxiv.org/abs/hep-ph/9910306), doi:10.1103/PhysRevD.62.074501.
- <sup>14</sup> [146] W. Detmold, C. J. D. Lin, Deep-inelastic scattering and the operator product expansion in lattice QCD, *Phys. Rev. D* 73 (2006) 014501. [arXiv:hep-lat/0507007](https://arxiv.org/abs/hep-lat/0507007), doi:10.1103/PhysRevD.73.014501.
- <sup>17</sup> [147] V. Braun, D. Müller, Exclusive processes in position space and the pion distribution amplitude, *Eur. Phys. J. C* 55 (2008) 349–361. [arXiv:0709.1348](https://arxiv.org/abs/0709.1348), doi:10.1140/epjc/s10052-008-0608-4.
- <sup>20</sup> [148] Y.-Q. Ma, J.-W. Qiu, Extracting Parton Distribution Functions from Lattice QCD Calculations, *Phys. Rev. D* 98 (7) (2018) 074021. [arXiv:1404.6860](https://arxiv.org/abs/1404.6860), doi:10.1103/PhysRevD.98.074021.
- <sup>23</sup> [149] Y.-Q. Ma, J.-W. Qiu, QCD Factorization and PDFs from Lattice QCD Calculation, *Int. J. Mod. Phys. Conf. Ser.* 37 (2015) 1560041. [arXiv:1412.2688](https://arxiv.org/abs/1412.2688), doi:10.1142/S2010194515600411.
- <sup>26</sup> [150] Y.-Q. Ma, J.-W. Qiu, Exploring Partonic Structure of Hadrons Using ab initio Lattice QCD Calculations, *Phys. Rev. Lett.* 120 (2) (2018) 022003. [arXiv:1709.03018](https://arxiv.org/abs/1709.03018), doi:10.1103/PhysRevLett.120.022003.
- <sup>29</sup> [151] A. Radyushkin, Nonperturbative Evolution of Parton Quasi-Distributions, *Phys. Lett. B* 767 (2017) 314–320. [arXiv:1612.05170](https://arxiv.org/abs/1612.05170), doi:10.1016/j.physletb.2017.02.019.
- <sup>31</sup> [152] A. J. Chambers, R. Horsley, Y. Nakamura, H. Perlt, P. E. L. Rakow, G. Schierholz, A. Schiller, K. Somfleth, R. D. Young, J. M. Zanotti, Nucleon Structure Functions from Operator Product Expansion on the Lattice, *Phys. Rev. Lett.* 118 (24) (2017) 242001. [arXiv:1703.01153](https://arxiv.org/abs/1703.01153), doi:10.1103/PhysRevLett.118.242001.
- <sup>35</sup> [153] S. Bethke,  $\alpha_s$  2002, *Nucl. Phys. B Proc. Suppl.* 121 (2003) 74–81. [arXiv:hep-ex/0211012](https://arxiv.org/abs/hep-ex/0211012), doi:10.1016/S0920-5632(03)01817-6.

- [154] H.-W. Lin, W. Melnitchouk, A. Prokudin, N. Sato, H. Shows, First Monte Carlo Global Analysis of Nucleon Transversity with Lattice QCD Constraints, Phys. Rev. Lett. 120 (15) (2018) 152502. [arXiv:1710.09858](https://arxiv.org/abs/1710.09858), doi:10.1103/PhysRevLett.120.152502.
- [155] J. Bringewatt, N. Sato, W. Melnitchouk, J.-W. Qiu, F. Steffens, M. Constantinou, Confronting lattice parton distributions with global QCD analysis, Phys. Rev. D 103 (1) (2021) 016003. [arXiv:2010.00548](https://arxiv.org/abs/2010.00548), doi:10.1103/PhysRevD.103.016003.
- [156] C. Alexandrou, K. Cichy, M. Constantinou, K. Jansen, A. Scapellato, F. Steffens, Transversity parton distribution functions from lattice QCD, Phys. Rev. D 98 (9) (2018) 091503. [arXiv:1807.00232](https://arxiv.org/abs/1807.00232), doi:10.1103/PhysRevD.98.091503.
- [157] S. Bhattacharya, K. Cichy, M. Constantinou, A. Metz, A. Scapellato, F. Steffens, Insights on proton structure from lattice QCD: The twist-3 parton distribution function  $g_T(x)$ , Phys. Rev. D 102 (11) (2020) 111501. [arXiv:2004.04130](https://arxiv.org/abs/2004.04130), doi:10.1103/PhysRevD.102.111501.
- [158] J.-W. Chen, H.-W. Lin, J.-H. Zhang, Pion generalized parton distribution from lattice QCD, Nucl. Phys. B 952 (2020) 114940. [arXiv:1904.12376](https://arxiv.org/abs/1904.12376), doi:10.1016/j.nuclphysb.2020.114940.
- [159] C. Alexandrou, K. Cichy, M. Constantinou, K. Hadjyiannakou, K. Jansen, A. Scapellato, F. Steffens, Unpolarized and helicity generalized parton distributions of the proton within lattice QCD, Phys. Rev. Lett. 125 (26) (2020) 262001. [arXiv:2008.10573](https://arxiv.org/abs/2008.10573), doi:10.1103/PhysRevLett.125.262001.
- [160] P. Shanahan, M. Wagman, Y. Zhao, Collins-Soper kernel for TMD evolution from lattice QCD, Phys. Rev. D 102 (1) (2020) 014511. [arXiv:2003.06063](https://arxiv.org/abs/2003.06063), doi:10.1103/PhysRevD.102.014511.
- [161] Q.-A. Zhang, et al., Lattice QCD Calculations of Transverse-Momentum-Dependent Soft Function through Large-Momentum Effective Theory, Phys. Rev. Lett. 125 (19) (2020) 192001. [arXiv:2005.14572](https://arxiv.org/abs/2005.14572), doi:10.1103/PhysRevLett.125.192001.
- [162] J. J. Aubert, et al., The ratio of the nucleon structure functions  $F_{2n}$  for iron and deuterium, Phys. Lett. B 123 (1983) 275–278. doi:10.1016/0370-2693(83)90437-9.
- [163] M. Arneodo, Nuclear effects in structure functions, Phys. Rept. 240 (1994) 301–393. doi:10.1016/0370-1573(94)90048-5.
- [164] D. F. Geesaman, K. Saito, A. W. Thomas, The nuclear EMC effect, Ann. Rev. Nucl. Part. Sci. 45 (1995) 337–390. doi:10.1146/annurev.ns.45.120195.002005.
- [165] O. Hen, D. W. Higinbotham, G. A. Miller, E. Piasetzky, L. B. Weinstein, The EMC Effect and High Momentum Nucleons in Nuclei, Int. J. Mod. Phys. E 22 (2013) 1330017. [arXiv:1304.2813](https://arxiv.org/abs/1304.2813), doi:10.1142/S0218301313300178.
- [166] J.-W. Chen, W. Detmold, Universality of the EMC effect, Phys. Lett. B 625 (2005) 165–170. [arXiv:hep-ph/0412119](https://arxiv.org/abs/hep-ph/0412119), doi:10.1016/j.physletb.2005.08.041.

- <sup>1</sup> [167] J. R. Smith, G. A. Miller, Polarized quark distributions in nuclear matter, Phys. Rev. C 72 (2005) 022203. [arXiv:nucl-th/0505048](https://arxiv.org/abs/nucl-th/0505048), doi:10.1103/PhysRevC.72.022203.
- <sup>3</sup> [168] I. C. Cloet, W. Bentz, A. W. Thomas, Spin-dependent structure functions in nuclear matter and the polarized EMC effect, Phys. Rev. Lett. 95 (2005) 052302. [arXiv:nucl-th/0504019](https://arxiv.org/abs/nucl-th/0504019), doi:10.1103/PhysRevLett.95.052302.
- <sup>6</sup> [169] J.-W. Chen, W. Detmold, J. E. Lynn, A. Schwenk, Short Range Correlations and the EMC Effect in Effective Field Theory, Phys. Rev. Lett. 119 (26) (2017) 262502. [arXiv:1607.03065](https://arxiv.org/abs/1607.03065), doi:10.1103/PhysRevLett.119.262502.
- <sup>9</sup> [170] W. Detmold, M. Illa, D. J. Murphy, P. Oare, K. Orginos, P. E. Shanahan, M. L. Wagman, F. Winter, Lattice QCD constraints on the parton distribution functions of  $^3\text{He}$  (2020). [arXiv:2009.05522](https://arxiv.org/abs/2009.05522).
- <sup>12</sup> [171] F. Winter, W. Detmold, A. S. Gambhir, K. Orginos, M. J. Savage, P. E. Shanahan, M. L. Wagman, First lattice QCD study of the gluonic structure of light nuclei, Phys. Rev. D 96 (9) (2017) 094512. [arXiv:1709.00395](https://arxiv.org/abs/1709.00395), doi:10.1103/PhysRevD.96.094512.
- <sup>16</sup> [172] Y. X. Zhao, A. Deshpande, J. Huang, K. S. Kumar, S. Riordan, Neutral-Current Weak Interactions at an EIC, Eur. Phys. J. A 53 (3) (2017) 55. [arXiv:1612.06927](https://arxiv.org/abs/1612.06927), doi:10.1140/epja/i2017-12245-2.
- <sup>19</sup> [173] P. E. Shanahan, A. W. Thomas, R. D. Young, Charge symmetry breaking from a chiral extrapolation of moments of quark distribution functions, Phys. Rev. D 87 (9) (2013) 094515. [arXiv:1303.4806](https://arxiv.org/abs/1303.4806), doi:10.1103/PhysRevD.87.094515.
- <sup>22</sup> [174] B. Buck, E. Anderssen, J. Bessuelle, M. Cepeda, T. Johnson, J. Kelsey, G. van Nieuwenhuizen, G. Visser, Design and fabrication of a highly integrated silicon detector for the star experiment at brookhaven national laboratory (2014). doi:10.48550/ARXIV.1404.0993.  
URL <https://arxiv.org/abs/1404.0993>
- <sup>27</sup> [175] J. N. Butler, T. Tabarelli de Fatis, A MIP Timing Detector for the CMS Phase-2 Upgrade (2019).
- <sup>29</sup> [176] sPHENIX Collaboration, [sphenix technical design report](#) (2019).  
URL <https://indico.bnl.gov/event/7081/>
- <sup>31</sup> [177] S. Inaba, M. Kobayashi, M. Nakagawa, T. Nakagawa, H. Shimizu, K. Takamatsu, T. Tsuru, Y. Yasu, A Beam test of a calorimeter prototype of PWO crystals at energies between 0.5-GeV and 2.5-GeV, Nucl. Instrum. Meth. A 359 (1995) 485–491. doi:10.1016/0168-9002(95)00022-4.
- <sup>35</sup> [178] Y. D. Prokoshkin, A. V. Shtannikov, Energy resolution calculation of the PWO calorimeter, comparison with the beam tests, Nucl. Instrum. Meth. A 362 (1995) 406–409. doi:10.1016/0168-9002(95)00226-X.

- 1 [179] T. D. Beattie, et al., Construction and Performance of the Barrel Electromagnetic  
2 Calorimeter for the GlueX Experiment, Nucl. Instrum. Meth. A 896 (2018) 24–42.  
3 [arXiv:1801.03088](https://arxiv.org/abs/1801.03088), doi:10.1016/j.nima.2018.04.006.
- 4 [180] O. D. Tsai, et al., Results of \& on a new construction technique for W/ScFi Calorime-  
5 ters, J. Phys. Conf. Ser. 404 (2012) 012023. doi:10.1088/1742-6596/404/1/012023.
- 6 [181] C. A. Aidala, et al., Design and Beam Test Results for the 2-D Projective sPHENIX  
7 Electromagnetic Calorimeter Prototype, IEEE Trans. Nucl. Sci. 68 (2) (2021) 173–  
8 181. [arXiv:2003.13685](https://arxiv.org/abs/2003.13685), doi:10.1109/TNS.2020.3034643.
- 9 [182] C. A. Aidala, et al., Design and Beam Test Results for the sPHENIX Electromagnetic  
10 and Hadronic Calorimeter Prototypes, IEEE Trans. Nucl. Sci. 65 (12) (2018) 2901–  
11 2919. [arXiv:1704.01461](https://arxiv.org/abs/1704.01461), doi:10.1109/TNS.2018.2879047.
- 12 [183] F. Guber, I. Selyuzhenkov (Eds.), Technical Design Report for the CBM Projectile  
13 Spectator Detector (PSD), GSI, Darmstadt, 2015.  
14 URL <https://repository.gsi.de/record/109059>
- 15 [184] F. Bock, et al., Design and Simulated Performance of Calorimetry Systems for the  
16 ECCE Detector at the Electron Ion Collider (7 2022). [arXiv:2207.09437](https://arxiv.org/abs/2207.09437).
- 17 [185] C. E. Allgower, et al., The STAR endcap electromagnetic calorimeter, Nucl. Instrum.  
18 Meth. A 499 (2003) 740–750. doi:10.1016/S0168-9002(02)01971-X.
- 19 [186] Electron Ion Collider Generic R&D Program (2011-2021), [https://wiki.bnl.gov/conferences/index.php/EIC\\_R%25D](https://wiki.bnl.gov/conferences/index.php/EIC_R%25D) (2011-2021).
- 21 [187] Electron Ion Collider Project R&D Program, [https://wiki.bnl.gov/conferences/index.php/General\\_Info](https://wiki.bnl.gov/conferences/index.php/General_Info) (2022).
- 23 [188] Electron Ion Collider Generic R&D Program (2022-present), [https://www.jlab.org/research/eic\\_rd\\_prgm](https://www.jlab.org/research/eic_rd_prgm) (2011-2021).
- 25 [189] A. Boehnlein, et al., Colloquium: Machine learning in nuclear physics, Rev. Mod.  
26 Phys. 94 (3) (2022) 031003. [arXiv:2112.02309](https://arxiv.org/abs/2112.02309), doi:10.1103/RevModPhys.94.031003.
- 28 [190] C. Fanelli, et al., AI-assisted Optimization of the ECCE Tracking System at the  
29 Electron Ion Collider (5 2022). [arXiv:2205.09185](https://arxiv.org/abs/2205.09185).
- 30 [191] E. Cisbani, et al., AI-optimized detector design for the future Electron-Ion Collider:  
31 the dual-radiator RICH case, JINST 15 (05) (2020) P05009. [arXiv:1911.05797](https://arxiv.org/abs/1911.05797),  
32 doi:10.1088/1748-0221/15/05/P05009.
- 33 [192] F. Ameli, et al., Streaming readout for next generation electron scattering experi-  
34 ments, Eur. Phys. J. Plus 137 (8) (2022) 958. [arXiv:2202.03085](https://arxiv.org/abs/2202.03085), doi:10.1140/  
35 epjp/s13360-022-03146-z.

- <sup>1</sup> [193] C. Fanelli, J. Pomponi, DeepRICH: Learning Deeply Cherenkov Detectors, *Mach. Learn. Sci. Tech.* 1 (2019) 015010. [arXiv:1911.11717](https://arxiv.org/abs/1911.11717), doi:10.1088/2632-2153/ab845a.
- <sup>4</sup> [194] V. Andreev, et al., Measurement of Lepton-Jet Correlation in Deep-Inelastic Scattering with the H1 Detector Using Machine Learning for Unfolding, *Phys. Rev. Lett.* 128 (13) (2022) 132002. [arXiv:2108.12376](https://arxiv.org/abs/2108.12376), doi:10.1103/PhysRevLett.128.132002.



